ROCK GLACIER WATER VOLUMES IN THE SAN JUAN MOUNTAINS, COLORADO: A MACHINE-LEARNING APPROACH

A Thesis

by

BENJAMIN A. GRUNAU

Submitted to the Office of Graduate and Professional Studies of
Texas A&M University
in partial fulfillment of the requirements for the degree of

MASTER OF SCIENCE

Chair of Committee,	John R. Giardino
Co-Chair of Committee,	George H. Allen
Committee Members,	Hongbin Zhan
Head of Department,	Ronald A. Kaiser

May 2021

Major Subject: Water Management & Hydrological Sciences

ABSTRACT

Today, issues pertaining to anthropogenic and climate forcing are threatening available water resources on a global scale. For remote alpine regions whose primary water resources are seasonally derived from snowmelt and runoff, these issues are particularly threatening. Changes in climate, and global population growth, mandate efforts for further exploration and monitoring of available water resources. This thesis explores the hydrologic significance of rock glaciers via machine-learning methodologies, in the form of a random forest image classifier, to classify rock glaciers in the 21,656 km^2 study area extent of the San Juan Mountains, CO. A procedural estimation of volume was developed and run using ArcGIS®, estimating water and ice volumes contained within all predicted rock glacier landcover in the study area. Water and ice volumes on the order of 0.94 – 1.41 km^3 were estimated for a predicted 69.691 km^2 rock glacier surface area based on these procedures. In response to the lack of any available validation data in the study area, all observable rock glaciers were mapped manually in ArcGIS®, resulting in a total of 1,052 observed features. The location of all mapped rock glaciers, and the morphometric data for these locations, served as validation for the semi-automated machine-learning methods used in this thesis. Statistical similarities between manually mapped rock glaciers, with regard to two trial-runs of the random forest image classifier, produced positive statistical results indicating the efficacy of these methods. The present results suggest that machine-learning decision-tree based image classifiers, in addition to the volumetric estimation procedure developed herein, provide a potentially effective means of estimating water and ice volumes present in rock glaciers.

DEDICATION

While the wealth of this world is quickly measured by gold and silver, precious gems, and shares of great corporations, I consider myself a truly rich man though countless friendships, and the love and wisdom shared by my family.

Shirk comfort, and smile!

ACKNOWLEDGEMENTS

This thesis is a testament of realization, perseverance, and growth, and marks one of the most noteworthy adventures of my life. My thanks and respect are greatly owed to my committee chair Dr. Rick Giardino for taking a chance on a new student with an awful undergraduate GPA, and for sharing his time, his stories, his scientific curiosities, and his delicious food with me. Rick's passion for his students is unprecedented, and has served to inspire and promote growth within all those who have had the pleasure of his company and interactions. In addition, I want to also thank Rick's wife Mrs. Fran Giardino, for her kind words, her humor, and for breaking the illusion of exclusivity in academia, making me feel welcome and appreciated as one of Rick's students. I also owe my most humble and sincere thanks to my committee member Dr. Hongbin Zhan for his overflowing exuberance as an educator, his complete dominion and mastery over the intricacies of groundwater hydrology, his contagious passion for physics and fluids – Dr. Zhan's powerful oratory as a lecturer is perhaps only superseded by the great Cicero. Additionally, the ambitious pursuit of applying remote sensing and machine-learning approaches to estimate water volumes in rock glaciers would have been a true burden to complete without the guidance of Dr. George Allen and his experimental 'Remote Sensing in Geomorphology' course. Despite his status as a new professor, Dr. Allen demonstrated an immediate sense of responsibility for his student's welfare as scientists, challenging our critical thinking and showing us the path towards meaningful and impactful work as researchers – his lessons were given not as a lecturer to an audience, but as wisdom from an older sibling.

My capacity for effective work, and the maintenance of my sanity during the global Covid-19 pandemic, was tremendously nurtured by the affirmation, love, and support of my wonderful

friends, family, and colleagues. I am deeply grateful to Derek Cheung for the time spent pondering science, woodworking, and fishing - for the wonderful food and lessons shared by the fireside. To Panshu Zhao I owe sincere thanks for his experience and advice shared regarding machine learning and GIS, his words alleviated much confusion and frustration, and served as genuine inspiration for my work. I cannot begin to describe the care and consideration shown by Raquel Granados-Aquilar, a true and noteworthy friend and colleague. Despite her busy schedule completing her dissertation, Raquel took the role of mother-hen over several of Rick's students, constantly checking in to see how our progress was going, sharing important papers and data, providing advice, answering questions, and offering much needed motivation through difficult and stressful times. To my newfound friends Luna and Alex, I must express my sincere gratitude for the wonderful times sharing jokes, stories, food and drink, and for their patience and selfless consideration enduring my vented frustrations and stress from grad school – their friendship is an ever-present source of happiness in my life. I was additionally blessed with a wonderfully surprising friendship by meeting my friend and colleague Daniel Acevedo, otherwise known as Ricky. In the midst of completing his own thesis, Ricky continues to emanate nothing but positivity, humor, and introspective thought-provoking conversation – a true friend, a brilliant scientist, a man destined to change the world. I am a truly blessed individual to be able to express my gratitude for a number of friendships fostered since middle school, friendships that have aged like wine and grown like vines – to my friends and brothers Brian Hine, Nolon Young, and Nick Pawelka, three men of abounding intelligence, loyalty, patience, respect, endearing generosity, my words of admiration ring hollow, thank you dudes for never changing. As iron sharpens iron, three more great men have given me the inspiration to pursue great things, and have helped sculpt me into an individual with more form than my former shapeless mass. To Jon Virdell, Daniel Valencia,

and Eric Stinson – scientists, philosophers, and dreamers of men – I have grown and suckled upon the teat of wisdom shared by these men; attempting to describe the impact each of you have had on my life would be a disgraceful and futile act, but I can say with words absolute that I would not be typing these words had we never met, thank you brothers.

In addition to my wealth of friendships and wonderful colleagues, my very existence, growth, and survival as a human being would be unworthy of mention without the nurturing love shown by my family and loved ones. To the entire Rambo household – to Tina, Kevin, and Sierra, I struggle to express my sincere respect, and my love for each of you. So much wonderful food shared, so many wonderful memories, so much laughter, you have all welcomed me into your home and treated me as your own; I am beyond blessed to have you all in my life. To my own family, how do I even describe my love. It is difficult to image how far I have come from the snot-nosed brat, the clueless child, that I once was. While I am still clueless about a great number of things, the love for science fostered within me from our camping trips, and the lessons shared with me after the countless times I have fallen, have kindled my passion for geology, and have taught me the importance of humility, patience, kindness, love and respect for others. Between the time sacrificed by my loving mom driving a fresh pair of shorts to my elementary school after wetting my pants, the time spent sitting next to my dad listening to music and his comforting words of strength after getting my heart broken, and the adventures and conversations I have shared with my younger brother and sister discussing relationships and the terrifying chasm of the future, I often catch myself pondering how deeply fortunate I am to have a family that loves me, cares for me, and promotes my growth as a person. And lastly, to Jackie, the flame within me who gives me strength, hope, and peace. To the woman who has climbed mountains of rock and overcome challenges responsible for the demise of so many who have come before us. I am constantly filled

with awe, and sometimes terror, at the capabilities and accomplishments you have demonstrated to the world. A humble human inspired by visions of a better world, an individual whose accolades are derived from efforts of sharing knowledge, wisdom, and truth. My efforts have been so deeply inspired by you, I have learned so much, grown so much, just through my admiration and adoration. The boundless love poured into her work and relationships is naught but a small fractal of her heart. My words, whether typed on a page or etched into stone, are inadequate to express my love, adoration, and respect. Perhaps the inspiration you have given me will help better the world, even a tiny bit – only through a better world can I begin to express these things.

CONTRIBUTORS AND FUNDING SOURCES

Contributors:

This project was supervised by committee chair Dr. Rick Giardino, committee co-chair Dr. George Allen, and committee member Dr. Hongbin Zhan, from the departments of Water Management & Hydrological Sciences, Geography, and Geology respectively.

Assistance with portions of the Google Earth Engine® Random Forest procedure was provided by colleague Jacqueline Rambo. Jacqueline also served ably as a field assistant throughout the mapping of the Camp Bird rock glacier during the summer of 2020. The simplified 3D rock glacier model, The Acevedo-Grunau Rock Glacier Model, for the calculation of water and ice volumes using ICESat-2 data was created with the help of colleague Daniel Acevedo. A preexisting rock glacier polygon database for the San Juan Mountains, created by Kriti Swami, was used as reference for manually mapped rock glacier inventory.

All remaining work performed in this thesis was carried out independently by the author.

Funding sources:

This thesis was supported in part by the departmental Water Management & Hydrological Sciences scholarship.

NOMENCLATURE

ANN	Artificial Neural Network
AUROC	Area Under the Receiver-Operator Curve
CNN	Convolutional Neural Network
DCG	Debris Covered Glacier
DEM	Digital Elevation Model
GAM	Generalized Additive Model
GEE	Google Earth Engine
LST	Lans-surface Temperature
MNDWI	Modified Normalized Difference Water Index
NDVI	Normalized Difference Vegetation Index
NIR	Near-infrared
ML	Machine Learning
RF	Random Forest
RG	Rock Glacier
SJM	San Juan Mountains
SVM	Support Vector Machine

TABLE OF CONTENTS

Page

LIST OF FIGURES

LIST OF TABLES

1. INTRODUCTION

Historically, studies on rock glaciers have primarily focused on age, kinetic mechanics of movement, formation processes, and general form and structure (Capps, 1910; Gerhold, 1964; Giardino et al., 1984; Haeberli, 1985), with limited attention paid to quantitative measurements of water and ice volumes and rock glacier water inventories. Much of the reasoning behind former research initiatives was underpinned by the common perception of rock glaciers as general geomorphic curiosities. Further understanding of their potential significance as hydrologic resources (Bajewsky & Gardner, 1989; Johnson, 1978; Jones et al., 2018; Jones et al., 2019), however, makes it necessary to develop a framework for precise remote identification and volumetric measurements of rock glaciers so that metrics on available water quantities can be readily collected and monitored.

In the context of water shortage and climate changes, rock glaciers may offer potentially valuable unconventional water resource assets. The water-storage potential of rock glaciers is unique among cryospheric landforms, resulting primarily from their diagnostic talus debris blankets which effectively provide insulation and solar-shielding for the internal permafrost and ice-debris matrix. To better understand the contribution of rock glaciers to the global hydrologic cycle, it is necessary to first establish a firm understanding of the volumetric water and ice content of rock glaciers at a much smaller localized scale. This thesis makes no attempts to establish the runoff contribution of rock glaciers on a global scale, but instead provides a preliminary first-order approximation of water volumes contained within rock glaciers in the San Juan Mountains, CO.

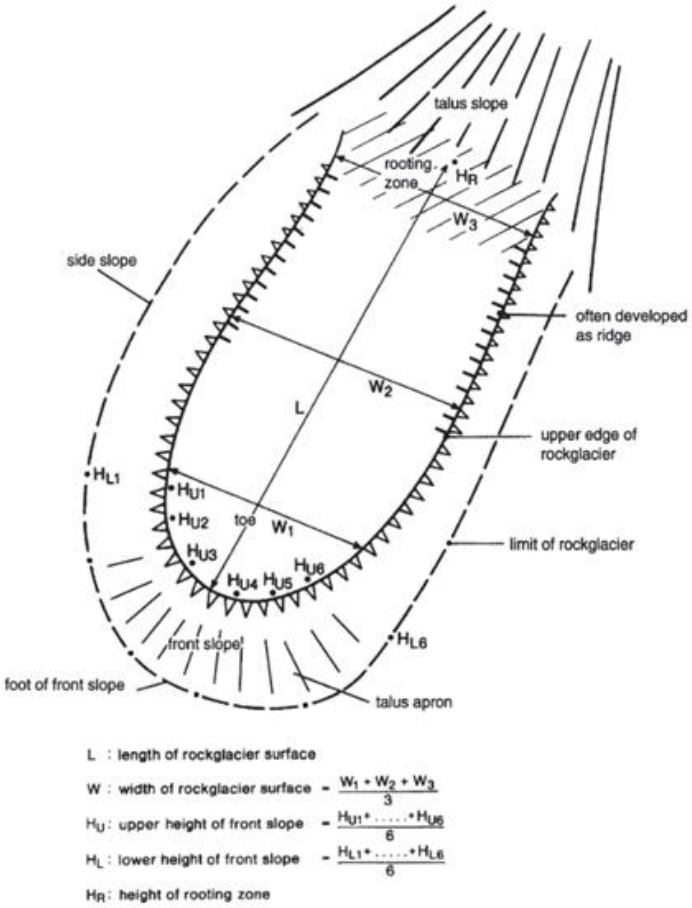

Fig. 3.1. Schematic diagram of geometric parameters and descriptive terms of a normal (active) talus rockglacier. In the case of a debris rockglacier, a moraine or (today) the relict of a glacier is situated at the base of the talus slope. The length is measured along the stromstrich (center flow line)

Fig. 1. Rock glacier volume estimation approach, reprinted from Barsch (1996).

Barsch (1996) provides descriptions of the morphometric and geometric parameters dictating the shape and form of rock glaciers (Figure 1). More recent studies (Brenning & Azocar, 2010; Brenning et al., 2007; Jones et al., 2019; Millar & Westfall, 2019; Munroe, 2018) have expanded upon these and other approaches for the estimation of rock glacier water and ice volumes. For this thesis, a similar integrated approach to volumetric estimation has been adopted

from these studies, in conjunction with semi-automated machine-learning and remote sensing methodologies utilized in more current studies.

These approaches have been shown in various other studies to offer precise quantitative water volume estimates in rock and debris-covered glaciers, allowing for important determinations to be gathered pertaining to periglacial water resource status and exploration (Xie et al., 2020; Zhang et al., 2019; Pfeffer et al., 2014; Jones et al., 2018; Barcaza et al., 2018; Grasser, 2006; Brenning, 2009).

In terms of rock glacier water inventories, the only existing first-order approximation of a near-global rock glacier database was demonstrated by Jones et al. (2018), suggesting volumetric water estimates of 83.72 ± 16.74 Gt, though these estimates are significantly limited in-part by methodological uncertainties, technical limitations, and primarily by lacking study area coverage. A different study by Pfeffer et al. (2014), representing the first true glacier and debris-covered glacier inventory - the Randolph Glacier Inventory – was created in response to needs posited by the Intergovernmental Panel on Climate Change. This database is the culmination of international collaboration between climate and Earth scientists, and the integration of a variety of datasets, truly highlighting the importance of local studies as they pertain to ultimate global investigations. The Randolph Glacier Inventory, however, focuses primarily on clean glacier-ice, which is significantly easier to observe and monitor using remotely-sensed datasets. In light of the inherent difficulties associated with rock glacier mapping and classification, and in ultimate pursuit of truly global-scale rock glacier inventories, it is necessary to first determine rock glacier water volumes at a much finer localized scale, and to additionally integrate new methods with existing approaches.

Estimates of available rock glacier water inventories in the San Juan Mountains of southwestern Colorado have only been posited by one study (Brenning et al., 2007). The resulting estimates, however, rely solely on analyst interpretation of aerial photography and the fitting of a statistical generalized additive model based off 84 rock glacier points. To bolster and add-upon the excellent work provided by Brenning et al. (2007), I undertook a detailed investigation and analysis of the available water inventories present within the near-entire extent of the San Juan Mountains by incorporating modern semi-automatic machine-learning and remote sensing approaches.

2. PROBLEM

2.1 Problem Statement & Questions:

The main emphasis for this thesis stems from global concerns over anthropogenic forcing of global climate and hydrology, especially concerning dwindling water resources and worldwide water shortages. Specifically, available water inventories are globally finite and dwindling in response to anthropogenic impacts on climate and global population expansion, mandating unique approaches for water resource exploration and monitoring.

In response to these concerns, I explored the viability of alpine rock glaciers as effective "perched aquifers", specifically in the San Juan Mountains, Colorado. The objectives and methods of this study are driven by the following research questions:

1. **Do rock glaciers in the San Juan Mountains contain hydrologically significant water stores?**
2. **Can water volumes contained within alpine rock glaciers be estimated using remotely sensed data?**

2.2 Objectives and Hypothesis:

In pursuit of the aforementioned challenges, this study has three objectives:

1. **To explore the reliability of modern geospatial approaches, and to expand the potential scale of study areas, GIS and remote-sensing methods will be used to map the distribution and number or rock glaciers in the San Juan Mountains, CO.**
2. **To better enhance random forest classifier accuracy, and to bolster understanding of supraglacial talus blankets, physical morphometric parameters and thermal characteristics of rock glaciers will be compiled and examined.**
3. **To estimate water and ice volumes contained within rock glaciers in the San Juan Mountains, non-invasive semi-automated machine-learning methods using remotely-sensed data and random forest image classification will be applied.**

The primary driving theme of this thesis is an investigation into, and estimation of, the potentially available water resources contained within rock glaciers in the San Juan Mountains. The hypothesis for this study, with preceding null hypothesis, can be summarized henceforth as:

H_0. The water and ice volumes contained within rock glaciers in the San Juan Mountains cannot be reasonably estimated using remotely sensed data, machine-learning, and geospatial approaches.

H_1. The water and ice volumes contained within rock glaciers in the San Juan mountains can be reasonably estimated using remotely sensed data, machine-learning, and geospatial approaches.

2.3 Purpose of Study

The scope of this thesis is the efficient, systematic understanding and validation of estimated water and ice volumes contained within rock glaciers in the San Juan Mountains. By incorporating current geospatial technology and methodologies, this thesis aims to explore the efficacy of GIS data, remotely-sensed data, and elevation data for the identification of rock glaciers in satellite imagery using machine-learning image classification approaches.

It is clear that the dynamics of cryogenic water storage in rock glaciers are complex, largely resulting from meteorologic fluctuations and differences in supraglacial debris thermal properties. As such, accurate estimates of available water and ice volumes are time-sensitive, and mandate continual monitoring over time. Concrete understanding of the water-storage potential of rock glaciers can further highlight their importance as shallow perched aquifers.

3. BACKGROUND

3.1 Literature Review

The study of rock glaciers is a remarkably aged realm of periglacial research. In the unique discipline of landform evolution, rock glaciers have long been muzzled in the category of geomorphic curiosities. Literature dating back to the 19th and early 20th centuries records early observations and interpretations of rock glaciers, glacial mechanics, and their role in periglacial geomorphic and hydrologic systems - (i.e. Steenstrup, 1883; Spencer, 1900; Cross & Howe, 1905; Capps, 1910; Brown, 1925; Howe, 1909).

Field methodology for research and observation of these landforms has taken a rather comical meandering path ever since rock glaciers were first observed in the late 19th century (Steenstrup, 1883). Where once trenches and boreholes were dug to reveal the internal structure of alpine rock glaciers (Barsch, 1977b; Brown, 1925; Giardino, 1979; Giardino & Vitek, 1985; Haeberli, 1989b; Haeberli et al., 1988), denudation has been cast to the wayside in lieu of non-invasive methods of structural observation (Barsch & Hell, 1975; King et al., 1987; Rothlisberger, 1972; Petersen et al., 2020; Xie et al., 2020).

With increasing interest in the effects of anthropogenic and climate changes on the global hydrologic cycle, interest in rock glaciers has been recently revived. Interest has even ventured to planetary disciplines with studies being conducted using radar sounding such as the SHARAD satellite program to look at the water content and structure of rock glaciers on Mars - (Degenhardt & Giardino, 2003; Holt et al., 2008; Plaut et al., 2009). Whether study areas be terrestrial or extraterrestrial, a prevalent consistency remains - rock glaciers remain highly-regarded for their capacity to store water and ice.

Indeed, even early miners in the late 19th and early 20th centuries first noted ice-cemented rock slides as fairly commonplace (Brown, 1925). It was not until the early 20th century with the famous Hurricane Basin excavation pit by the Golconda Mines Consolidated, however, that Brown published his 1925 report on rock glacier structural composition, garnering attention to the resource potential of rock glaciers. Soon thereafter, a notable body of research made its way into the library of periglacial studies on rock glaciers.

Excavations and direct field observations of the internal structure of rock glaciers began shortly after Brown's initial Hurricane Basin report. It was noted early on that permafrost material could be confronted at depths of under 1 m, and reports of flowing water underneath the bouldery sediment-apron layer led to the "ice-core hypothesis" in the early 1970's (Potter, 1972). The excavation into the side of a rock glacier located in the combe de Prafleuri, Swiss alps, was reported in an early study by Fisch et al. (1978). Fisch noted that interstitial, ice-cemented material was discovered at a depth of roughly 10 m, cementing coarse angular sediment and revealing a heavily fine-grained ice-matrix supported composition that differed from nearby local glacial ice (Barsch, 1996). Giardino and Vitek (1988a) made unique observations of a rock glacier near Mount Mestas, Colorado, performing internal fabric analysis in a 100m-long trench. Their observations led to the conclusion that three potential catastrophic depositional events produced the feature in question, as opposed to slow plastic-creep, suggesting that the landform was not a rock glacier, echoing the shared opinion of Wahrhaftig (1987). Where the utility of excavation and boring provided invaluable direct observations of the composition of rock glaciers and other similar landforms early on, largely providing their distinct classification as unconventional water resources, non-invasive methods of observation quickly, and simultaneously, became preferential.

The field of seismology, already well established by the mid-19th century, proved immensely effective for early non-invasive studies of rock glaciers. Early studies employed traditional geophones, arranged in transverse and longitudinal profile lines, relying on crude explosive and percussive vibrational shock waves powerful enough to reach bedrock. Additionally, sledgehammer percussion proved effective enough to provide information on the upper 20 m of rock glaciers (Barsch, 1996). By 1968, geophysical field work was conducted on the rock glacier Macun I, in the Lower Engadin Swiss Alps (Barsch, 1971b). The Macun I study presented the first deep-seismic soundings in an active rock glacier, paving the way for non-invasive techniques for the observation of buried mountain permafrost. The second deep-seismic survey shortly followed in 1971 on the Murtel I in the Upper Engadin Swiss Alps (Barsch & Hell, 1975). An unpublished study by Barsch & Schneider (1972) collected the first recorded geoelectric resistivity data on several rock glaciers in Upper Engadin, Graubunden, and a later study by Fisch et al. (1978) employed their same methodology on rock glaciers in the Wallis Mountains, Swiss Alps.

Advances in geophysical techniques have seen tremendous improvements since original geoelectric resistivity studies, with more advanced methods such as capacitive coupled electrical resistivity tomography (CCERT), transient electromagnetics (TEM), gravimetry, radio echo soundings, and ground penetrating radar (GPR) constituting more modern approaches for the investigation of internal composition and structure in rock and debris-covered glaciers (Barsch, 1996a, 1996c; Degenhardt & Giardino, 2003; Hauck et al., 2003; Hauck & Vonder Muhll, 2003; Janke et al., 2013; King et al., 1987; Kneisel et al., 2008; Maurer & Hauck, 2007; Petersen et al., 2020; Vonder Muhll & Klingele, 1994; Wagner, 1996). The application of multiple geophysical techniques is important to account for potential misinterpretations, and as validation (Janke et al., 2013; Schrott and Sass, 2008). By incorporating several forms of geophysical methodologies,

overwhelming consensus for the ice-rich internal structure of rock glaciers has been demonstrated by numerous studies. Thus, the intention of this study is not focused on further investigating the internal structure and composition of rock glaciers, and their water-storage potential, but is instead interested in utilizing modern geospatial, remote sensing, and machine-learning approaches for large-scale regional, and global, rock glacier inventory, analysis, and water budget estimations.

3.2 State of Knowledge

The alpine cryosphere is singlehandedly one of the most important global contributors of surface runoff, estimated to provide 32-60% of total runoff discharge globally (Apaloo, 2013). Many small mountain communities in southwestern Colorado are almost completely reliant on this form of surface water, and with increasing understanding of the hydrologic contribution mountains provide there has been a notable increase in attention and research recently. It is well-understood that a firm understanding of the actual runoff contribution that mountains provide is mandatory to ensure future water allocation for stakeholders and local communities, however the challenges associated with accurate runoff estimates require studies to begin at a more local scale. When much of this runoff contribution stems from rock glacier meltwater, it would be appropriate to note that this is easier said than done.

Interwoven throughout the lexicon of rock glacier studies, particularly those incorporating geospatial and remote-sensing approaches for observation and analysis, are the long-bemoaned challenges associated with the identification and observation of rock glaciers and other ice-debris landforms using satellite imagery. Periglacial landforms such as these are indeed effectively camouflaged by the surrounding denuded talus landscape in which they reside.

As a result of the inherent challenges associated with remote observation of rock glaciers, modern approaches incorporating a variety of multispectral data, machine-learning, and deep-learning methodologies have become quite commonplace. Specifically, the reason for the recent reliance on algorithmic image recognition in rock glacier studies is primarily the result of similarities in spectral signatures between the supraglacial talus debris blankets that cover rock glaciers, and the surrounding talus debris of the eroding mountain landscape (Berta, 1982; Brenning, 2009; Brenning et al., 2012; Johnson et al., 2020; Jones et al., 2018; Jones et al., 2019).

To overcome the problem of rock glaciers camouflaged in mountain terrain, it is necessary to view rock glaciers in wavelengths of the electromagnetic spectrum that are beyond the capabilities of human eyes (i.e., outside red, blue, and green RGB light). Additionally, textural morphometric characteristics of rock glacier surface features, derived from digital elevation models (DEMs), can be similarly used to distinguish them from surrounding terrain. Thus, a major caveat exists when leveraging these types of remotely-sensed multispectral and textural data across large study areas to identify rock glaciers – to avoid discrepancies between analyst interpretations of rock glaciers in satellite imagery, and to reduce the time required to process these data, it is necessary to rely on machine-learning image classification algorithms to identify and delineate rock glacier landcover. Because of these challenges and requirements, machine-learning and deep-learning approaches to rock glacier studies are very much in vogue (Bhardwaj et al., 2014; Brenning, 2009; Janke, 2005; Jones et al., 2018; Khan et al., 2020; Pfeffer et al., 2014; Xie et al., 2020; Zhang et al., 2019).

As a result of recent technological advances in the computational power available in consumer-grade computers, satellite sensor technology, and open-source machine-learning and deep-learning software, several studies have successfully produced image classification maps of

rock and debris-covered glaciers in regions including the Parlung Zangbo Basin of the Tibetan Plateau (Zhang et al., 2019), the Karakoram and Nepal Himalayas (Xie et al., 2020), the Eastern Italian Alps (Kofler et al., 2020), the Hunzu Basin in Pakistan (Khan et al., 2020), the Rocky Mountain National Park of Colorado (Janke, 2013), and the Hamtah and Patsio glaciers in India (Bhardwaj et al., 2014). Remarkably, Jones et al. (2018) has even leveraged these methods to produce a near-global rock glacier water inventory, citing equivalent water volumes of 83.72 ± 16.74 Gt. Currently, only three studies have looked at rock glacier populations contained within the San Juan Mountains (Brenning et al., 2007; Johnson, B. 2017; White, P. 1979). Of these, only the study by Brenning et al. (2007) has attempted to estimate rock glacier water volumes in the San Juan Mountains using a statistical generalized additive model, estimating a water equivalence of 0.5-0.76 km^3 for a surface area of 70 km^2. By applying modern semi-automated machine-learning methodologies, and integrating observations of effective band combinations and input data at a localized scale, this thesis provides an alternate approach to rock glacier water volume estimation in the San Juan Mountains.

3.3 Hydrologic Significance of Rock Glaciers

As previously mentioned, rock glacier studies have historically focused on depositional and geomorphologic processes responsible for these landforms, as they are unique features (Barsch, 1971a; Capps, 1910; Cross & Howe, 1905; Mateo, 2017; Spencer, 1900; Steenstrup, 1883; Wahrhaftig & Cox, 1959; White, 1979). As interest shifted from formation processes to ongoing debates of flow characteristics and mechanics of rock glaciers, understanding of the water-bearing potential of rock glaciers became a topic of much focus (Baltensperger et al., 1990;

Giardino et al., 1992; Johnson, 1981; Outcalt & Benedict, 1965). It was not until these observations of water-induced creep, the presence of the unfrozen “active-layer”, and eventual observations of rock glacier meltwater chemistry, that the arguably most pertinent and compelling quality of rock glaciers (i.e., water-storage characteristics) was fortunately discovered (Azocar & Brenning, 2010; Bajewsky & Gardner, 1989; Corte, 1976; Mateo, 2017; Petersen et al., 2020; Potter, 1972).

Seasonal discharge patterns have been observed in a variety of studies, with observations demonstrating consistent meltwater flow and runoff volumes equal to or greater than clean glacier-ice meltwater (Caine, 2010; Corte, 1976; Johnson et al., 2020; Mateo, 2017; Millar & Westfall, 2019). Many of these studies have also made important observations of the seasonally driven storage-discharge trends of rock glaciers, noting that necessary storage accommodation space is readily supplied as warm-season meltwater is removed from storage. While the presence of interstitial ice and water matrices and observations of consistent seasonal meltwater suggest a cyclical recharge system in rock glaciers, warming climates have also been observed to cause a decline in water storage (Azocar & Brenning, 2010; Jones et al., 2019; Millar & Westfall, 2019; Wagner et al., 2020). Multiyear observations by Caine (2010) of rock glacier runoff trends in the Colorado Front Range reveal an unexplainable increased discharge despite changes in precipitation patterns. Such results indicate the possibility of increased melting of internal ice, and suggest a projected decline in meltwater into the future.

Projections of changing climates in alpine regions certainly indicate an overall decrease in the water-storage potential of rock glaciers, however observations of seasonal meltwater patterns during droughts still demonstrate reliable runoff contribution, at least for the time being (Wagner et al., 2020). Observations of the resilience of rock glacier water storage, owing to their insulating supraglacial talus debris cover, highlight the hydrologic significance of these landforms. Indeed,

even throughout the summer months dataloggers have recorded rock glacier meltwater temperatures near 0 °C in the Uinta Mountains, Utah (Munroe, 2018). Additional observations of the thermal buffering provided by supraglacial rock glacier taluses in the Innere Olgrube, Austrian Alps revealed fast and slow-flow discharge components owing to suprapermafrost and subpermafrost flow paths which are present within active rock glaciers (Wagner et al., 2020). The subpermafrost water storage for the observed rock glaciers was attributed to the presence of an unconsolidated ice-free sediment layer approximately 10-15m thick, resting above bedrock, which provided consistent baseflow discharge even during winter months. This subpermafrost layer demonstrated characteristics which were interpreted as activity of a shallow groundwater aquifer. Such observations of the radiative buffering provided by supraglacial rock glacier taluses, and the consistent baseflow from the subpermafrost layers, indicate that the hydrologic contribution and role of rock glaciers should continue to be investigated and considered in larger regional alpine hydrologic systems.

3.4 Remote Sensing & Machine-Learning Approaches for Rock Glacier Research

Recent advances in computer and sensor technologies have given rise to semi and fully-automated approaches to geomorphic research, and particularly have garnered tremendous interest in machine-learning methodologies (Bhardwaj et al., 2014; Brenning, 2009; Jones et al., 2018; Pfeffer et al., 2014; Xie et al., 2020). Automation and machine-learning approaches truly mark the state of the science when it comes to regional-scaled landform studies, as they provide consistent reproducibility, eliminating human error, and produce rapid results. In terms of their potential applications to rock glacier research, these types of automated approaches offer the ability for

exploration and long-term monitoring of these important water resources, especially in the context of anthropogenic and climatic changes. While the idea of automated, machine-learning approaches to ice-debris landform detection and monitoring is not new, this field of computer-based research has seen a wide range of methodologies employed, with an equally wide range of results.

First-order approximations for a near-global rock glacier inventory have been posited by Jones et al. (2018), motivated greatly by a similar near-global glacier and debris-covered glacier inventory, The Randolph Glacier Inventory (Pfeffer et al., 2014), though estimates of water resources are highlighted by the disclaimer of uncertainties associated with correct land-cover identification, and missing study areas. In the San Juan Mountains, limited work has been done combining these technologies and methods for rock glacier detection and monitoring (Brenning, 2009). To date, one available study has been conducted utilizing image classification in the San Juan Mountains, Brenning (2009), though the study focuses primarily on comparisons of image classifiers and their respective performances. The previous best estimate of rock glacier volumes of water by Brenning et al. (2007) provides a reasonable first-order approximation of the water resources contained within rock glaciers in the San Juan Mountain study area. His approach, however, assumes rock glacier thicknesses of 20 m for all rock glaciers in the study area, and additionally relies on analyst interpretations of rock glaciers in aerial photography, and the fitting of a statistical generalized additive model, based solely off eighty-four identified rock glacier points and their respective morphometric characteristics. This thesis eliminates analyst bias, in-part, by relying on a machine-learning image classifier. Additionally, the use of raw DEM data, and an interpolation procedure used to generate estimated rock glacier bases, provides an updated approach to rock glacier thickness estimates over the thickness estimation approach posited in Brenning (2005) and Azocar & Brenning (2010). By incorporating novel and successful semi-

automated machine-learning methods of previous studies it is hoped that similar approaches for the study of ice-debris landforms in the San Juan Mountains can be demonstrated as effective.

Methods of automation applied to geomorphic research typically rely on image classification, which itself arguably represents an entire genre of computer-based automation approaches for landform studies. Historically, early studies on the topographic controls and modeling of rock and debris-covered glaciers focused simply on location and distribution (Brenning, 2005a; Brenning & Trombotto, 2006; Brenning et al., 2007; Brenning, 2009; Janke, 2005). Some early studies applied novel remote-sensing approaches to the detection and mapping of rock glaciers (Bishop et al., 2001; Bolch & Kamp, 2006; Bolch et al., 2008; Bonk, 2002; Grasser, 2006; Janke, 2001; Paul et al., 2004), though results only provided basic understanding of the complications associated with spectral identification of rock glaciers in remotely-sensed data. Later novel efforts of combining machine-learning classifiers with remotely-sensed data revealed inherent challenges associated with the detection and mapping of these landforms (Brenning, 2009), nevertheless standing as noteworthy efforts for the identification and classification of rock and debris-covered glaciers.

Whereas many of these early studies used complex statistical and machine-learning classification methods, including logistic regression, support vector machine (SVM), generalized linear and additive modeling, and decision tree classifiers such as random forests (RF), lacking advancements in sensor and computer technologies presented a major bottleneck to effective autonomous classification (Brenning et al., 2007; Brenning, 2009). Since then, major advancements in these fields have allowed for greatly improved algorithmic identification and mapping of ice-debris landforms, and seen tremendous improvement in validation and accuracy. Approaches utilizing high-resolution digital elevation models, multispectral satellite imagery, and

supervised semi-automatic machine-learning methodologies have been applied to the study of ice-debris landform identification and mapping with noteworthy results. The application of artificial neural networks (ANNs) was shown to accurately identify and delineate rock and debris-covered glacier boundaries in the Karakoram and Nepal Himalaya, with high accuracy when validated against glacier-boundary outlines provided by the Global Land Ice Measurements from Space (GLIMS) database (Xie et al., 2020). Similarly, the application of ANNs, SVMs, and RF classifiers for the identification of debris-covered glaciers in the Passu watershed, Pakistan, presented highly accurate results with accuracies >95% using RF classifiers, and >92% using ANN classifiers (Khan et al., 2020). Another study strictly relying on the use of automated RF classifiers revealed identification and classification results >98% for ice-debris landforms in the Tibetan Plateau (Zhang et al., 2019). These results serve as the motivation and emphasis to utilize semi-automated machine-learning approaches for the identification and classification of rock glaciers in the San Juan Mountains, and the ultimate quantification of water resources contained within them.

4. STUDY AREA

4.1 San Juan Mountains, CO.

The San Juan Mountains in southwestern Colorado are of geomorphological significance, housing upwards of 658-756 documented rock glacier landforms as recorded by White (1973; 1979). Regionally, the San Juan's contain 14 peaks exceeding 4,260 meters of elevation (approx.. 14,000 feet) (Cross & Larsen, 1935). A majority of the rock glaciers observed in this study are found above 2500 meters of elevation (approx. 8,202 ft). The landscape alternates between vast plateaus and semiarid lowlands, where seasonal meltwater nourishes pastures, farmlands, and densely forested areas. The entirety of the San Juan's span roughly 90 miles from east to west, and approximately 70 miles from north to south, covering an approximate area of 25,800 km^2 (Atwood & Mather, 1932). As a result of no observable rock glacier landforms in certain southernmost areas, specifically the southern region spanning into northern New Mexico, the study area extent investigated in this thesis covers an approximate area of 21,656 km^2 (Figure 2).

Field observations from the Camp Bird rock glacier, at the northwestern edge of the San Juan Mountains, were gathered during late summer 2020, and have been referenced as a form of ground-truth validation data. This rock glacier is located within Imogene Basin, near the historic Ouray Mining District, and lies on a north-facing slope near the northwestern portion of the San Juan Mountains (37.94588, -107.73170) between Ouray and Telluride, Colorado (Figure 2. Red dot). The portal of the Upper Camp Bird Level-3 mine, and the proximal Camp Bird rock glacier, are located directly off the path of a historic mining trail, now a popular off-roading trail, to Imogene Pass.

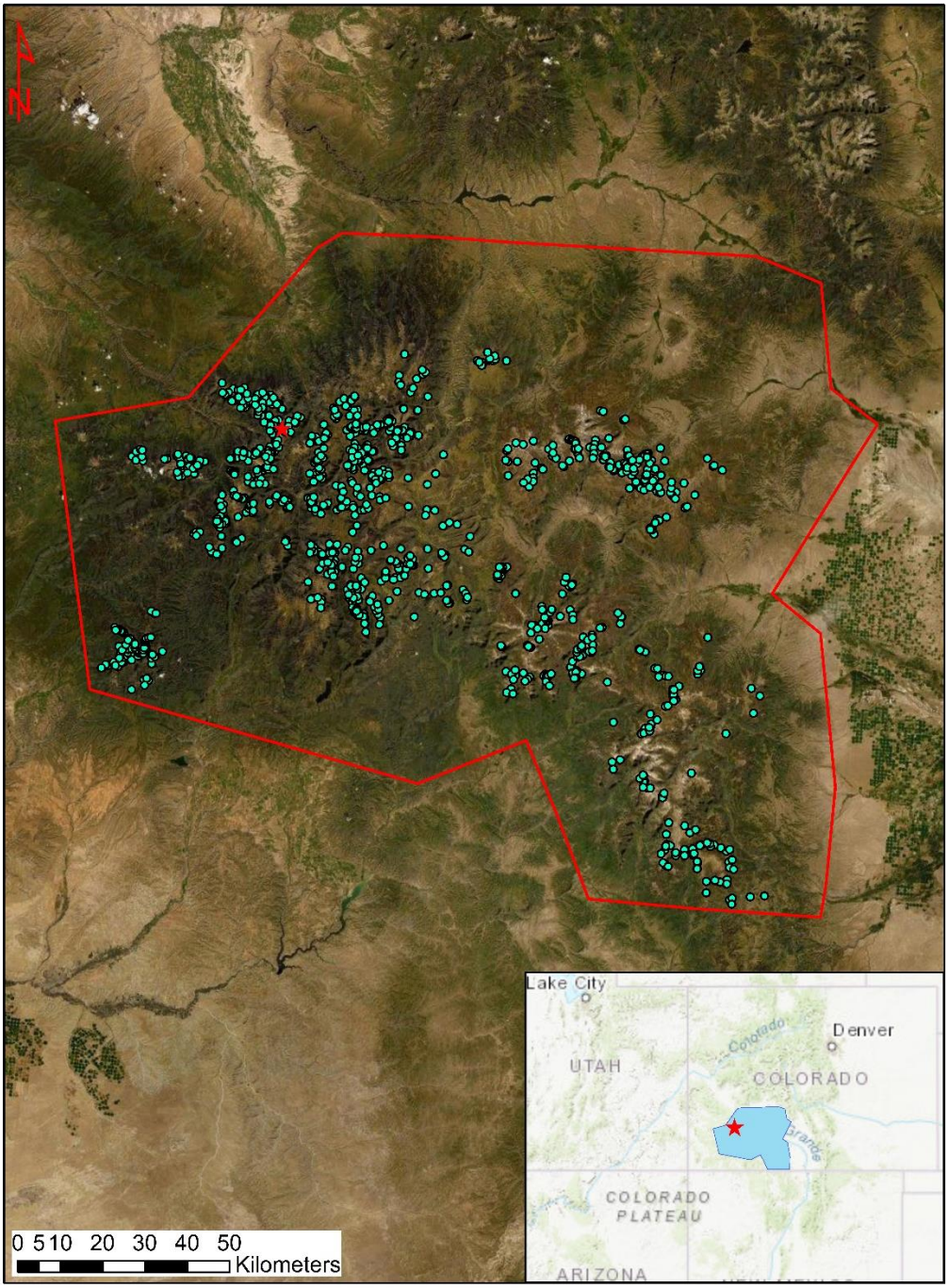

Fig. 2 - Study area extent (red outline) for the San Juan Mountains, CO. Manually mapped rock glaciers shown as blue points. Mapping based off analyst photo-interpretation of satellite imagery. Camp Bird field site shown as red star.

4.2 Geology of the San Juan Mountains

The geologic history of the San Juan Mountains is complex. The oldest rocks in the area are Archean gneisses, schists, and amphibolites of plutonic origin (Cross & Larsen, 1935). The Algonkian aged Irving greenstone was erupted, deposited, and metamorphosed after erosion of preexisting Archean rocks, followed by the highly deformed and folded Needle Mountains group which was ultimately injected with Precambrian plutonic rocks. Late Precambrian erosional processes regionally smoothed the landscape, and subsequent deposition of Paleozoic, Mesozoic, and Tertiary rocks formed much of what now constitutes the San Juan Mountains (Burbank & Luedke, 2008; Cross & Larsen, 1935).

Regionally, a majority of the present geology displays the product of several uplift events, crosscutting igneous intrusions, deformational erosional sequences, and volcanic eruptions, occurring between Proterozioc to the Paleozoic and Mesozoic. Regional basement rocks constituted by the Paleozoic Uncompahgre Formation, consisting of metamorphic quartzites and slates, comprise some of the oldest rocks in the region. Near the Ouray district, a significant angular unconformity exists between the underlying Uncompahgre Formation and the overlying sedimentary limestones, dolomites, sandstones, and shales representing the Paleozoic Devonian Elbert Formation, Ouray Limestone, and Mississippian Leadville Limestone. These units are further overlain by Pennsylvanian Molas and Hermosa Formations, and the Permian Cutler Formation; these formations consist of sedimentary conglomerates, sandstones, limestones, and shales. A thick sequence of Mesozoic rocks further overlay these units, resting conformably on a dramatic angular unconformity. The Mesozoic rocks are predominantly sedimentary shales, mudstones, and sandstones, with occasional limestones, conglomerates, and breccias. These rocks fall into a series of formations including the Triassic Dolores Formation, Jurassic formations

including the Entrada Sandstone, Wanakah Formation, and the Morrison Formation, as well as the Cretaceous Dakota Sandstone and Mancos Shale Formations. Subsequent erosional processes occurring during the early Tertiary were followed by a series of volcanic eruptions, covering the region in mid-Tertiary volcanic rocks comprising the San Juan Formation. Structural processes affecting the region are primarily attributed to uplifting in the early Proterozoic, Paleozoic, and Mesozoic with the infamous Laramide Orogeny. The result of igneous laccolithic intrusions occurring during these events deposited a rich trove of ores and minerals, giving the area considerable notoriety as a successful mining district (Burbank & Luedke, 2008). Aside from the noteworthy economic geology of the San Juan Mountains, and arguably of greater significance, this region offers rich hydrologic value in the way of abundant surface and groundwater resources, in addition to an unknown amount of unconventional water resources contained within rock and debris-covered glaciers.

Rock glaciers are geomorphic features which exist in various forms; however, they can be generally classified by their external morphological features (i.e. furrowed longitudinal ridges, ogives, lobate form, cirque rooting zone) with classifications of ice-cored and ice-cemented (i.e. interstitial-ice) rock glaciers being applied as a diagnostic comparative factor (Janke et al., 2013). The first documented occurrence of interstitial ice, and tongue-shaped glacial landforms, in the San Juan Mountains was mentioned by Spencer (1900) in an edition of Science, in which he noted them simply as a “peculiar form of talus”. Not long after, research in the Silverton Quadrangle of Southwestern Colorado marks the first efforts to excavate an active rock glacier, as documented in the famous Hurricane Basin study conducted by Brown (1925). While obviously unrefined in approach, the study remains a remarkable achievement in rock glacier studies, by providing the first ground-truth regarding the internal structure of an active rock glacier.

The depositional formation process of ice-cored rock glaciers occurs in mountainous alpine environments (Petersen et al., 2020), and typically results from slope failure and mass-wasting events, where pure exposed periglacial ice becomes rapidly buried beneath sediment debris - insulating the internal ice structure. The internal structure and composition of ice-cemented rock glaciers is the product of similar mass-wasting slope-failure events. Ice-cemented rock glaciers, however, are produced after slope-failure occurs, where surface melt-runoff and precipitation infiltrate into the porous structure of the lobate rock-glacier debris fans, and become subsequently frozen and preserved with time. Ice-cemented rock glaciers have been noted to contain anywhere from 30-60% ice content (Barsch, 1996a; Janke et al., 2013; Jones et al., 2019), whereas ice-cored rock glaciers have been observed to contain upwards of 60-90% ice content (Mateo, 2019).

4.3 Hydrology of the San Juan Mountains

In terms of seasonal melt regimes of rock glaciers in high alpine environments, the relationship between flow patterns and climatic trends is widely considered the most influential to discharge characteristics. Nevertheless, observations of rock glacier melt regimes as a function of slope/basin aspects, and geographic distribution, have indicated that the factors affecting flow are multifaceted (Mateo, 2017).

In the San Juan Mountains of southwestern Colorado, local hydrology is largely controlled by seasonal snowmelt (Mateo & Daniels, 2019). Regional topographic constraints on hydrologic flow behavior are a subsequent result of multiple glaciation events.

The San Juan Mountains are situated on the eastern edge of the Colorado River Basin, diverting seasonal meltwater into a handful of major tributaries. Flow characteristics, as a result of

the prevailing landforms, effectively channel meltwater and precipitation runoff into seven major tributaries, namely the Uncompahgre River, the Gunnison River, the San Miguel River, the Dolores River, the Animas River, the San Juan River, and ultimately the Colorado River (Figure 3).

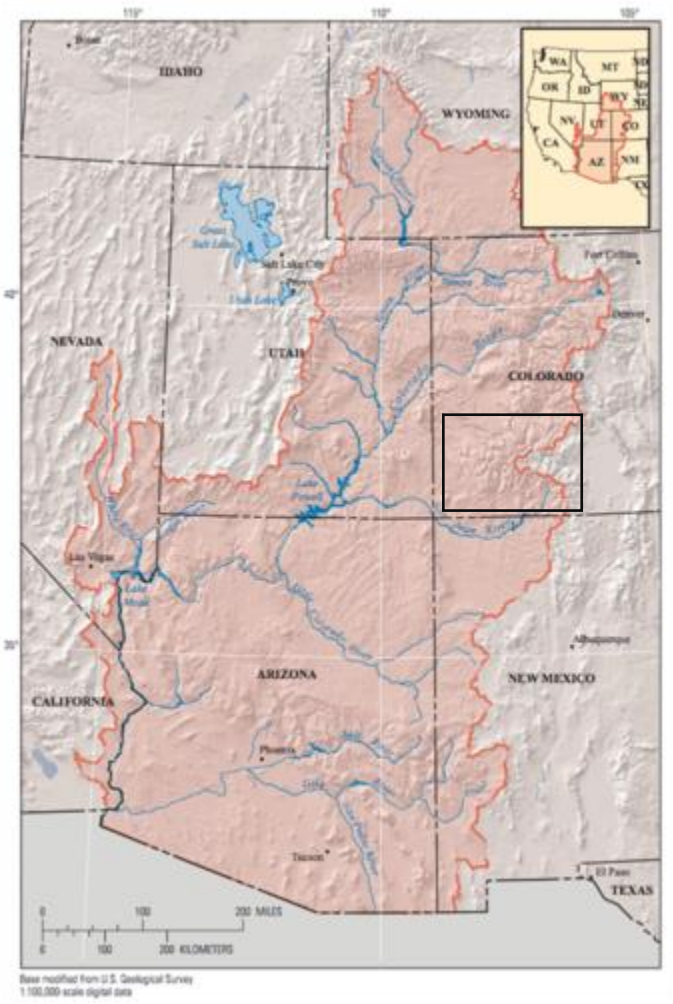

Fig. 3 - Colorado River basin delineation. San Juan Mountain study area shown by black box. Figure adapted from the USGS.

Northern-facing slopes generally outsource flow into the Uncompahgre and Gunnison rivers, whereas southern-facing slopes generally outsource their flow into the San Miguel and Dolores rivers. The Gunnison River is fed by the Uncompahgre River and eventually feeds the Colorado River around Grand Junction, whereas the Dolores River is fed by the San Miguel River and ultimately feeds the Colorado River near Dewey, Utah.

The Camp Bird rock glacier, representing the site of collected in-situ data, is situated within the Imogene Basin, and feeds Imogene Creek, which ultimately connects with Sneffels Creek forming Canyon Creek, which feeds the Uncompahgre River near Ouray. These major tributaries span five states, ultimately feeding into the Pacific Ocean near the Baja Peninsula, and provide a large majority of the water resources required by many communities (Figure 4). Local Colorado communities such as Ouray, Telluride, Silverton, Durango, and Montrose heavily rely on water resources that are provided by runoff in high-alpine regions like the San Juan Mountains.

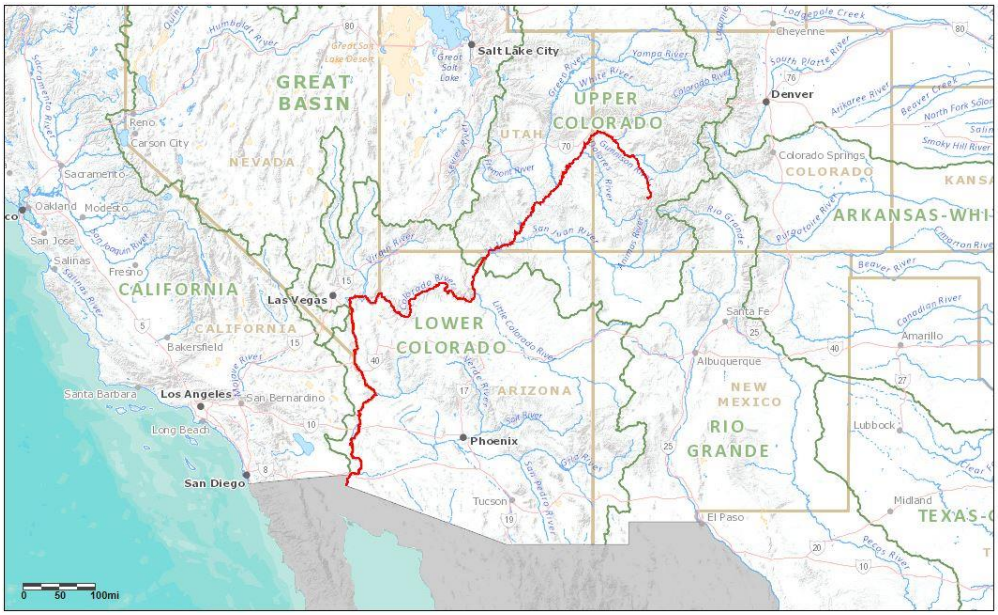

Fig. 4 - Generalized meltwater runoff course for San Juan Mountains, CO. Figure provided courtesy of the USGS.

Whereas a majority of flow input that is sourced from the San Juan Mountains is a result of seasonal snowmelt, an unknown amount of input is directly sourced from local rock glaciers. Previous studies in the San Juan region have shown the predominance of ice-cored internal structures in many rock glaciers in this area (Giardino et al., 1992).

4.4 Climate and Meteorology of the San Juan Mountains

Local weather trends in the San Juan Mountains experience significant seasonal fluctuations, with topography and elevation acting as primary controls (Mateo & Daniels, 2019). Seasonal fluctuation trends in Southwestern Colorado coincide with the North American Monsoon System, also known as the Southwest Monsoon, during mid to late summer months, producing orographic lift of warm, moist air systems flowing inland from the Gulf of California (Sheppard et al., 2002; Mateo, 2017). The effect of these intrusive weather systems produces high-intensity precipitation events during the summer months, with cool and dry weather trends following into the winter.

The National Weather Service (NWS) and the National Oceanic and Atmospheric Administration (NOAA) record daily, monthly, and annual weather data including temperature, precipitation, and snow accumulation with weather forecast offices located around the periphery of the San Juan Mountain region; their field office located in Montrose provides weather data relevant to the study area. In addition, the Center for Snow and Avalanche Studies (CSAS) manages a highly monitored field site at Senator Beck Basin, off the nearby Red Mountain Pass, providing access to archived meteorological data in the vicinity of the San Juan Mountain area.

The mean annual precipitation value for the period of 2005-2012 recorded by CSAS in the Senator Beck Basin study area was recorded to be 1190mm (Landry et al., 2014), whereas the mean annual precipitation value recorded by NWS at their nearby Montrose field site for the period of 2010-2020 was 255.02mm (NWS; NOAA). Snow depth in the San Juan Mountains is quite variable, largely because of changes in topography and as a result of wind effects. Maximum recorded snow depths measured in one plot area of Senator Beck Basin for the recorded period between 2005-2012 ranged from 1.37-2.91 m, and 618-1101 mm as measured in an adjoining plot area for the same period, yielding an overall mean snow depth of 1499.8mm. Mean hourly air temperatures recorded by CSAS at their upper Senator Beck Basin field site ranged from -31.5-22.3°C for the period between 2004-2012 (Landry et al., 2014), whereas the mean monthly average air temperatures recorded by NWS and NOAA at their Montrose field site for the period between 2010-2020 ranged from -2.56-23.78°C (NWS; NOAA).

4.5 Rock Glaciers in the San Juan Mountains

The San Juan Mountains of Colorado are the result of a variety of geologic processes. Precambrian and Tertiary volcanics constitute a majority of the landscape, which was subsequently reshaped by dominant erosional and glacial processes (Mateo, 2017; White, 1979). Following Pleistocene glaciation events, the landscape was denuded creating a dramatic relief of horns, aretes, cirques, and U-shaped valleys (Carrara & Andrews, 1975; White, 1979). The eventual retreat of valley glaciers following the Late Wisconsin deglaciation event 16,000 years ago, and complete melting around 8-9000 years ago, left behind the carved landscape that is still visible today (Carrara & Andrews, 1975; Mateo, 2017; White, 1979).

As a result of the prevalence of volcanic rocks in the area, and the historic glacial and periglacial forces, a great majority of the landscape spanning the San Juan Mountains is highly fractured and broken. As White (1979) noted early on, regions above the timberline (>3550m) are almost entirely dominated by periglacial erosional processes, especially mass wasting events. In addition, the intrusion of warm moist air regionally compelled by orographic lift, known as the Southwest Monsoon, causes summer months in the San Juan Mountains to experience high intensities of precipitation. The culmination of these preexisting conditions creates the perfect environment for rock glaciers.

Some of the earliest recorded rock glacier studies (Brown, 1925; Cross & Howe, 1905, Spencer, 1900) were conducted in the San Juan Mountains, each of them providing groundbreaking observations and noting their uniqueness among other periglacial landforms. Notably, the study by Brown (1925) in Hurricane Basin provided one of the earliest observations of the internal ice content of rock glaciers. Following these landmark studies, however, interest in San Juan Mountain rock glaciers has only been shown by a handful of other publications (Bailey, 2020; Brenning et al., 2007; Janke, 2007; Johnson, 2017; White, P. 1973, 1979; White, S. 1971, Mateo, 2017; Mateo & Daniels, 2019). Of these, only one (Brenning et al., 2007) has attempted to estimate the available water resources contained within San Juan Mountain rock glaciers. The study published by P. White (1973) reported 756 observed rock glaciers located at elevations between approximately 2975-4109 m in the San Juan Mountains, whereas Brenning (2007) statistically estimated 900-1300 rock glacier features above elevation of approximately 3600 m. In either case, the population of rock glaciers contained within the San Juan Mountains is reportedly one of the largest global populations contained within a single mountain range.

5. METHODS

5.1 GIS and Remote-Sensing Approaches to Rock Glacier Mapping

Quantitative assessments of rock glacier inventories and estimations of their volumetric water stores present significant challenges in remote alpine regions where they are located. Accessibility presents one of the greatest challenges when studying these landforms, and sufficient field observations necessary to produce such inventory estimates and analyses are time and labor intensive. In light of these challenges, remotely-sensed satellite data provide valuable resources for local and regional scale rock glacier inventory studies, and provide means of rock glacier water volume estimation. By utilizing a variety of remote sensing datasets and techniques, this study will provide a better understanding of the available water resources contained within rock glaciers in the San Juan Mountains. Additionally, this thesis will highlight constraints and challenges posed by these methods, as well as the ultimate benefits these methods can offer for understanding rock glacier water inventories.

The major diagnostic property of rock glaciers and debris-covered glaciers (DCGs), jointly referred to as "ice-debris landforms" for simplicity (Berthling, 2011), is the talus supraglacial debris cover. Unfortunately, this renders their spectral signature difficult to parse from remotely-sensed spectral indices (Berta, 1982). In efforts to surmount this problem, thermal data have been used, with some success, to observe and measure ice-debris landforms. The distinguishing characteristic of these landforms from the surrounding terrain is the internal composition, consisting of permafrost and ice-lenses, and the behavior of heat emission from the earth's surface is a result of the internal temperature of the underlying soil and rock; thus, it has been posited that differences in heat emission of ice-debris landforms and the surrounding terrain can aid in

identification and mapping in imagery (Brenning et al., 2011). Because of these observations, this thesis utilizes remotely-sensed thermal bands from Landsat-8 to estimate changes in land surface temperature (LST) by converting thermal surface radiation emissions to radiant surface temperature (Lillesand et al., 2004). Google Earth Engine®, a cloud-based geospatial and remote-sensing platform, was used to source and manipulate LST data, and ArcMap 10.7® was used to overlay these data and perform calculations of thermal emissions.

Because of the complex and unique structure, composition, and location of alpine rock glaciers, it is necessary to integrate a variety of data and methodologies to observe these landforms remotely. The research approaches adapted in this thesis combine a large variety of open-source data including 10-meter digital elevation model (DEM) data derived from the USGS' 3D Elevation Program, DEM-derived morphometric parameter layers calculated in ArcMap 10.7®, Landsat-8 multispectral data, ICESat-2 lidar data, 1-meter National Agriculture Imagery Program (NAIP) multispectral data, landcover spectral indices including the normalized difference vegetation index (NDVI) and the modified normalized difference water index (MNDWI), textural layers calculated in Google Earth Engine®, and in-situ field data collected during the Summer of 2020. In addition to all open-source GIS and remotely-sensed data analyzed, and as a result of the lacking availability of validation data in this study area, all observable rock glaciers within the entire San Juan Mountain extent were manually mapped in ArcMap® to provide comparative validation data – these positional validation data were ultimately used to assess the accuracy and efficacy of the semi-automated and machine-learning methods used later on. A database including morphometric parameter values and positional data was also created in ArcMap® based off the manual rock glacier point map. For further comparative validation and analysis of elevation measurements,

ICESat-2 data was examined and applied towards generalized first-order water volume approximations.

5.1.1 ICESat-2 Data for Elevation Measurements

The ICESat and ICESat-2 missions, conducted by NASA, collect Ice, Cloud, and land elevation data via Satellite (ICESat). ICESat and ICESat-2 use LIDAR laser altimeter sensors to provide updated ice and glacier mass-balance estimates, vegetation indices, and land topography information. All data collected by ICESat and ICESat-2 satellites are open-source and managed by the National Snow and Ice Data Center (NSIDC), available for download from NASA's interactive cyberinfrastructure data platform OpenAltimetry. ICESat-2 data are primarily used in this thesis for comparison of elevation values, however rough, first-order approximations of rock glacier water volumes for five miscellaneous rock glaciers in the San Juan Mountain study area have been produced by means of a very generalized 3D rock glacier model, henceforth, referred to as the Acevedo-Grunau or A.G. rock glacier model.

While still in their infancy, the ICESat and ICESat-2 missions offer noteworthy advantages over traditionally collected lidar data, primarily owed to the precision of elevation measurements and the variety of landcover types capable of being measured, including land-ice height, sea-ice height, land and vegetation height, ocean surface height, sea-ice freeboard measurements, and inland water surface height. The laser altimeter utilized by ICESat is the Geoscience Laser Altimeter System (GLAS), capable of performing roughly 40 photon measurements a second. Notable improvements were made to the laser altimeter housed on ICESat-2, known as the Advanced Topographic Laser Altimeter System (ATLAS), which is capable of performing over

10,000 photon measurements per second. Orbital coverage of the ICESat GLAS instrument can be observed in Figure 5 for the San Juan Mountain study area, and global coverage of the ICESat-2 ATLAS instrument can be observed in Figure 6. Datasets were filtered by location, data product, and orbital period.

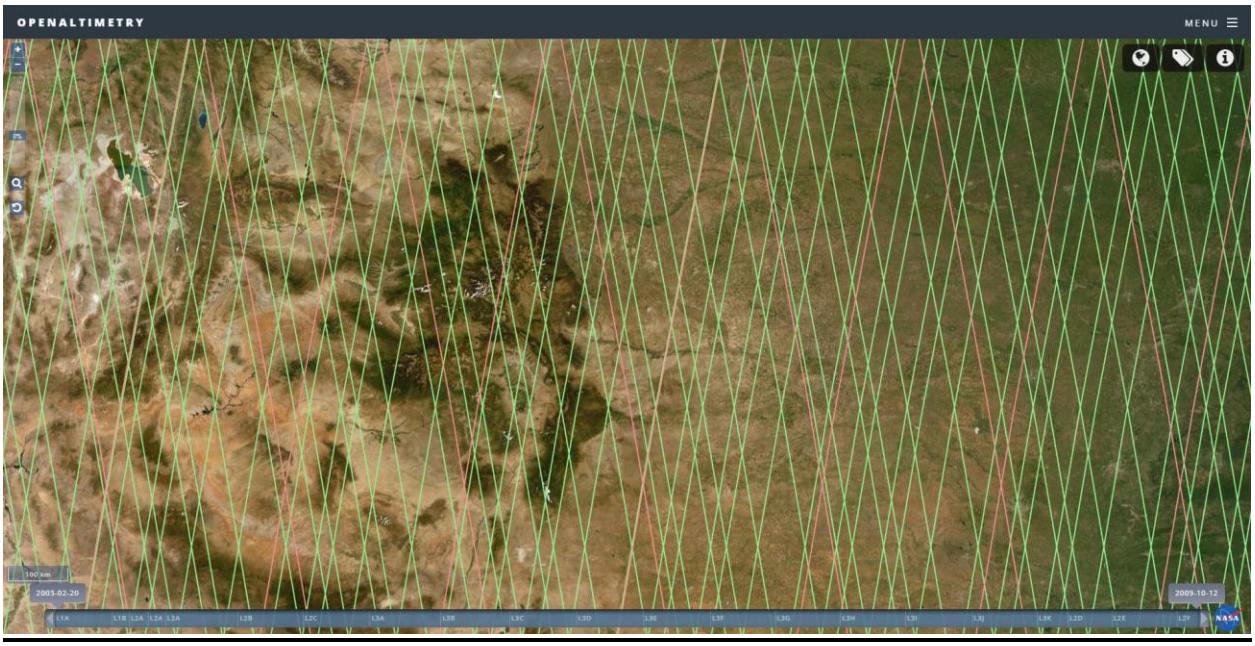

Fig. 5 – ICESat ground tracks over the San Juan Mountain study area. From NASA's OpenAltimetry portal.

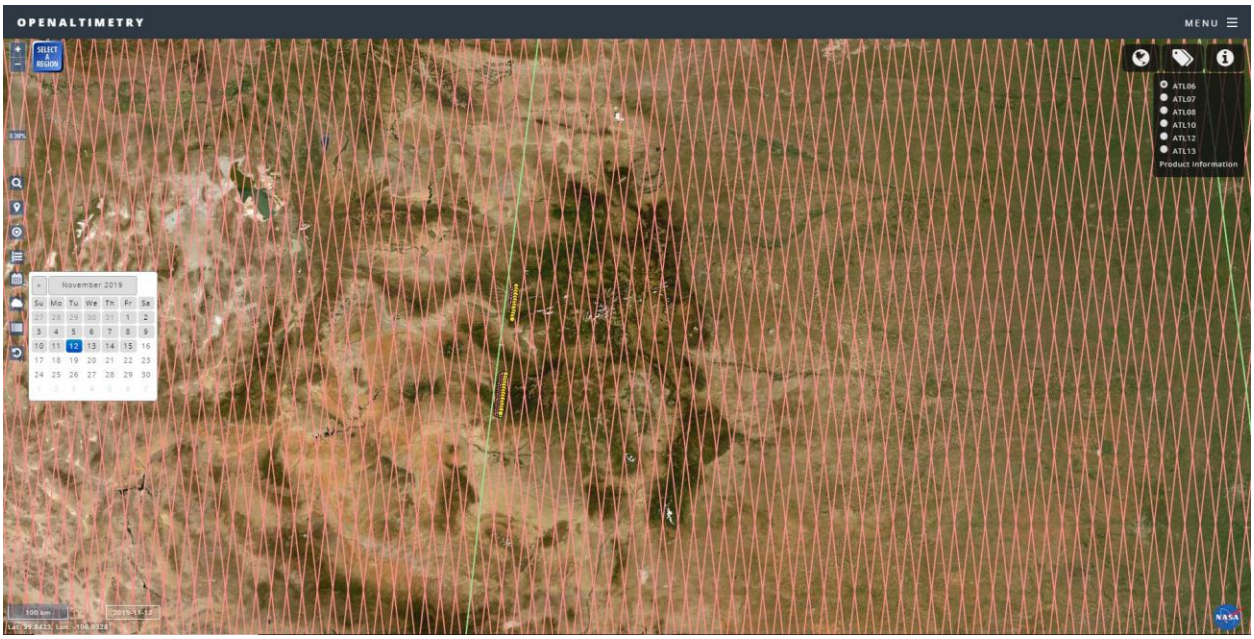

Fig. 6 – ICESat-2 ground tracks over the San Juan Mountain study area. From NASA's OpenAltimetry portal.

While offering extremely precise elevation measurements, a significant drawback of the ICESat and ICESat-2 missions is the very low temporal resolution. The orbital return time for the satellite to return to a given location is 91 days, which currently corresponds to the minimal amount of available data. The spatial coverage of the ground tracks is also very low (Figures 5-6). The spatiotemporal constraints arising from ICESat and ICESat-2 orbital coverage lend to the difficulties in finding good elevation profiles in the San Juan Mountains. Good elevation profiles require ground tracks to intersect rock glaciers either perpendicular or horizontal to the direction of creep (i.e., down-dip). Additionally, the availability of good rock glacier elevation profiles only allow very generalized thickness metrics to be manually gathered and incorporated into the A.G. model. To investigate the efficacy of using ICESat-2 data to derive generalized rock glacier water

and ice volume estimates, elevation profiles from six rock glaciers were used to determine thickness measurements, and ultimately were used to estimate water and ice volumes.

Both ICESat and ICESat-2 datasets used in this report are for the same study area, allowing for comparison of data coverage and spatiotemporal resolution. The following ICESat data were collected from the NSIDC website using their interactive download interface:

GLAH06_634_2129_002_0153_4_01_0001.H5 - 2009-03-24
GLAH06_634_2129_002_0087_2_01_0001.H5 - 2009-03-19
GLAH06_634_2127_001_0153_4_01_0001.H5 - 2008-11-29
GLAH06_634_2125_002_0087_2_01_0001.H5 - 2008-10-15

The following ICESat-2 data were similarly collected directly from the NSIDC website using the same interactive download interface:

ATL06_20190913063941_11790402_002_01.h5 – 2019-09-13
ATL06_20190614105952_11790302_002_01.h5 – 2019-06-14
ATL06_20190315152016_11790202_002_01.h5 – 2019-03-15
ATL06_20181214194017_11790102_002_01.h5 – 2018-12-14

The interactive NSIDC dataset for ICESat and ICESat-2 land-ice height data can be respectively found at: https://nsidc.org/data/GLAH06/versions/34 ; https://nsidc.org/data/atl06

ICESat and ICESat-2 data and elevation profiles can also be downloaded directly from NASA's OpenAltimetry data portal, which was ultimately used in lieu of NSIDC data. Elevation profiles generated within the OpenAltimetry platform were produced for four different rock glaciers using ICESat-2 data, and for one rock glacier using ICESat data. Elevation data for the measured rock glaciers were incorporated into a generalized model, the Acevedo-Grunau rock glacier volume model (Figure 7, Eq.1), developed for this report and based off the 1996 study by Barsch (Figure 1).

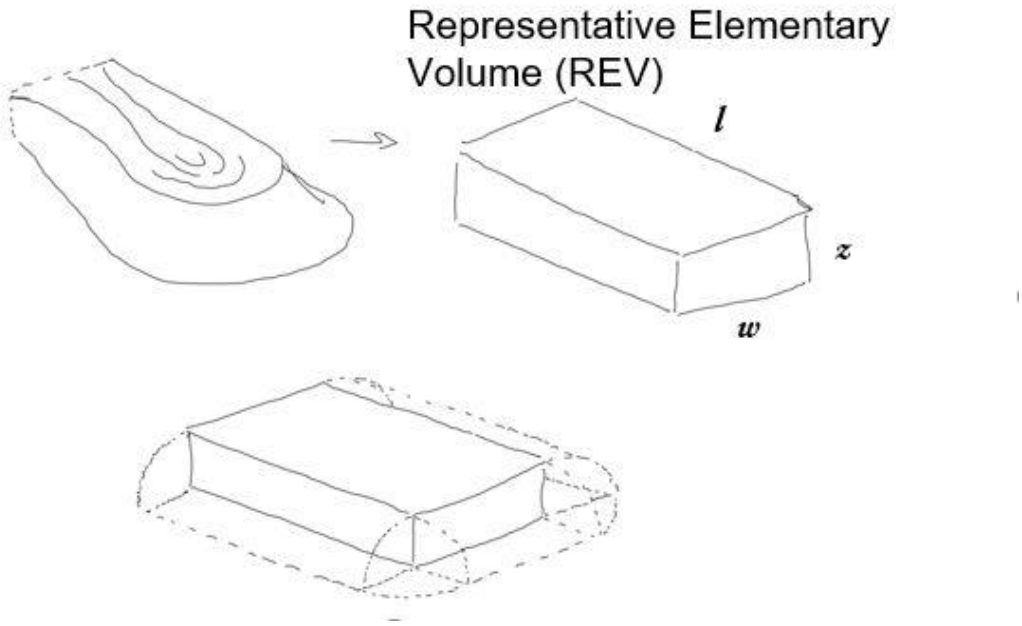

Fig. 7 – Generalized rock glacier volume model (i.e., A.G. model). Block diagram sketched by Grunau, B.

The Acevedo-Grunau (A.G.) model for volumetric rock glacier water estimation is mathematically expressed as:

$$R_{vol} = ((lwz + (0.5\pi z^2 l) + (0.25\pi z^2 w) + (0.33\pi z^3))*0.75)*0.9095 \quad \textbf{Eq. 1}$$

The length, width, and height (lwz) values are taken of a representative elementary volume (REV) of a rock glacier, and added to the partial volumes of three quarters of a cylinder, and a quarter of a sphere. The addition of the partial volumes with a rectangular prism REV forms what is a very rough basic three-dimensional volume closely related to the actual shape of a rock glacier, albeit

with some serious shortcomings. For the rock glaciers measured in this study, three dimensional measurements of the rock glaciers were made with both ICESat-2 data for height, whereas lateral and longitudinal (i.e., width, length) measurements were made using the measuring tool in ArcMap 10.7®.

5.1.2 Rock Glacier Mapping in ArcGIS

As previously mentioned, only three available rock glacier inventory studies have been conducted within the San Juan Mountains. In each case, the study area extents examined did not contain the entire San Juan Mountain region. Additionally, only the studies conducted by Johnson (2017) and White (1979) mapped rock glacier locations, however, the specific location data for these mapped rock glaciers are still unavailable. Because of the lack of available mapped rock glacier location data, all observable rock glaciers contained within the near-entire San Juan Mountain extent spanning 21,656 km^2 have been mapped in this thesis to serve as validation data for the algorithmically classified rock glacier landcover generated by a random forest image classifier in Google Earth Engine®.

Manual mapping of all observable rock glaciers was performed in ArcMap 10.7®. The standard World Imagery basemap provided by Maxar Technologies was the primary imagery used for mapping. Additionally, all DEM-derived morphometric parameters including slope, aspect, curvature, and hillshade were combined as a stacked-raster which was also useful for visualizing areas where terrain was obscured. A preexisting rock glacier polygon dataset created by Texas A&M student, Kriti Swami, was also available and referenced for manually mapped rock glacier locations.

The identification of landcover constituting rock glaciers was performed based off several criteria. Foremost, longitudinal ridges and furrows have long been accepted as diagnostic features of rock glaciers distinguishing them from other forms of talus debris, a result of their ice-rich internal structure and plastic form of creep (Barsch, 1971a; Giardino, 1983; Giardino & Vick, 1987; Wahrhaftig & Cox, 1959; White, 1979; Janke et al., 2013). As noted by Barsch (1971a), Wahrhaftig & Cox (1959), and White (1979), the element of rock glacier form especially shown by the presence of steep frontal slopes is another key feature indicative of active rock glaciers. In many cases, steep frontal slopes were easily visible when viewing DEM-derived slope maps (Figure 8).

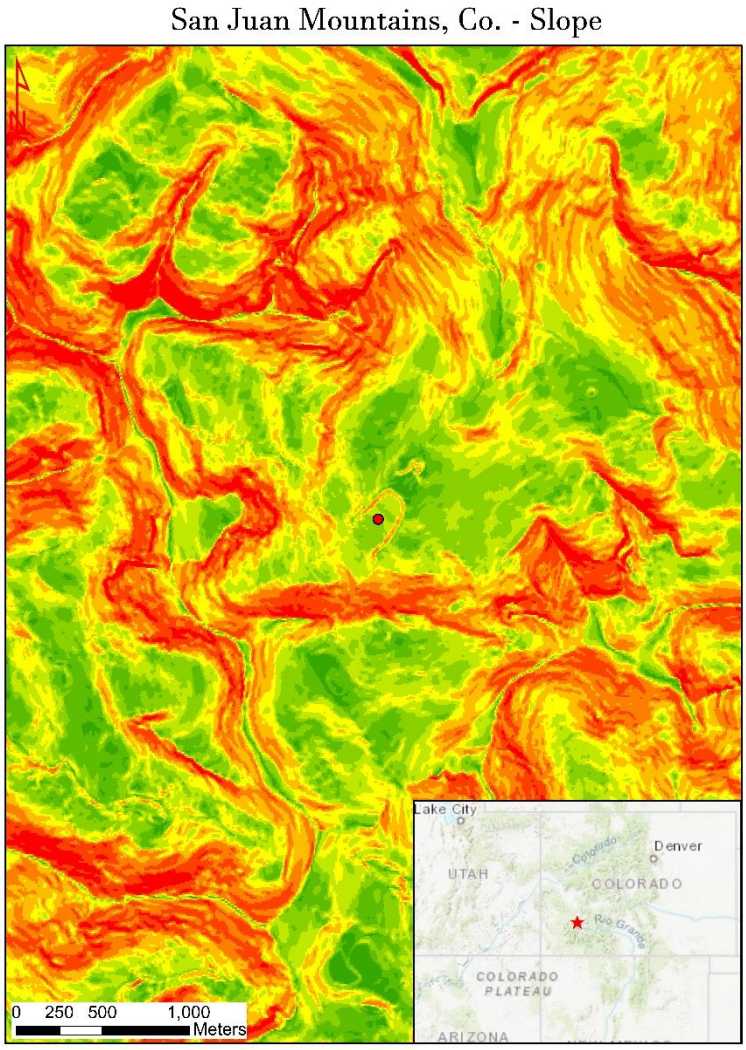

Fig. 8 - Morphometric slope map at the Camp Bird field site. Camp Bird shown by red dot on inset map.

Their primary location above the timberline, in sparsely to completely unvegetated areas, was also a helpful diagnostic feature. Additionally, a majority of the identified rock glaciers were observed to have small streams discharging from their toe, and in many cases ponds and lakes were seen to accumulate at their base. Whereas color was certainly not a highly indicative characteristic, many observed rock glaciers demonstrated a dull gray to tan appearance. Also, many rock glaciers had

noticeably large boulder-sized rock fragments entrained on their surface, whereas large boulders in surrounding areas were seen to simply roll downhill and accumulate in low points.

A point feature-class was created to mark their geographic locations. Points were strategically placed away from the headwall, above the estimated centroid of the active layer, however due to the wide range of shapes and sizes of local rock glaciers these estimated active layer centroid locations are admittedly not precise. In many areas, especially in large amphitheater-sized cirques, multiple abutting rock glaciers can be observed. In cases where multiple rock glaciers are juxtaposed, the delineation of individual features was determined based off the presence of separate frontal lobes, and individual sets of longitudinal ridges and furrows. Throughout the mapping procedure, no attempt was made to distinguish relict from active rock glaciers.

It is worth noting that there are fundamental drawbacks to geomorphic studies primarily conducted with the use of remote-sensing approaches, especially considering that geomorphology is a discipline rooted in field observations – the field aspects of geomorphic research cannot be ignored, even in the context of exponential advances in computer and sensor technologies (Leupold et al., 1964). Because of this, efforts to leverage in-situ observations and manually mapped rock glacier point data as a form of ground truth have been made in this study, and it is hoped that additional in-situ data can be collected in the future to further bolster the results of this work. Nevertheless, in an effort to provide large-scale regional and even global implications, remote-sensing approaches are indispensable for the results of this study. Furthermore, conceptually, accurate analysis of regional and global water inventories contained within ice-debris landforms is largely controlled by climate variations, meaning that water budgets are in a state of constant flux. To account for these fluctuations, it is necessary to devise methodologies

for the continued monitoring of these resources into the future. With time being a major constraint, remote observations provide the most viable and effective way to maintain widespread monitoring of water inventories, especially those contained within ice-debris landforms. The implementation of automated approaches to these methodologies can provide additional standardization, reproducibility, and robustness to global water budget monitoring, invaluable in the context of climate and population changes.

5.2 Rock Glacier Morphometric and Thermal Properties

To effectively classify and distinguish rock glaciers remotely using satellite imagery, it is necessary to understand the physical morphometric and thermal characteristics of these landforms. Moreover, to fully grasp the water and ice-storage potential of rock glaciers, it is important to understand the thermal regime and behavior of their internal structure. In essence, rock glacier surface textures display diagnostic features from surrounding land surfaces, which greatly aids machine-learning image classifier detection of these and other ice-debris landforms. Furthermore, the unique thermal responses of rock glaciers can be leveraged using remotely-sensed data to further bolster image classifier reliability.

The majority of these physical textural characteristics can be readily determined from simple digital elevation models using software such as ArcGIS® and Google Earth Engine®, however traditional field mapping methods can be additionally applied to estimate morphometric parameters, providing important in-situ measurements for comparison and validation. For this thesis, field mapping was conducted on the Camp Bird rock glacier.

5.2.1 Morphometric Field Observations of the Camp Bird Rock Glacier

Field observations were collected at the Camp Bird rock glacier during late summer, July 2020, and include: manual morphometric measurements of longitudinal and transverse rock glacier profiles, slope aspect measurements, GPS latitude and longitude point measurements, elevation point measurements, and manual stream gage measurements of rock glacier meltwater. A longitudinal transect was manually obtained by walking from the rock glacier's rooting zone, near the cirque wall, to the tip of the frontal slope. A 100-foot tape measure was used for measuring distance, and a Brunton® compass was used to maintain a straight line for the transect. Transverse profiles were collected similarly, with three total transects taken, one near the rock glacier toe, one near the middle above the active layer, and one near the rooting zone (Figure 9). Additionally, the entire rock glacier perimeter was manually measured in similar fashion. Frontal and peripheral slope angles were also measured using the Brunton® compass.

Fig. 9 - Field work conducted at the Camp Bird rock glacier July 2020. Transverse profile measurements were manually collected with GPS data and a 100 ft tape measure. Photograph captured by field assistant Jacqueline Rambo, July 2020.

Latitude/longitude and elevation data were recorded using GPS data collected from cell phones with simple and free surveying apps, and were later imported into ArcMap ®, allowing for

the creation of a generalized digital elevation model using the Kriging tool found in the Spatial Analyst® package (Figure 10). The generated DEM constitutes the only true in situ field observations of this thesis and was eventually used to estimate stored water volumes for the Camp Bird rock glacier, which was subsequently compared with estimated water volumes using ICESat-2 data and the generalized A.G. model.

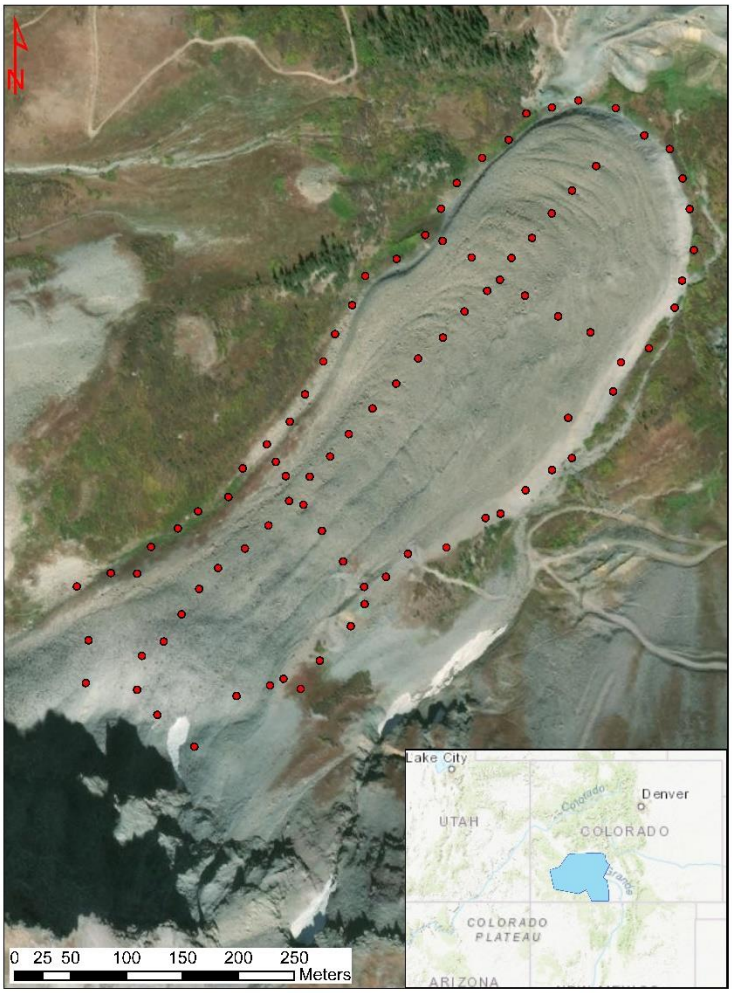

Fig. 10 - Camp Bird rock glacier. Red points represent locations of in-situ field measurements. Point measurements collected during July 2020 by author and field assistant Jacqueline Rambo.

This *in situ* DEM also provides a first-order ground-truth comparison of a single rock glacier against other open-source DEM data such as those provided by the USGS and ICESat-2. Indeed, almost every rock glacier study conducted using remotely-sensed data notes the importance of DEM data, primarily as they are necessary to compute important morphometric parameters such as slope, curvature, hillshade, and aspect (Bishop et al., 2004; Bhardwaj et al., 2014; Brenning et al., 2011; Brenning, 2009; Brenning et al., 2007; Charbonneau & Smith, 2018; Gamache et al., 2018; Janke, 2013; Janke, 2008; Khan et al., 2020; Rau et al., 2005; Robson et al., 2020; Schmid et al., 2015; Xie et al., 2020; Zhang et al., 2019). As noted in the study conducted by Janke (2013), satellite-derived LiDAR DEM data were more than sufficient for observing textural and morphometric features of rock glaciers located in the Front Range of Colorado, in the northern Colorado Rocky Mountain National Park. His study did note, however, that detailed observations of micro-topography of rock glaciers were best made using aerial LiDAR data. While aerial LiDAR is costly and difficult to acquire, the study indicates that a simple 10m USGS DEM can provide meaningful measurements of rock glacier geomorphic features. This thesis similarly utilizes a 10 m DEM from the USGS, from which all morphometric parameters and terrain statistics for this thesis have been computed. Furthermore, the creation of a generalized DEM using field-collected GPS measurements from cell phone app data demonstrates the ability for fine-scaled localized studies of rock glacier morphometries to be readily performed at low cost.

5.2.2 Morphometric Parameters in ArcGIS® and Google Earth Engine®

The USGS 3D Elevation Program provides publicly available DEMs, with 1 arc second (30m), 1/3 arc second (10m), and 1-meter spatial resolutions available in the San Juan Mountain

study area. Because 1-meter DEM data are only available in small portions of the San Juan Mountains, the lowest available spatial resolution (i.e., 1/3 arc second) was used for this thesis.

Software such as ArcMap® provides tools through their Spatial Analyst® and 3D Analyst® toolboxes to calculate morphometric parameters from imported DEM data, including: slope, aspect, curvature, and hillshade. Google Earth Engine® provides similar tools to calculate additional morphometric textural parameters such as the gray level co-occurrence matrix (GLCM), gradient, direction, entropy, contrast, angular second momentum, and Geary's C. In addition to hyperspectral satellite data, textural morphometric parameters such as these have been observed to more reliably distinguish rock glacier and other talus-debris landforms when using image classifiers (Bhardwaj et al., 2014; Brenning et al., 2007; Brenning, 2009; Khan et al., 2020; Robson et al., 2020; Xie et al., 2020; Zhang et al., 2019). While thermal data have been shown to provide some means of identifying rock glaciers using satellite data (Brenning et al., 2011), almost every rock glacier study utilizing remotely-sensed data has echoed the importance of rock glacier morphometry, each of them noting the use of morphometric parameters as unequivocally necessary to distinguish ice-debris landforms from surrounding talus terrain.

All calculated morphometric parameters in this thesis include normal curvature, profile curvature, plan curvature, slope, hillshade, aspect, gradient, direction, the gray-level co-occurrence matrix (GLCM), and derivatives of the GLCM including contrast, angular second momentum, and entropy. Additionally, a Laplacian edge-detection kernel was used in Google Earth Engine® to identify rock glaciers with well-defined form. The calculation of each morphometric parameter resulted in individual raster layers, which were eventually combined into a large multi-band stacked raster feature which was incorporated into the random forest image classifier.

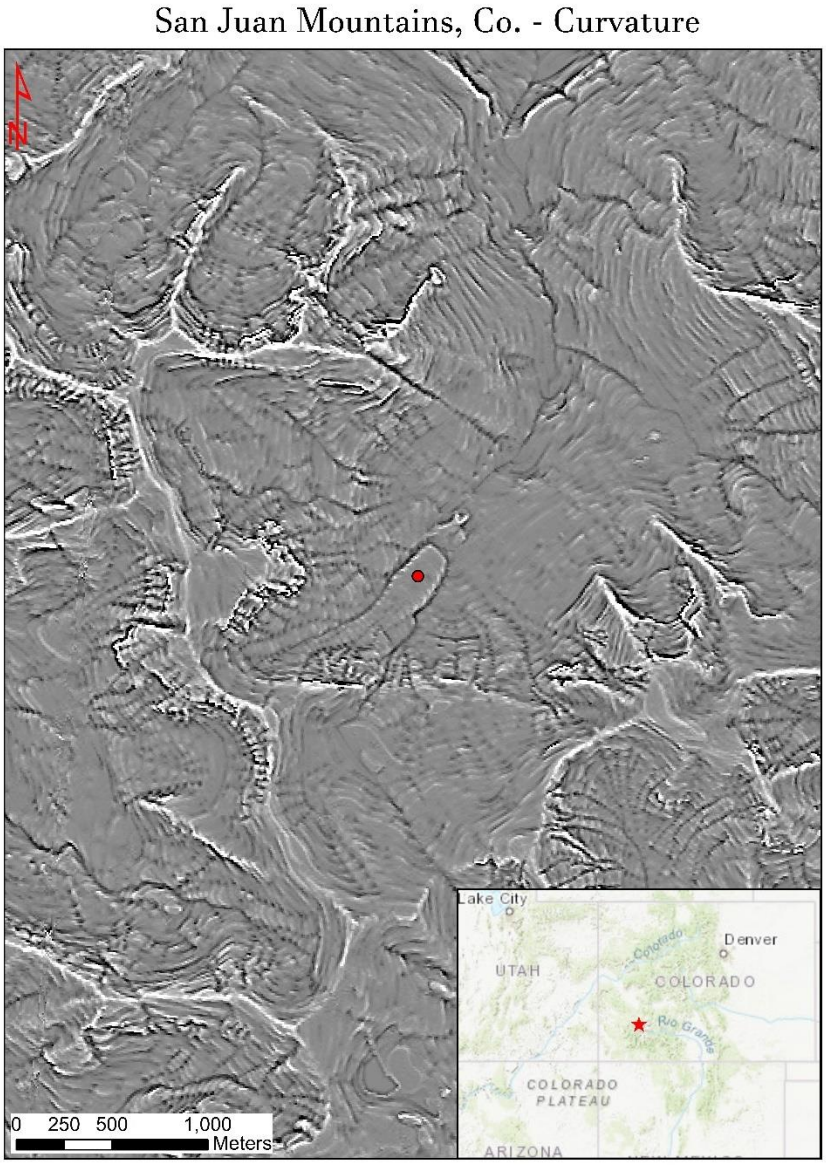

Fig. 11 – Morphometric curvature map at Camp Bird field site. Camp Bird shown as red dot on inset map.

Curvature is one of the most important rock glacier morphometrics, as noted by almost every study cited above. It is the second derivative of terrain surfaces, more succinctly noted as the slope-of-the-slope. and is a measurement of convexity vs concavity of terrain. Three types of

curvature are capable of being calculated in ArcMap, normal curvature, profile curvature, and plan curvature. Normal curvature (Figure 11) is computed as stated above, whereas profile curvature is measured in the direction of maximum slope, and plan curvature is measured perpendicular to the direction of maximum slope. Positive values for both normal and plan curvatures indicate the ground surface is upwardly convex, with negative values indicating the surface is upwardly concave, and values of 0 indicate the surface is flat. For profile curvatures, positive values indicate the surface is upwardly concave, negative values indicate the surface is upwardly convex, and values of 0 similarly indicate the surface is flat. The units of curvature are $1/100^{th}$ of a z-unit.

Slope, aspect, and hillshade were also calculated in ArcMap. Slope and aspect use a 3x3 kernel moving window to calculate topographic values between pixels, and hillshade is computed assuming an infinite amount of illumination sources, with brightness values ranging from 0-255. Textural properties including gradient and direction were calculated in Google Earth Engine®, and represent spatial changes in pixel elevation values akin to the computation of slope. The GLCM is a very important textural parameter for understanding topographies, and is computed using a matrix of specified dimensions, in this case a 4x4 kernel matrix was used. The GLCM calculates the frequency of grey-to-white pixel brightness variations over space, which is extremely useful for rock glaciers as their longitudinal ridges and furrows are diagnostic and demonstrate consistent patterns of grey-to-white. Brenning et al. (2012) expanded on this idea using Gabor textural filters and IKONOS satellite imagery to detect flow structures based off grey-to-white variations represented by ridges and furrows. From the GLCM, contrast, angular second momentum, and entropy were also calculated. Contrast represents overall local contrast of the imagery based off grey-to-white pixel values, angular second momentum is a measurement of repeated pairs of grey

and white pixels, and entropy is a measurement of the overall randomness of grey and white pixel values. The efficacy of individual bands used in the random forest image classifier was assessed iteratively by sequentially adding and removing individual bands upon each classification test run, and analyzing the predicted rock glacier surface area and mean slope values in comparison with observed mean slope values from White (1979) and Brenning et al. (2007), and predicted rock glacier surface area estimates from Brenning et al. (2007). Band combinations with estimated surface areas and mean slope values closest to these studies were ultimately chosen for testing in the final image classification procedure.

5.2.3 Thermal Characteristics of Rock Glaciers

Without doubt, the primary characteristic of rock glaciers designating them as hydrologically significant, aside from their capacity for water storage, it the thermal insulation provided by their supraglacial talus debris cover (i.e., debris blankets). Rock glaciers are relatively unaffected by local climate and thermal controls, allowing them to exist as prolonged and insulated water stores unlike clean glacier ice (White, 1979). Their insulated thermal properties are particularly important as climate changes persist and change alpine landscapes. To better understand the temperature characteristics present in the San Juan Mountains, temperature fluctuation trends in the study area were derived from Band-10 of Lansdat-8 surface reflectance imagery in Google Earth Engine®, based off the locations of digitized rock glacier training data used in the random forest image classifier. Additionally, the results and findings of a variety of thermal regime rock glacier studies have been compiled and incorporated below. From these

findings, a simplified thermal model of rock glaciers in the San Juan Mountains was created, demonstrating the efficacy of supraglacial talus insulation.

The thermal resilience of rock glaciers has been historically heralded by almost every study, and more recently an understanding of the mechanics behind their insulating characteristics have been examined more in depth. A study conducted by Staub et al. (2015) indicated the additional insulating factors of overlying snow cover as proven by various other studies, noting that an overlying snow layer of at least 80 cm effectively thermally decoupled ground permafrost from the atmosphere, whereas an overlying snow layer of 5-20 cm can lead to the "autumn snow effect" during cooler weather, which may intensify ground cooling especially for unconsolidated course-grained surfaces by decreasing the thermal insulation (Goodrich, 1982; Hoelzle et al., 1999; Ishikawa, 2003; Keller & Gubler, 1993; Luetschg et al., 2008; Staub et al., 2015). The average snow cover recorded between two different study plots in Senator Beck Basin, of the San Juan Mountains, is 149.98 cm. Another study conducted in the Swiss Alps by Haeberli et al. (1998) on the famous Murtel-Corvatsch rock glacier marked one of the longest ongoing thermal studies of a rock glacier. In the study, a borehole was drilled to a depth of 58 m in 1987, whereby temperature trends were recorded at intermittent depths for a period of over 10 years. At depths of 10 m and deeper, mean internal temperatures ranged from -2.6°C to -1.2°C. Another similar study was conducted by Vonder Muhll et al. (2003) on the same rock glacier. Thermistor sensors were placed in boreholes in 1993, recording temperature trends at similar depths as the study by Haeberli et al. (1998). Similar temperature fluctuations were noted, with warm periods around June registering warmer internal temperatures ranging from -0.05°C to 0.15°C. The study by Vonder Muhll also noted that internal rock glacier temperatures may be governed by mean annual surface temperatures and the internal permafrost base.

The cooling effects of openwork blocky debris have been noted as a particularly governing factor for internal thermal regimes of rock glaciers (Jones et al., 2019; Wicky & Hauck, 2020). Several thermophysical mechanisms occur in unconsolidated, openwork blocky matrices such as rock glaciers, including: the Balch effect, the chimney effect, continuous air exchange with the atmosphere, summer-time evaporation or sublimation of water and/or ice, and conductive heat loss via boulder protrusion (Jones et al., 2019). One particular mechanism of cooling, aptly named the chimney effect, was proposed in a study by von Wakonigg (1996). The chimney effect describes the seasonal thermally-driven circulation of air through rock glacier matrices. During cooler winter months, warm air masses move upslope through open rock glacier interstices, allowing cold air to build-up in lower areas of rock glaciers. During warmer summer months, the mechanism is reversed and cool air is driven downward, exiting at the foot of the rock glacier toe (Wakonigg, 1996). The discharge of cool air from rock glacier toes has been observed as a gentle breeze exiting from the frontal slope (Delaloye & Lambiel, 2005; Jones et al., 2019), and was also observed at the Camp Bird rock glacier during field work conducted in this thesis in July 2020. Conductive heat loss via boulder protrusion is another effective mechanism of rock glacier thermal regimes, as has been observed in the Solen Mountains, central-eastern Norway by Juliussen & Humlum (2008). Large boulders entrained in supraglacial rock glacier taluses act as heat bridges, increasing surface area and thermally coupling openwork blocky debris with surrounding surface air, promoting heat conduction. In their study, Juliussen & Humlum (2008) reported mean annual ground surface temperatures of openwork blocky debris cover 1.3-2.0°C lower than surrounding till and bedrock surfaces (Jones et al., 2019). Wicky and Hauck (2020) reported similar observations of the thermal regimes of openwork blocky debris cover of rock glaciers at the Murtel-Corvatsch and Schafberg rock glaciers in the Swiss Alps. Their study modeled heat

convection in an openwork blocky, porous media using a Darcy approach based off Darcy's law, and found that in addition to heat conduction resulting from similar mechanisms as the aforementioned 'conductive heat loss via boulder protrusion', free air convection has a significant influence on the internal thermal regime of rock glaciers. The results of the study by Wicky & Hauck (2020) demonstrate how highly porous openwork blocky debris cover constituting the supraglacial taluses of rock glaciers promote strong air circulation, ultimately leading to increased ground cooling.

While a rigorous understanding of the thermal regimes and thermophysical processes of rock glacier taluses is beyond the scope of this thesis, temperature fluctuation data was collected from Band-10 of Landsat-8 surface reflectance imagery using Google Earth Engine® for the period of March 2013 to November 2020. The overall trend of temperature fluctuations can be shown by the raw data in Figure 12.

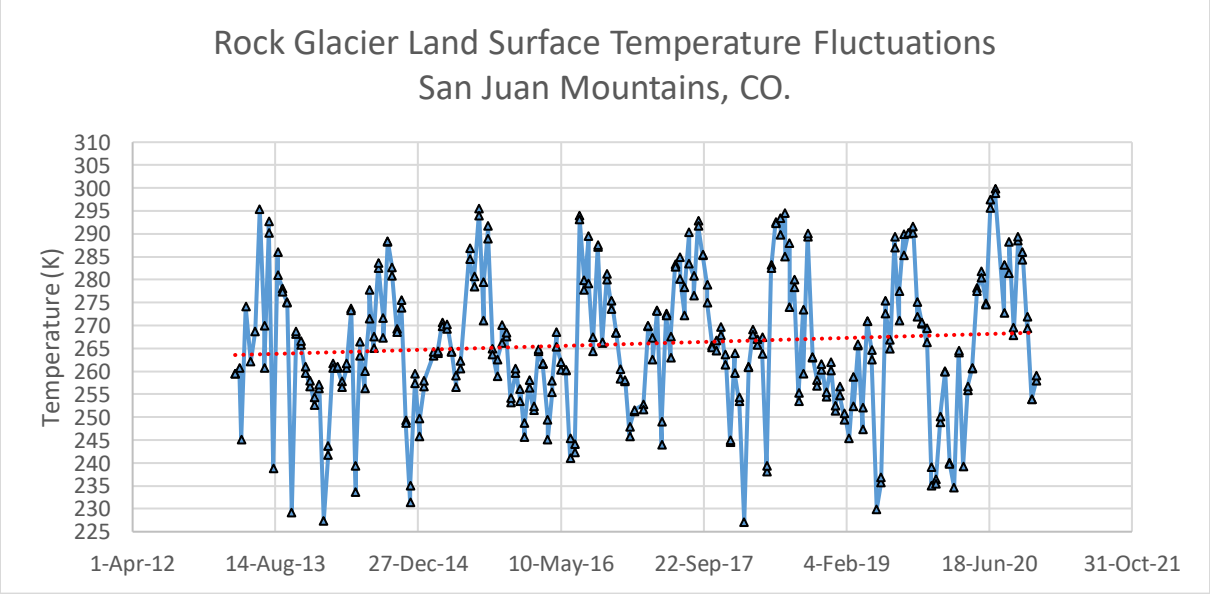

Fig. 12 – Raw Landsat-8, Band-10 surface reflectance temperature data, generated in GEE®.

A harmonic oscillatory wave function was ultimately fit to these temperature data, allowing trends of temperature fluctuations to be more easily seen (Figure 26). The use of satellite thermal bands such as Bands 10 and 11 from Landsat-8 offer potentially valuable data for remote areas with little to no existing temperature datasets, or whose study areas area inaccessible. Additionally, satellite-derived thermal data provide regional and even global-scale coverage. These types of data will likely be extremely valuable in the coming years as climate changes dictate more widespread and consistent monitoring of hydrologic resources such as those contained within rock glaciers. Based off the results of the previously mentioned studies, a schematic diagram illustrating thermal processes in rock glaciers was sketched to demonstrate the interactions, variables, and thermal-coupling present within alpine rock glaciers (Figure 13).

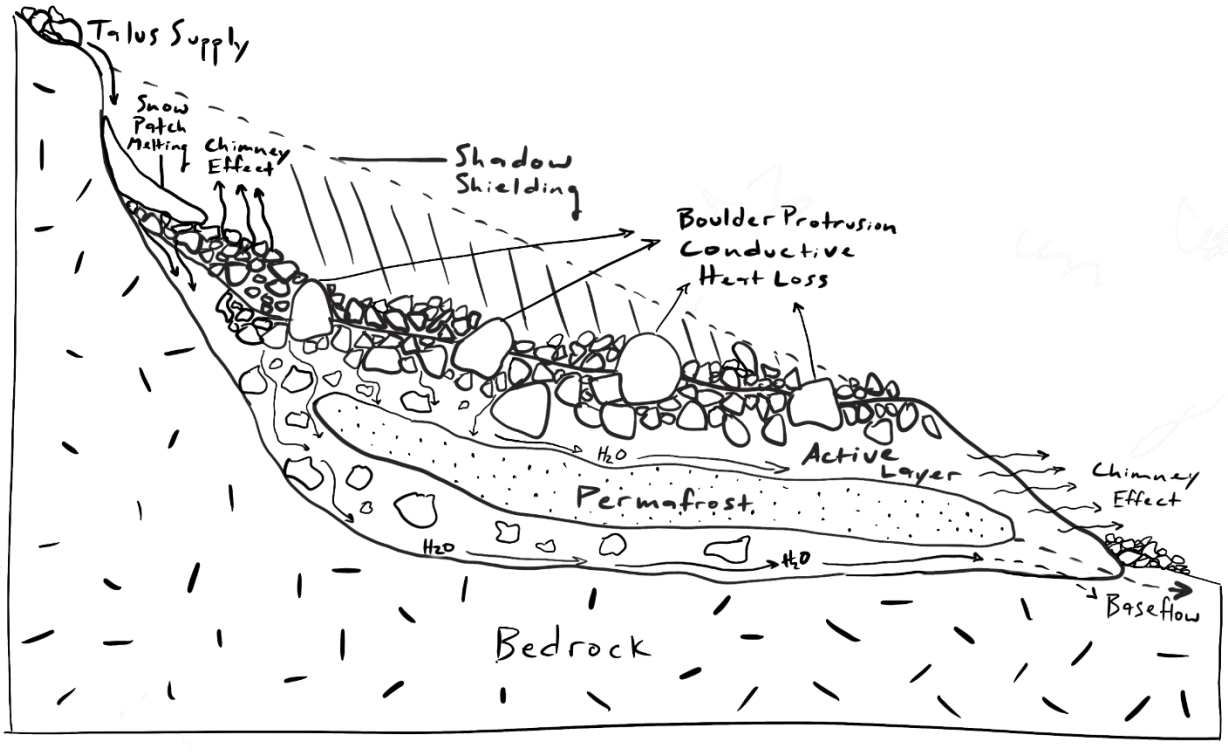

Fig. 13 – Generalized schematic diagram demonstrating thermal convective and conductive heat distribution processes present within rock glaciers. Diagram illustrated by the author.

While still very generalized, schematic diagrams such as these help communicate the hydrologic value of ice-debris stores contained within rock glaciers, and may provide more context to individuals and entities such as legislators or local communities who are necessary to help protect and monitor these important landforms into the future.

5.3 Machine-Learning Approach for Rock Glacier Water & Ice Volume Estimation

The primary objective of this thesis focuses on the quantitative estimation of water resources contained within rock glacier landforms within the entire San Juan Mountain extent. Because of the large extent of the San Juan Mountain study area (i.e., 21,656 km^2) it was necessary to utilize remotely-sensed data. As previously mentioned, the remotely-sensed data used to achieve this objective include a USGS 10 m DEM sourced from the 3D Elevation Program database, and a variety of multispectral satellite imagery including NAIP, Landsat-8 raw imagery, and Landsat-8 surface reflectance imagery all sourced directly from Google Earth Engine®. Three different spectral indices including the Normalized Difference Vegetation Index (NDVI), the Modified Normalized Difference Water Index (MNDWI), and the normalized difference built-up index (NDBI), were additionally computed using the multispectral imagery to aid in the identification of vegetation, water, and urban landcover; of these, only NDVI was ultimately used. A multi-band stacked raster image containing morphometric derivatives of slope, hillshade, normal curvature, profile curvature, plan curvature, and aspect, was created in ArcMap® and was imported into Google Earth Engine® as an input. Additional DEM morphometric derivatives including GLCM,

and GLCM derivatives including gradient, direction, contrast, angular second momentum, entropy, and a Laplacian edge detection filter, were additionally utilized and ultimately incorporated into a random forest image classifier developed in Google Earth Engine®.

By incorporating raw DEM data, DEM morphometric derivatives, and multispectral satellite data, the structure and spectral response of rock glaciers were more readily identifiable. Multispectral satellite data such as Landsat-8 raw imagery, Landsat-8 surface reflectance imagery, and NAIP imagery provide thermal bands which measure land surface temperature using long wavelengths such as infrared. These types of data have been noted to be useful for characterizing thermophysical properties of different types of landcover and landforms, especially rock glaciers (Brenning, 2011). Land surface temperatures derived from these types of thermal bands are directly measuring surface radiation emissions, which are a function of the internal temperature of the landcover being measured. Previous studies have demonstrated the spectral similarity of rock glaciers with surrounding terrain in visible wavelengths (i.e., RGB), which has long constituted the major challenges associated with image classification of ice-debris landforms (Berta, 1982; Brenning, 2009; Brenning, 2011; Jones et al., 2018). Studies such as Brenning (2011), however, have shown how land surface temperature can provide a means of distinguishing rock glaciers from surrounding terrain based solely off differences in surface radiation emissions. Observing regional morphometric and thermal characteristics, and referencing the results of previously conducted rock glacier thermal regime studies (Apaloo, 2013; Millar et al., 2012; Millar & Westfall, 2019; Wagner et al., 2020), provides a better understanding of the scope of surface energy fluxes in the region.

5.3.1 GEE RF structure and data

The random forest image classifier developed and run using Google Earth Engine® incorporates all aforementioned data as inputs. Rock glacier training polygons were manually digitized in Google Earth Engine®, in addition to training polygons for four other landcover classes including: water, vegetation, urban/miscellaneous, and mountaintop ridges. Digitized rock glacier polygons constitute the training data inputs required for the training of the random forest image classifier, from which the resultant classification map was later compared with manually mapped rock glacier point data which were mapped using ArcMap®. In response to the lack of available validation data in the San Juan Mountain study area, the comparison of manually mapped rock glacier point data with algorithmically generated rock glacier landcover maps created in Google Earth Engine® serves as validation of the procedure. By calculating the physical morphometric characteristics of rock glaciers in the San Juan Mountain study area, these landforms were more easily distinguished and isolated from the surrounding terrain for the determination of number and distribution, imparting more effective identification and classification in satellite imagery by machine-learning algorithms.

The random forest image classifier used in Google Earth Engine® is humbly provided as a pre-loaded function. Random forest classification is, for lack of a better description, “the child of the computer age” (Brieman et al., 1998). The general procedure of regression tress is, for lack of a better term, “rooted” in decision tree logic, which itself has roots stemming from the blossoming research into computer logic and artificial intelligence that was largely advanced in the 1960’s. To posit a humble explanation of random forest decision trees, input data (i.e., training data) are ingested by the classifier, whereby the classifier “votes” on subsequent classes in which to place

the ingested data (Figure 14). The five landcover classes defined at the beginning of the classification procedure (i.e., rock glacier, vegetation, water, ridges/peaks, and urban/miscellaneous) constitute the classes that training data (i.e., training polygons) are iteratively voted on and placed within.

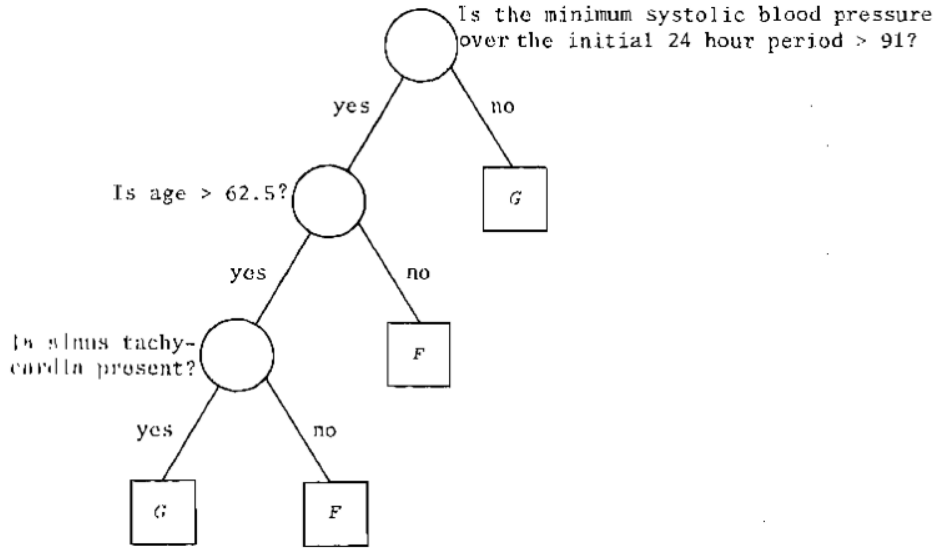

Fig. 14 - Generalized random-forest decision-tree structure, reprinted from Brieman et al. (1998).

Prior to running the image classifier, remotely-sensed data inputs were combined as a large multi-band stacked raster, which contained a total of 352 bands. Of these bands, 46 were ultimately chosen to be used for model prediction. The final band selection was based off multiple iterations of various band combinations, where the total surface area, mean elevation, and mean slope values of all classified rock glacier pixels were used as basis for band combination efficacy. The random forest (RF) classifier was run multiple times with a variety of band combinations to assess the best combination of bands for classifier performance. The ultimate best-performing band combination was based off predicted rock glacier surface areas that were close to the 70 km^2 rock glacier surface

area estimated by Brenning et al. (2007) for the San Juan Mountain study area, as well as predicted mean slope values of rock glaciers that fell close to the overall mean rock glacier slope of 17.1° that was determined by White (1979) for the San Juan Mountains. An accuracy assessment of classifier performance was computed for each run, with all but two band combination trial runs achieving accuracy performances greater than 95%. The number of training polygons for each landcover class, for the first round of classification, included 45 rock glacier training polygons, 7 water training polygons, 90 vegetation training polygons, 72 ridge/peak training polygons, and 46 urban/miscellaneous training polygons. The generalized workflow for the random forest machine-learning image classifier is shown in Figure 15.

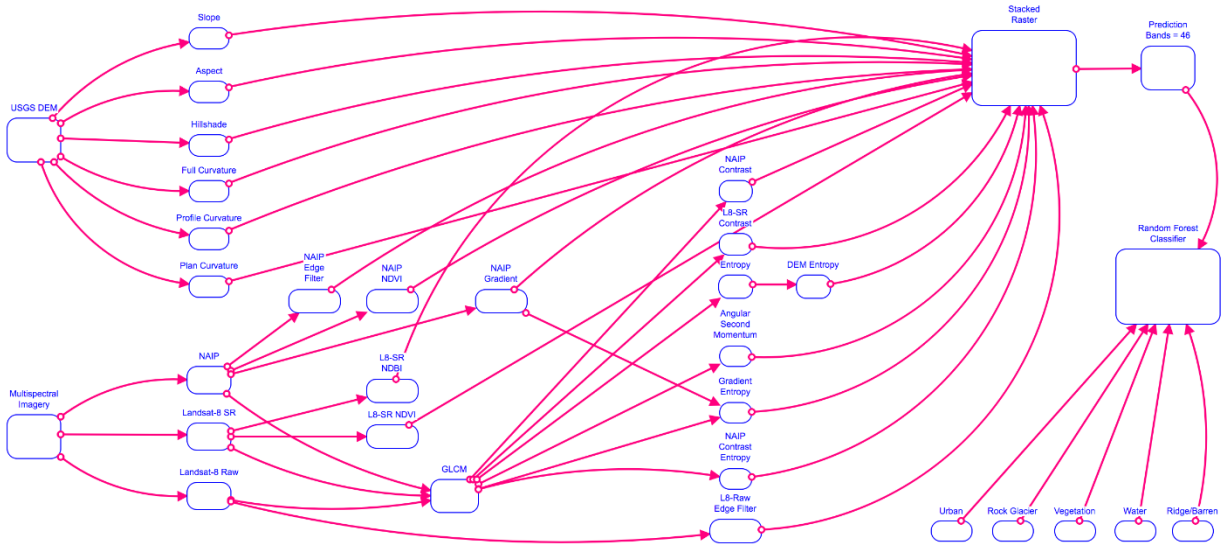

Fig. 15 – Random-forest workflow procedure developed in Google Earth Engine®.

Upon determining the most effective band combination, all pixels contained within the resulting classified rock glacier landcover area was isolated and exported as a GeoTIFF image, which was ultimately imported into ArcMap® for the final volume estimation procedure. After the first volume estimation of rock glacier water content was computed in ArcMap®, the number of

landcover class training polygons was increased to include 150 rock glacier training polygons, 7 water training polygons, 90 vegetation training polygons, 87 ridge/peak training polygons, and 46 urban/miscellaneous training polygons. The resulting classified rock glacier landcover pixels predicted by the second trial run were similarly exported as a GeoTIFF image and imported into ArcMap® for the final volume estimation procedure as before. To further assess the accuracy of the predicted rock glacier pixel locations, the manually mapped rock glacier point data feature class was ultimately used as validation.

5.3.2 Arc methods – GEE data import and final volume calculation

In addition to using ArcMap® to manually map all observable rock glacier features in the San Juan Mountain study area, it was also used for the final estimated volume calculation of rock glacier water storage. The final volume estimation procedure involved many steps, and utilized a variety of tools provided by ArcMap®. Whereas Brenning (2005) proposed an empirical rock glacier thickness model in his dissertation, which has been adopted in other studies to estimate rock glacier water volumes (Jones et al., 2018; Millar & Westfall, 2019), this thickness estimation approach is based off observations of rock glaciers in the Swiss Alps from a study by Barsch (1977). In pursuit of wider applicability, I applied a different and original approach to thickness estimations which is based strictly off the use of remotely-sensed data, where the training of a random forest image classifier in Google Earth Engine® was used to isolate predicted rock glacier locations, and the 10 m USGS DEM previously used to calculate morphometric parameters was additionally used to estimate rock glacier thicknesses, and ultimately used to derive water volumes.

The volume estimation workflow (Figure 16) developed for this thesis first requires the importation of a binary (i.e., black and white) GeoTIFF image which constitutes the predicted rock glacier pixel locations derived from the random forest image classifier results from Google Earth Engine®. The imported GeoTIFF is the only input data necessary to estimate water volumes using this volume estimation approach. These classified rock glacier landcover pixels are manipulated and run through a series of ArcMap® tools including: Raster Calculator®, Majority Filter®, Raster to Polygon®, Dissolve®, Int®, Extract by Mask®, Erase (Analysis)®, Elevation Void Fill (raster function)®, Zonal Statistics & Zonal Statistics as Table®, and Tabulate Intersection®. An exhaustive explanation of the workflow procedure is not included here, but instead a conceptual and generalized explanation is sufficient to understand the process.

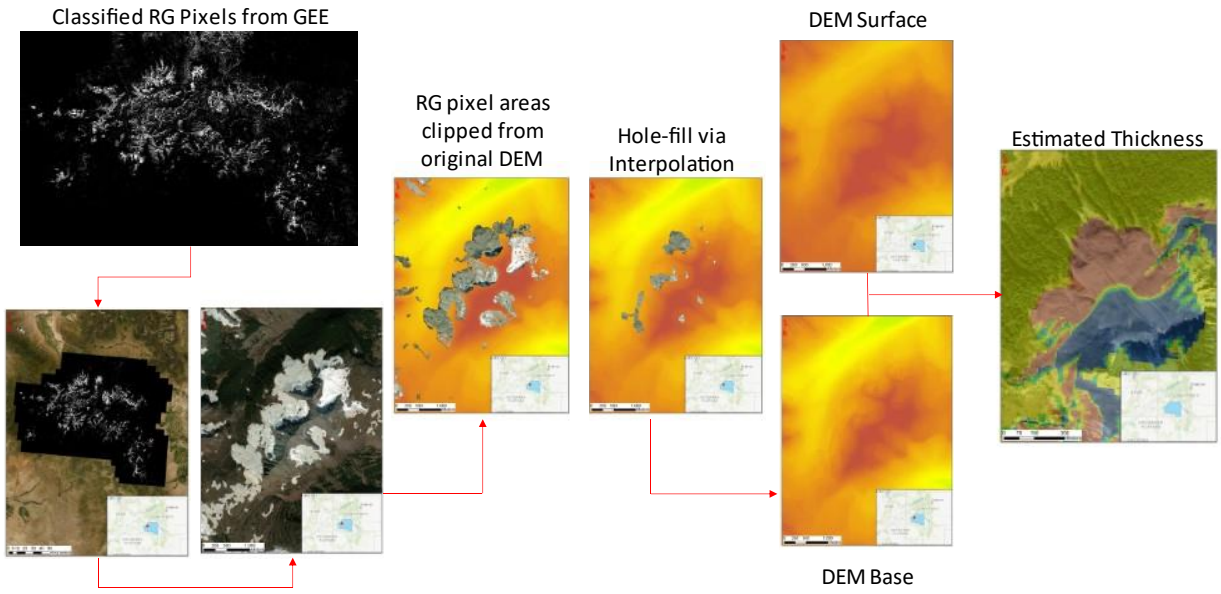

Fig. 16 – Generalized water volume estimation procedure developed and run via ArcMap®. Classified RG pixels from GEE used to clip holes in original DEM. Holes filled via interpolation procedure, creating a new DEM (i.e., DEM base) with inferred rock glacier bases. Estimated RG thickness maps produced by subtracting DEM base from original DEM surface.

Using this volume estimation approach, the classified rock glacier pixel locations are further isolated from the imported GeoTIFF image, and overlapping polygon features representing these locations are generated. The created polygon features are used to cut holes out of the original 10 m USGS DEM, which are later filled using the Elevation Void Fill® raster function to infer rock glacier bases. Elevation values from the DEM are additionally clipped to these polygon features, representing the rock glacier surface topography. By clipping rock glacier surface and base values to the overlapping polygon features, the two surfaces are subtracted (i.e., surface – base) to generate rock glacier thickness measurements for all classified rock glacier landcover pixels; the resulting output is saved as a raster image.

The process of filling all holes previously cut out of the DEM, using the Elevation Void Fill® function, is inferential and utilizes a combination of plane fitting and inverse distance weighting (IDW). As such, it is less precise when filling larger holes, and when inferring elevations over highly variable terrains. As a result, some areas are given negative thickness values resulting from the subtraction of rock glacier base raster values from rock glacier surface raster values. To eliminate negative thicknesses, all positive thickness values are isolated. These final rock glacier thicknesses are used to estimate rock glacier water volumes. The final volume calculation is performed by extracting the pixel thickness values (i.e., z-values) contained within respective polygons, stored in as an ArcMap® table, and multiplying each polygon by 100 representing the surface area of each pixel for a 10 m DEM. The result yields an estimated rock glacier volume in cubic meters per respective classified polygon areas, which may be summed together to get the total cubic meter volume of rock glacier features in the study area. Estimates of rock glacier ice

volumes are simply taken as a 40-60% value of the summed dimensional volume, and estimates of water volumes are additionally taken as a 90% value of the ice volumes.

6. RESULTS & DISCUSSION

6.1 ICESat-2

Data collected from ICESat-2 were used to derive elevation measurements, and ultimately generalized water and ice volume estimates, for six rock glaciers in the San Juan Mountains, including the Camp Bird rock glacier (Table 1). In an attempt to assess the accuracy of the generalized rock glacier model (i.e., A.G. model) for estimating water and ice volumes, the estimated water volume using ICESat-2 data for the Camp Bird rock glacier was subsequently compared with the estimated water volume for Camp Bird using in situ field observations and the resulting DEM created in ArcMap®.

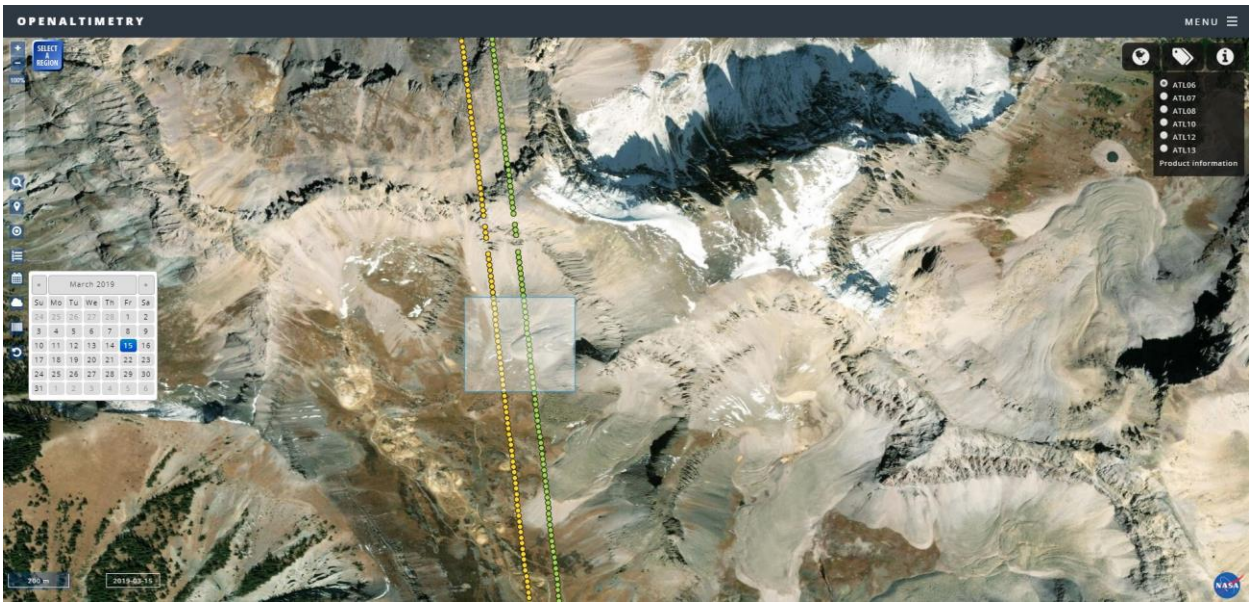

Fig. 17 – ICESat-2 ground track intersecting rock glacier RG2-3. The perpendicular intersection yielded the best elevation profile of all six rock glaciers investigated. Image provided courtesy of NASA's OpenAltimetry portal.

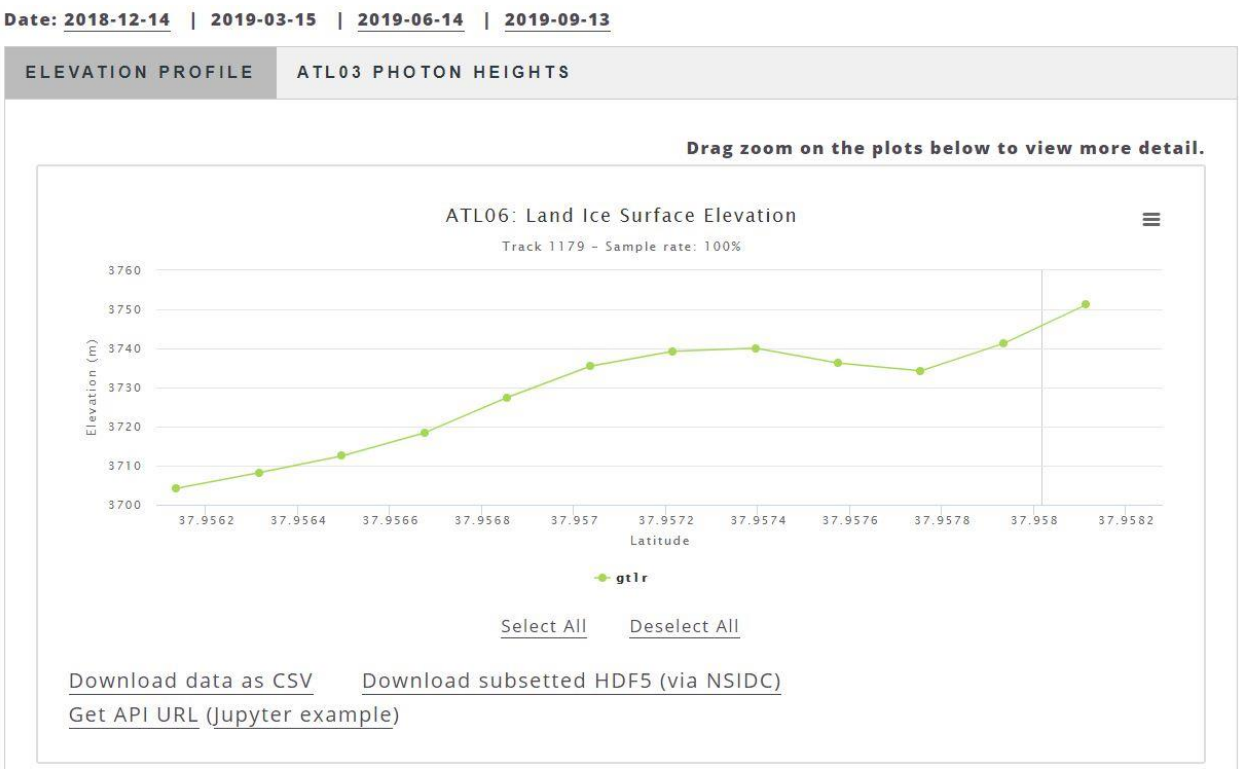

Fig. 18 – Elevation profile for rock glacier RG2-3, representing the best collected elevation profile of all six rock glaciers investigated. Profile provided courtesy of NASA's OpenAltimetry portal.

Of the six collected elevation profiles, only two rock glaciers were found with ground tracks intersecting horizontal and/or perpendicular to the rock glacier flow direction, namely RG2-1 and RG2-3. The best elevation profile out of the six rock glaciers came from RG2-3 (Figures 16-17). The other four rock glaciers were poorly intersected by ground tracks, leading the resulting water and ice volume estimates to be very generalized.

The Camp Bird rock glacier was one such rock glacier with a poorly oriented ground track (Figure 18). Coincidentally, the estimated water and ice volumes for the Camp Bird rock glacier, as compared with the volumes derived using the in situ-derived DEM created in ArcMap®, were very different. The estimated water volumes derived using ICESat-2 data and the generalized A.G.

rock glacier model, under conditions of 40% interstitial water content, was 0.0019 km^3 as compared with an estimated 0.00029 km^3 water volume estimated via the in-situ derived DEM and the water volume estimation procedure utilized to estimate water volumes for the entire San Juan Mountain study area. Thickness values incorporated into the A.G. model were estimated by taking the difference between the peak surface elevation at the rock glacier crest, and the inferred rock glacier base elevation which was assumed to be a concurrent continuous surface connected to the surrounding ground surface. Length and width measurements were determined via the measuring tool provided in ArcMap®. The large discrepancies between water volume estimates produced via the A.G. model and the volume estimation procedure developed in this study suggest that use of the generalized A.G. rock glacier model is inaccurate, and further highlight the difficulty of using ICESat and ICESat-2 data to estimate water and ice volumes in ice-debris landforms such as rock glaciers.

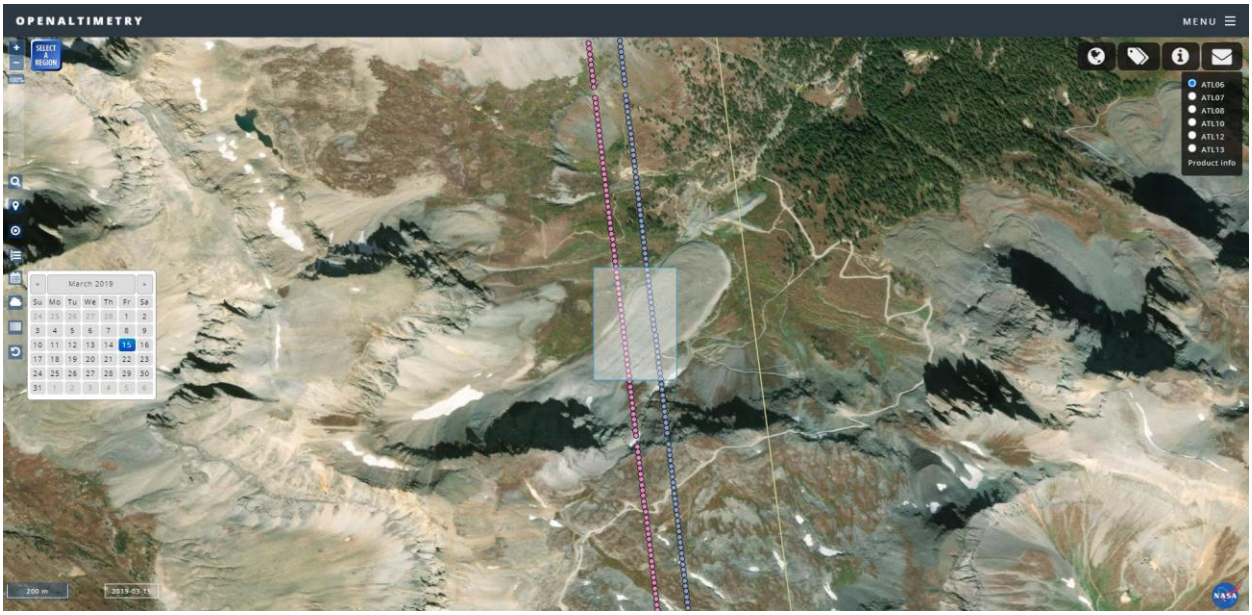

Fig. 19 – ICESat-2 ground track over the Camp Bird rock glacier. This ground track produced a poor elevation profile. Image provided courtesy of NASA's OpenAltimetry portal.

Table 1 - First-order rock glacier water/ice volume estimates produced via generalized A.G. rock glacier model and ICESat-2 data.

Volume Estimates	RG2-1	RG2-2	RG2-3	RG2-4	RG1-1	Camp Bird
Z (m)	45.5954	65.5	15.5	35.5	53	30.34
W (m)	1956.82	241.01	115.27	307.48	330	217.67
L (m)	553.27	727.71	287.26	822.62	1500	632.9543
Z*W*L	49363850.75	11487742.86	513243.1331	8979341.515	26235000	4180098.43
Ice Volume (m^3) - 75% content	40848714.41	13123669.12	485475.3333	8219241.527	25303116.11	3961446.591
Water Volume (m^3)	37151905.75	11935977.06	441539.8156	7475400.169	23013184.11	3602935.675
Water Volume (km^3)	0.037151906	0.011935977	0.00044154	0.0074754	0.023013184	0.003602936
Water Volume (acre ft)	30119.57012	9676.663709	357.9625101	6060.411572	18657.11054	2920.950393

6.2 Manual Rock Glacier Mapping

A total of 1,052 rock glacier features were identified and manually mapped within the 21,656 km^2 San Juan Mountain study area (Fig. 2). As previously mentioned, all mapping of observable rock glacier features was primarily done using the default basemap imagery in ArcMap 10.7® which is provided courtesy of Maxar Technologies. The number of observed rock glaciers falls within the range of the study by Brenning et al. (2007), who cited a statistically estimated rock glacier population for the San Juan Mountains of 900-1300 features.

Rock glacier distribution maps using latitude and longitudes of manually mapped rock glacier features were produced in RStudio®. Five separate maps were produced, with rock glacier location points colored based off respective elevation, slope, aspect, curvature, and hillshade values (Appendix B.1 – B.5). Whereas additional morphometric parameters were computed in Google Earth Engine®, including textural aspects such as the gray-level co-occurrence matrix (GLCM), angular second momentum, contrast, gradient, and entropy, the most diagnostic

parameters of rock glaciers appeared to be slope, elevation, hillshade, and especially curvature. The statistical results of these parameters are shown in Table 2.

Table 2 - Summary statistics for 1,052 manually mapped rock glacier features.

	Elevation (m)	Slope (deg)	Aspect (deg)	Curvature (*1e9)	Hillshade
Min	2919.245	1.8	0.828	-76.88	86.0
Max	4012.878	41.18	359.413	85.63	238.0
Mean	3612.138	17.73	188.79	1.3	195.289
Std. Dev	183.757	7.29	128.18	13.99	28.389

As echoed by several studies, rock glaciers are generally found above the timberline (Barsch, 1971a; Brenning et al., 2007; Wahrhaftig & Cox, 1959; White, 1979), as was observed in the San Juan Mountain region. The timberline for the San Juan Mountains lies between 3400-3500 m (Brenning et al., 2007). Of the two rock glacier inventory studies conducted in the San Juan Mountains, White (1979) and Brenning et al. (2007), White mapped a total of 756 rock glaciers while Brenning estimated an aforementioned population of 900-1300 features. White's study noted the majority of observed rock glaciers to occur at elevations above 3350 m, with the lowest observed occurrence at 2975 m and the highest occurrence at 4109 m. Brenning's study applied a statistical predictive generalized additive model, which was applied to areas only above 3400 m and based off sampling of 84 randomly selected rock glacier features, noting that elevations above 3600 m were significant for the formation of rock glacier features – the mean elevation of mapped rock glacier features in this thesis was ~3612 m.

Azimuthal orientation of rock glaciers in North America have been noted to be predominantly north-facing (Wahrhaftig & Cox, 1959; White, 1979). White noted that rock glacier orientations in the San Juan Mountains were preferentially north-facing as well, with active rock glaciers demonstrating a mean orientation of 1°, and inactive rock glaciers demonstrating a mean orientation of 354°. Brenning's study does not mention a statistically estimated mean rock glacier orientation. The mean aspect orientation for all manually mapped rock glaciers in this thesis was 188.79°, which disagrees with White's study. All aspect azimuth values were calculated in ArcMap 10.7®, based off the 10 m USGS DEM used in this study. The observations of both White, Wahrhaftig, and others indicate consistent preferential rock glacier orientations that are generally north-trending. The tool used to calculate terrain aspect values in ArcMap® comes from the Spatial Analyst® toolbox, and uses a 3x3 cell moving window to calculate aspect values based off eight neighboring pixels. Because the required computations for estimating aspect are directly dependent on the size and number of pixels in the imagery, the spatial resolution of DEMs is a significant factor in the accuracy of aspect values. A spatial resolution of 10 m corresponds to 10x10 m pixels, which may drastically skew estimated azimuth directions in mountainous regions where terrain is greatly variable. Because of the variability of calculated aspect directions stemming directly from the low-resolution 10 m DEM data used, the mean aspect orientations calculated for rock glacier features in this thesis are considered approximations at best, and inappropriate at worst.

6.3 Camp Bird Rock Glacier – In situ Field Observations

Field observations at the Camp Bird rock glacier were collected during Summer 2020, during the Southwest Monsoon season (Figure 19). Morphometric measurements of the rock glacier were collected, and were later incorporated into a DEM. One of the most important morphometric observations of this rock glacier were the measured frontal and peripheral slope values using the inclinometer on a Brunton® compass. The mean frontal slope value was 43°, whereas the mean peripheral slope value was 44.17°. These slope values are greater than the angle of repose (i.e., >35°), which is highly indicative of an active rock glacier. Observations of surface color variations were also made, noting the lighter color of frontal and peripheral slopes and darker colors on the upper rock glacier surface, indicating that the frontal and peripheral slopes are less weathered than the upper rock glacier surface. While my field assistant and I performed measurements of the rock glacier perimeter, a constant cool breeze exiting from the rock glacier toe was observed, which was ultimately explained by the chimney effect theory proposed by Wakonigg (1996), and additionally described by Delaloye & Lambiel (2005) and Wicky & Hauck (2017), (Jones et al., 2019).

Fig. 20 – Camp Bird rock glacier field site. Photograph captured by author - July, 2020.

The presence of an observable chimney effect strengthens the argument for an active permafrost layer within the Camp Bird rock glacier, as the chimney effect has been demonstrated to enhance the preservation of internal ice content (Delaloye & Lambiel, 2005; Wicky & Hauck, 2017). Stream gauge measurements were additionally taken from two small streams discharging from the mid-frontal toe (Figure 20). For each stream, multiple velocity measurements were taken at intervals of 0.5 ft for the smallest stream, and 1 ft for the larger stream, from which mean velocity measurements were derived ranging from 0.96 fps for the larger stream to 2.3 fps for the smaller stream.

Fig. 21 - Observed baseflow discharge at Camp Bird rock glacier toe. Photograph captured by author - July, 2020.

In addition to morphometric observations and stream gauge measurements, all manually collected latitude, longitude, and elevation values recorded from cellular GPS data were ultimately imported into ArcMap 10.7® and used to create a generalized digital elevation model of the Camp Bird rock glacier (Figure 21). As mentioned earlier, this DEM was used to estimate water and ice volumes within the Camp Bird rock glacier which was additionally used as comparison for the

volume estimates derived from the use of a generalized rock glacier volume model and ICESat-2 data. The water and ice volume estimate for the Camp Bird rock glacier was derived using the same volume estimation procedure used to estimate water and ice volumes for the entire San Juan Mountain study area. The aforementioned liquid water volume estimate produced from the generalized rock glacier volume model was 0.0019 km^3 – 0.0029 km^3 for 40-60% internal ice/water content, whereas the estimated liquid water volume derived from the in-situ DEM was 0.00029 km^3 – 0.00043 km^3 for 40-60% ice/water content. Based off the extreme differences between the water and ice volume estimate derived from ICESat-2 data, and the volume estimate derived from the primary DEM volume estimation procedure utilized in this thesis, it is assumed that using ICESat-2 data and an overly-generalized 3D-volume model to estimate water and ice volumes within rock glaciers results in significant overestimations.

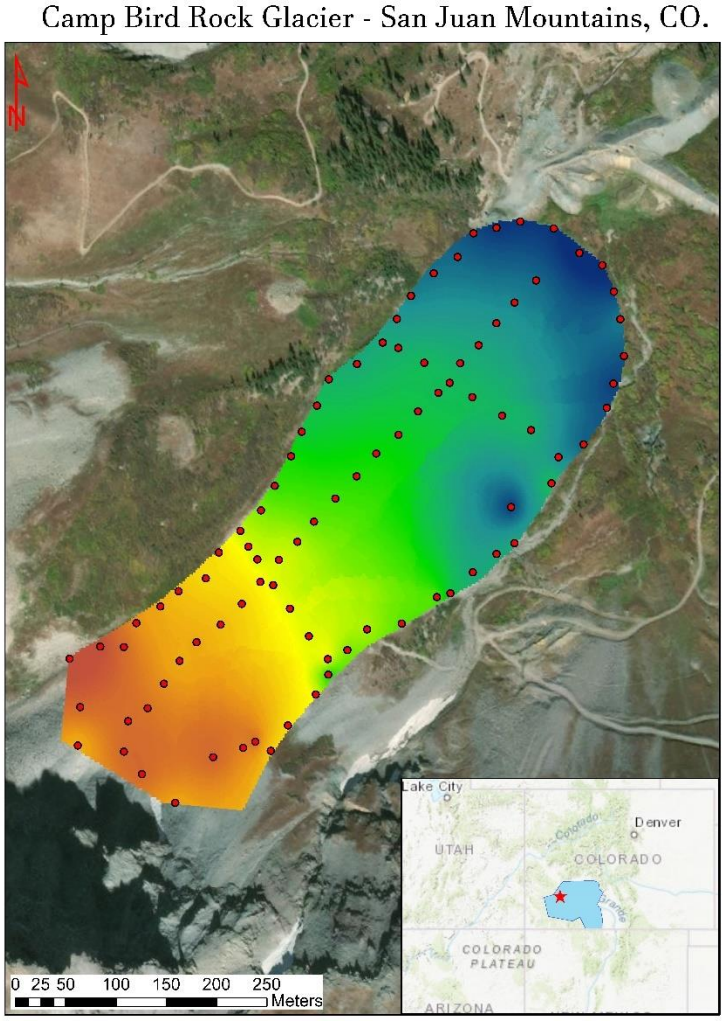

Fig. 22 - Camp Bird rock glacier DEM based off in-situ GPS measurements. Red dots represent GPS measurement locations collected by author and field assistant Jacqueline Rambo, July 2020. Created by author using the Kriging® analysis tool in ArcMap®.

The primary water volume estimation procedure used in this thesis, as mentioned before, calculates some negative thickness values in areas where large DEM voids (i.e., holes) exist and where topography is highly variable. This occurred during the water volume calculation for Camp Bird. To avoid a final volume estimation calculated with included negative thickness values, only positive thickness values were used in the final calculation. As a result, the estimated liquid water

volume of 0.00029 km^3 – 0.00043 km^3 is an underestimate. It is very likely that there is significantly more water included in the Camp Bird rock glacier, as well as within other rock glaciers in the San Juan Mountain, than was calculated using the volume estimation method utilized in this thesis.

6.4 Google Earth Engine® Classification Results

The random forest image classifier used in Google Earth Engine® was run twice covering the entire San Juan Mountain study area extent of 21,656 km^2. The number of landcover training polygons for rock glacier and ridge/peak landcover classes was increased for the second classification run, from 45 rock glacier training polygons to 150 and from 72 ridge/peak polygons to 87, based off erroneously classified areas resulting from the first classification. The result of each classification run was a predicted landcover map with predicted landcover classes shown by color: rock glaciers (gray), ridges/peaks (burgundy), vegetation (green), water (blue), and urban/miscellaneous (red) (Figures 22-23). The ridges/peaks landcover class was created primarily to isolate rock glaciers from the surrounding cirque areas, and performed quite well following the addition of textural input data such as GLCM and particularly GLCM-derivatives such as contrast.

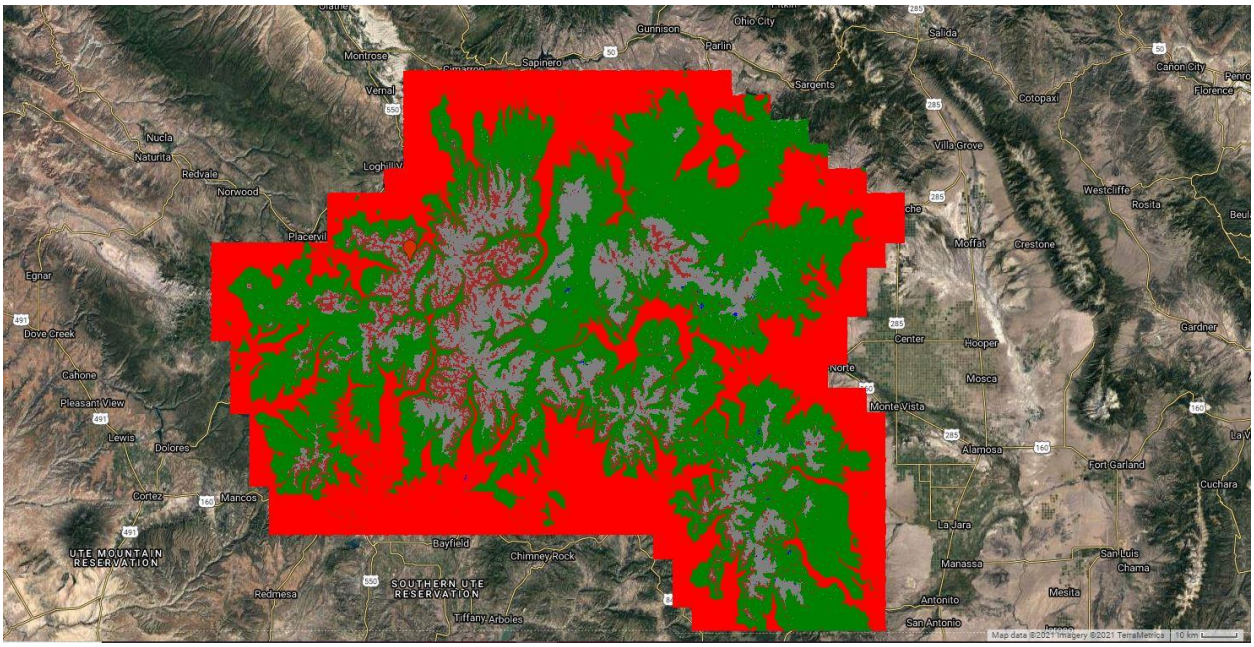

Fig. 23 - Trial-1 random-forest landcover classification map produced in Google Earth Engine® for the San Juan Mountains, CO. (grey = rock glacier; green = vegetation; blue = water; burgundy = ridges/peaks; red = urban/miscellaneous).

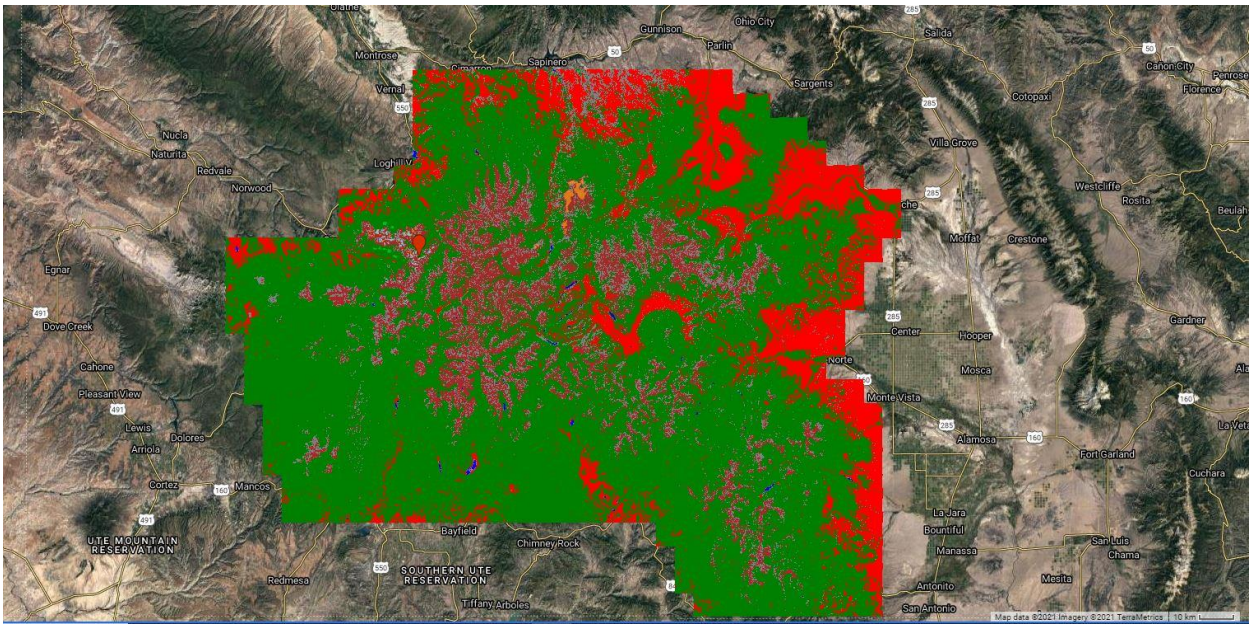

Fig. 24 - Trial-2 random-forest landcover classification map produced in Google Earth Engine® for the San Juan Mountains, CO. (grey = rock glacier; green = vegetation; blue = water; burgundy = ridges/peaks; red = urban/miscellaneous).

Whereas results from the first classification scheme greatly overestimated rock glacier landcover surface area, estimated at 76.9550 km^2, the addition of extra training polygons for both rock glaciers and ridges/peaks greatly enhanced the isolation of predicted rock glacier surface area, estimated at 69.6913 km^2. The predicted rock glacier surface area for the second classification scheme was close to the estimated rock glacier surface area of 70 km^2 predicted by the generalized additive model from Brenning et al. (2007). The resulting mean slope, aspect, and elevation values for the predicted rock glacier landcover area for both classification schemes is shown in Table 3. The predicted rock glacier landcover pixels were isolated in Google Earth Engine® using a binary thresholding procedure, resulting in a black-and-white GeoTIFF image which was ultimately exported, and later imported to ArcMap® for the final volume calculation (Figure 24, 26).

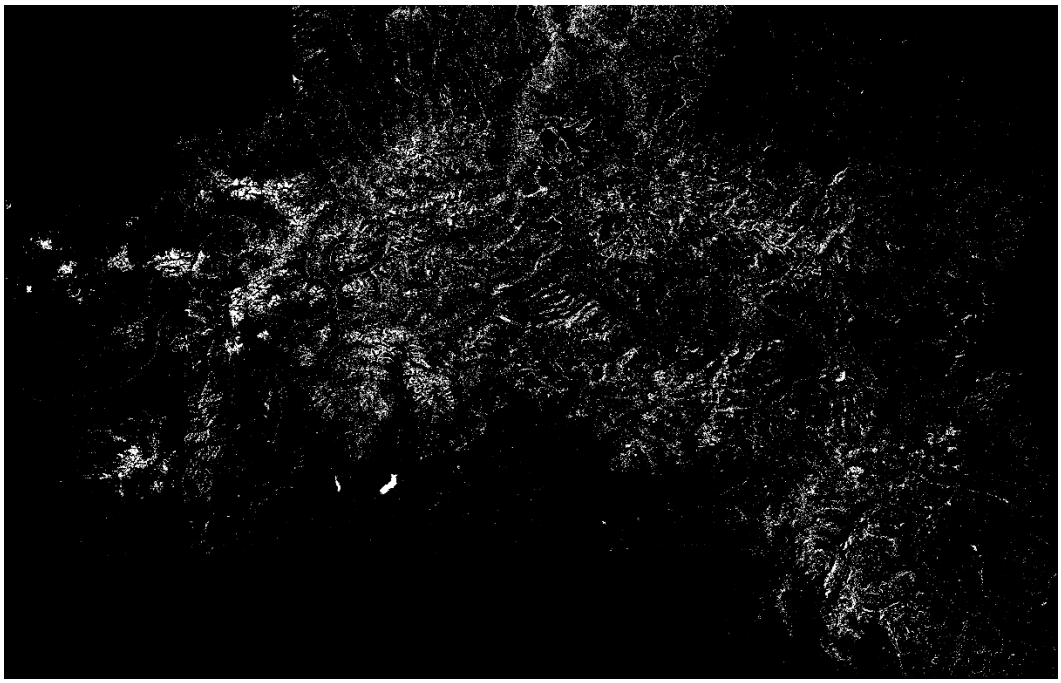

Fig. 25 - Binary-thresholding map produced in Google Earth Engine®, resulting from random-forest image classification of the San Juan Mountains. Classified rock glacier landcover pixels isolated and displayed in white.

Table 3 - Classified rock glacier morphometric parameter pixel results from trial-1 (GEE-1) and trial-2 (GEE-2) of the random forest image classifier used in Google Earth Engine®.

	Surface Area (km^2)	**Mean Elevation (m)**	**Mean Slope (deg)**	**Mean Aspect (deg)**	**Mean Curvature (*1e9)**	**Hillshade**
GEE-1	76.955	3633.219522	17.190057	196.110348	5.799024948	196.268514
GEE-2	69.6913	3435.486998	20.31	207.336203	5.861379792	194.9737

In addition to utilizing a random forest machine-learning image classifier to estimate predicted rock glacier landcover area, Google Earth Engine® was used to derive land surface temperatures based off the locations of digitized rock glacier training polygons. Landsat-8 surface reflectance data provide land surface temperature values, from which temperature data for the period of March 2013 to November 2020 were collected using Band-10. These Band-10 data were originally recorded at 100 m spatial resolution, and were subsequently resampled using cubic convolution to a spatial resolution of 30 m. While this thesis is not primarily focused on a rigorous thermal analysis of rock glacier insulation as it relates to internal permafrost residence time, and subsequently to baseflow discharge volumes, it is still necessary to illustrate temperature trends for rock glacier surfaces in the context of climate change – especially considering how the hydrologic importance of rock glaciers, as opposed to clean-ice glaciers, is directly related to the insulating characteristics of supraglacial rock glacier taluses. To better understand the temperature fluctuation trends, an oscillatory harmonic wave function was fit to the data, whereby temperature peaks and troughs can be observed with regard to seasonal variations (Figure 25).

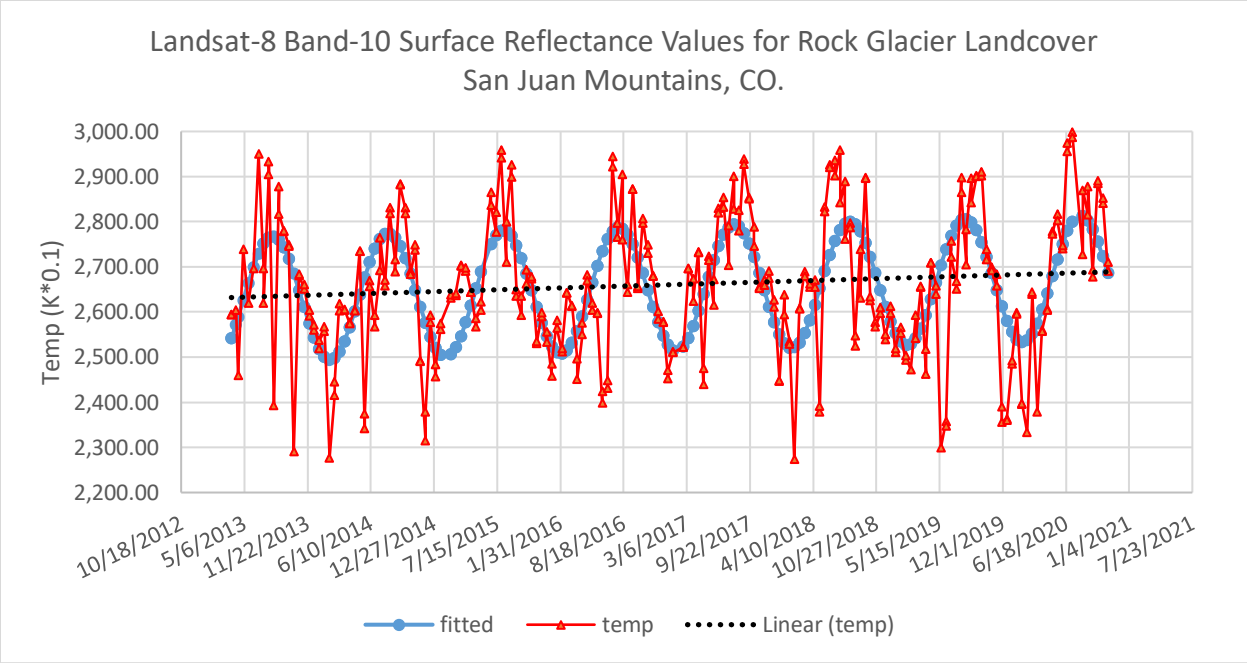

Fig. 26 - Lansdat-8 (Band-10) raw surface reflectance data (red) and fitted oscillatory harmonic wave model (blue) time-series of all 150 rock glacier training polygon locations between March 2013 to November 2020. Black dotted line represents linear temperature trend. Data and chart collected and generated by author using Google Earth Engine®.

Based off the temperature trendline for these Landsat-8 land surface temperature data, rock glacier surface temperatures for the time period of March 2013 to November 2020 have experienced an overall temperature increase of 4.45°C. The availability of remotely-sensed thermal data such as those provided by Landsat-8 thermal bands, in addition to the free access to cloud-computing GIS and remote-sensing platforms such as Google Earth Engine®, bodes well for future studies of rock glaciers and the importance of their water and ice stores.

6.5 Ice-debris Volume Estimation

The primary objective of this thesis is an investigation into volumetric estimation of water and ice inventories contained within rock glaciers in the 21,656 km^2 San Juan Mountain study area, specifically via the integration of remotely-sensed data and geospatial approaches. This was accomplished by incorporating multispectral satellite imagery, LiDAR-derived digital elevation model data, textural and morphometric derivatives of DEM data, and a random-forest machine-learning image classifier run in Google Earth Engine®. Following the classification of landcover classes in Google Earth Engine®, and the isolation of predicted rock glacier pixels via a binary-thresholding procedure, the resultant GeoTIFF image produced from the classification scheme constituted one of two necessary data inputs to perform the final rock glacier water volume calculation (Figure 24, 26).

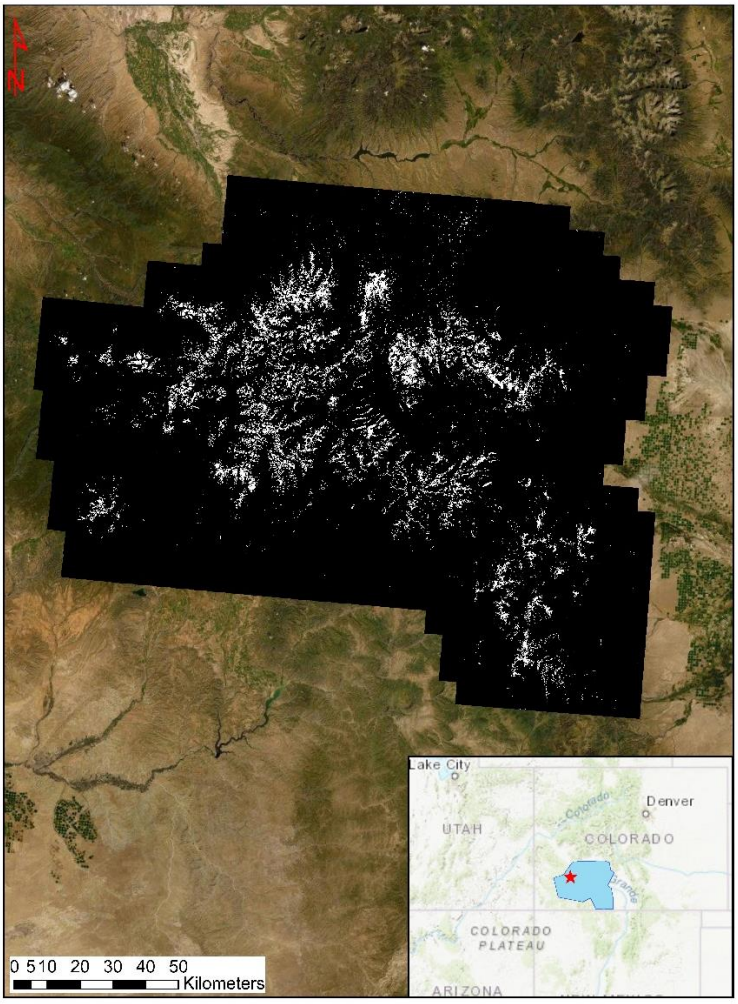

Fig. 27 - GeoTIFF image of classified rock glacier pixels (white) exported from Google Earth Engine®.

To ultimately validate efficacy of the machine-learning approach used in this thesis, the results of predictive rock glacier characteristics, namely mean elevation, slope, aspect, curvature, and hillshade values, for predicted rock glacier pixels were compared against the values of all 1,052 rock glacier points manually mapped in ArcMap®. Elevation, slope, aspect, curvature, and hillshade were chosen as comparative variables based off literature (Barsch, 1996; Brenning et al., 2007; Giardino, 1979; Giardino & Vitek, 1985; Wahrhaftig & Cox, 1959; White, 1979), as well

as the statistical summaries produced in ArcMap®. The results of the two image classification schemes (i.e. GEE-1 and GEE-2), yielded predicted rock glacier pixel surface areas of 76.955 km^2 and 69.691 km^2 respectively. Additionally, the results of GEE-1 yielded mean slope, elevation, aspect, curvature, and hillshade values of 3633.22 m, 17.19°, 196.11°, 5.80, and 196.27 respectively, while GEE-2 yielded values of 3435.49 m, 20.31°, 207.34°, 5.86, and 194.97 respectively. Mean elevation, slope, aspect, curvature, and hillshade values for all 1,052 manually mapped rock glacier points were 3612.14 m, 17.73°, 188.79°, 1.3, and 195.29, respectively.

The predicted rock glacier pixel locations generated for GEE-1 and GEE-2 were run through the volume estimation workflow as previously described, where estimated rock glacier thicknesses greater than 60 m were initially eliminated from the water and ice volume calculations (Table 4). Using the predicted rock glacier landcover areas generated by the random forest image classifier in Google Earth Engine®, rock glacier "thickness maps" were produced based off the differences between DEM surface terrain, and inferred rock glacier bases estimated in the volume estimation workflow as detailed earlier. These thickness maps seldom spanned the entire rock glacier extent, as a result of filtering out negative thickness estimates, so it is very likely that final water and ice volume calculations are underestimated (Figure 27).

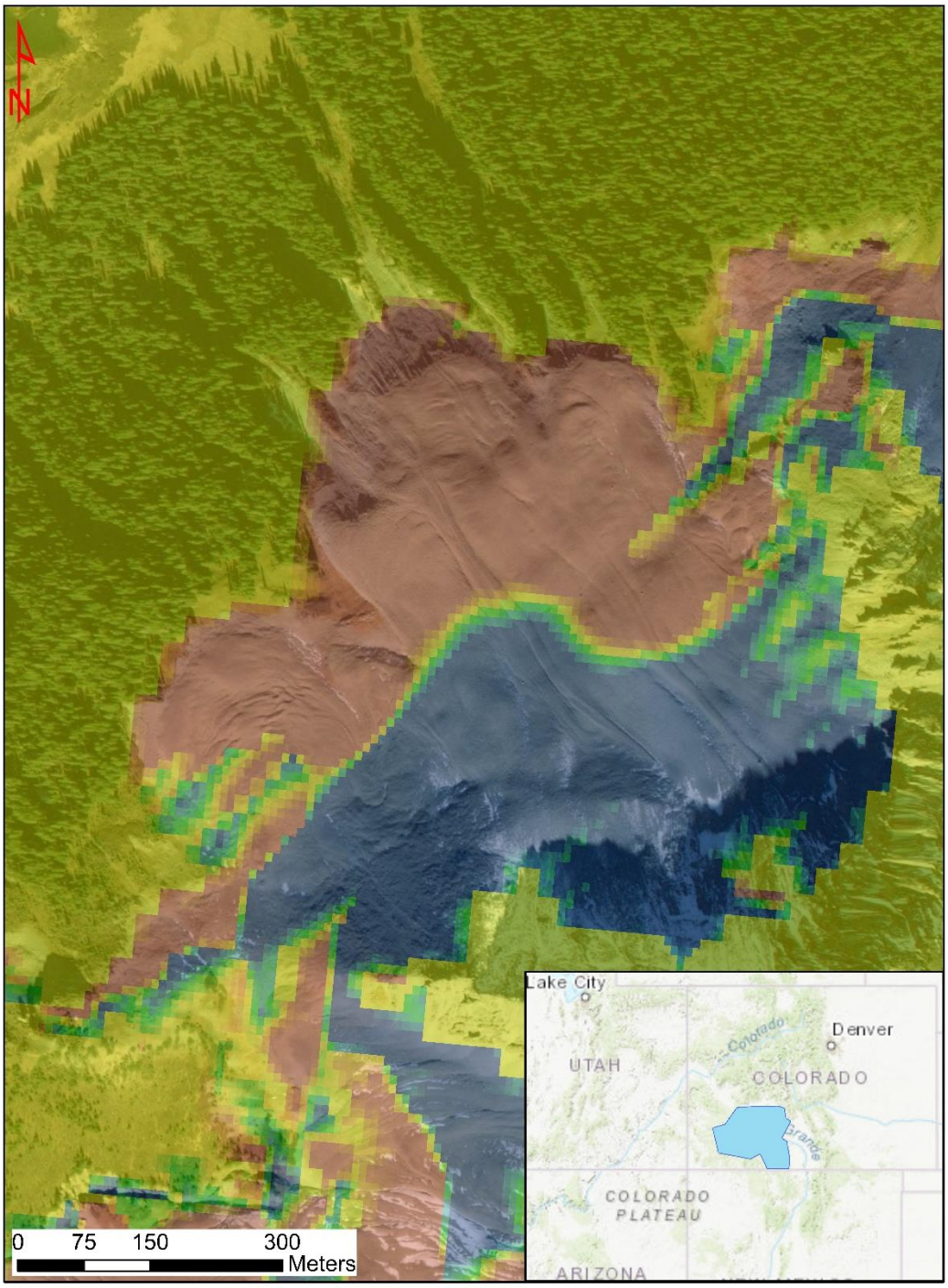

Fig. 28 - Rock glacier thickness map demonstrating positive (red) and negative (blue) thickness estimates. All negative thickness estimates were eliminated from the final calculations of water and ice volumes.

Table 4 – Rock glacier ice and water volume estimates from GEE-1 and GEE-2 for rock glaciers less than 60 m thick.

RG < 60m thickness	**40% ice (km^3)**	**60% ice (km^3)**	**40% water (km^3)**	**60% water (km^3)**
GEE-1	2.17303892	3.259558385	1.95573503	2.933602547
GEE-2	0.860429671	1.290644507	0.774386704	1.161580056

As mentioned by Barsch (1996a), rock glaciers are estimated to reach thicknesses up to 100 m, and it is estimated that rock glaciers in the San Juan Mountains, particularly in large amphitheater-cirques, can exceed these thicknesses. To determine a true, unfiltered, estimated water inventory based off the semi-automated machine-learning methods used in this thesis, maximum estimated rock glacier thicknesses generated by the volume estimation procedure were included in a secondary volume calculation. Including maximum estimated thickness values, the secondary volume estimates are shown in Table 5.

Table 5 – Rock glacier ice and water volume estimates from GEE-1 and GEE-2 for all predicted rock glacier thicknesses.

	ice (40%)	**ice (60%)**	**water (40%)**	**water (60%)**	**Max RG Thickness (m)**
GEE-1	2.357067872	3.535601809	2.121361085	3.182041628	127.3283
GEE-2	1.046120774	1.569181161	0.941508696	1.412263044	154.6757

Assuming an internal ice/water mixture of 40% - 60%, based off the updated GEE-2 results, the estimated water volumes in the San Juan Mountains are 0.94 – 1.41 km^3 spanning a predicted surface area of 69.691 km^2.

The emphasis for important rock glacier characteristics of elevation, slope, aspect, curvature, and hillshade were based off aforementioned studies, in addition to the statistical mean results of these variables as derived in ArcMap®. Of these five predictive variables, elevation, slope, and curvature were noted to be the most diagnostic features. The distribution of elevation, slope, and curvature values from GEE-1 and GEE-2 runs were compared against the raw data derived from the 1,052 manually mapped rock glacier points (Figures 28 – 33).

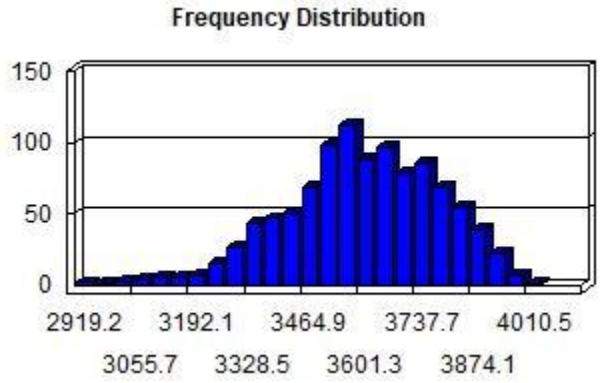

Fig. 29 - Elevation results from manually mapped rock glacier points.

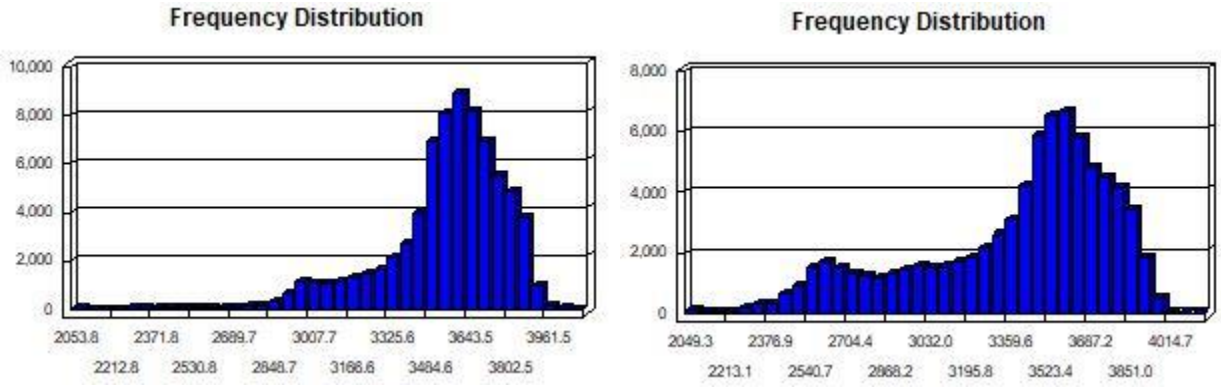

Fig. 30 - Mean elevation results from GEE-1 (left) and GEE-2 (right).

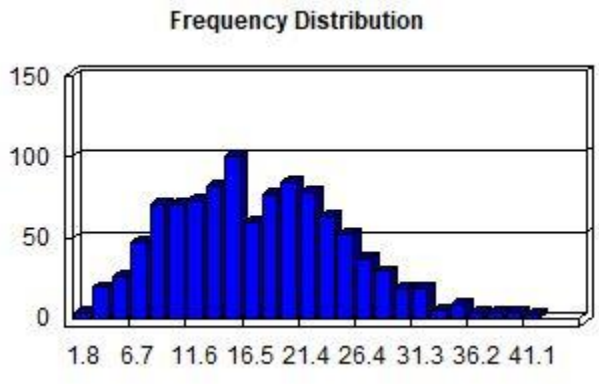

Fig. 31 - Slope results from manually mapped rock glacier points.

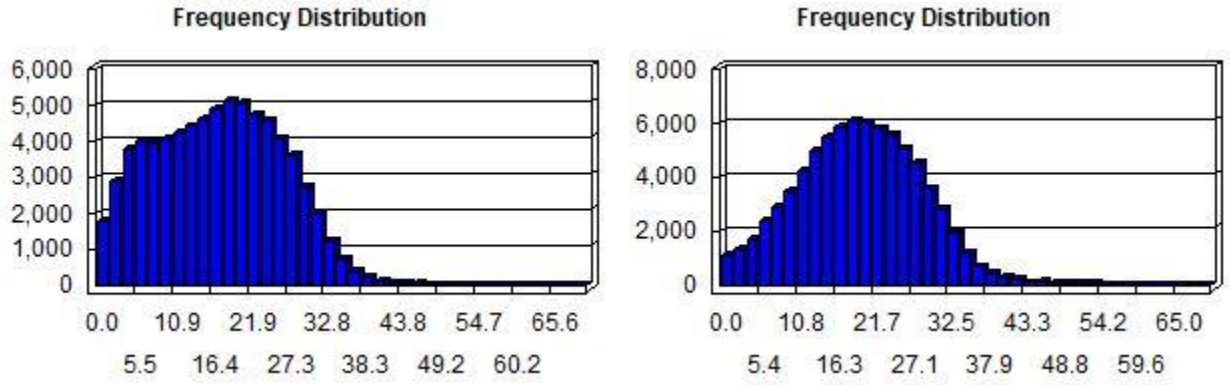

Fig. 32 - Mean slope results from GEE-1 (left) and GEE-2 (right).

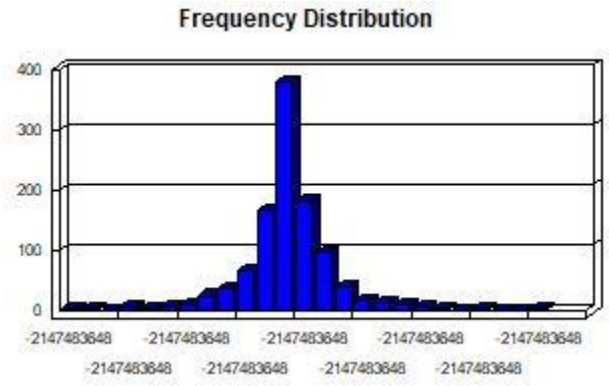

Fig. 33 - Curvature results from manually mapped rock glacier points.

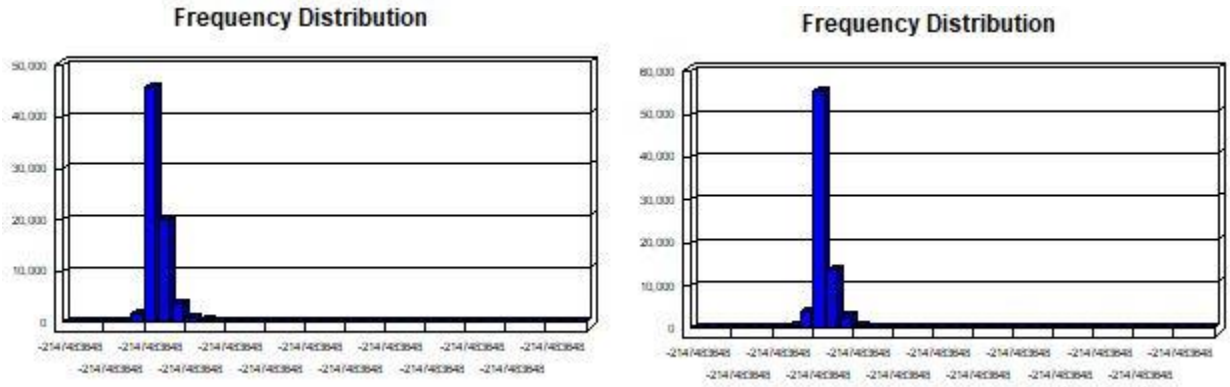

Fig. 34 - Mean curvature results from GEE-1 (left) and GEE-2 (right).

To fully demonstrate the clustered relationship between slope, curvature, and elevation as predictive rock glacier variables, mean values from all 1,052 manually mapped rock glacier points were plotted against one another on a series of 3-axis graphs in Rstudio® (Figures 34 - 36).

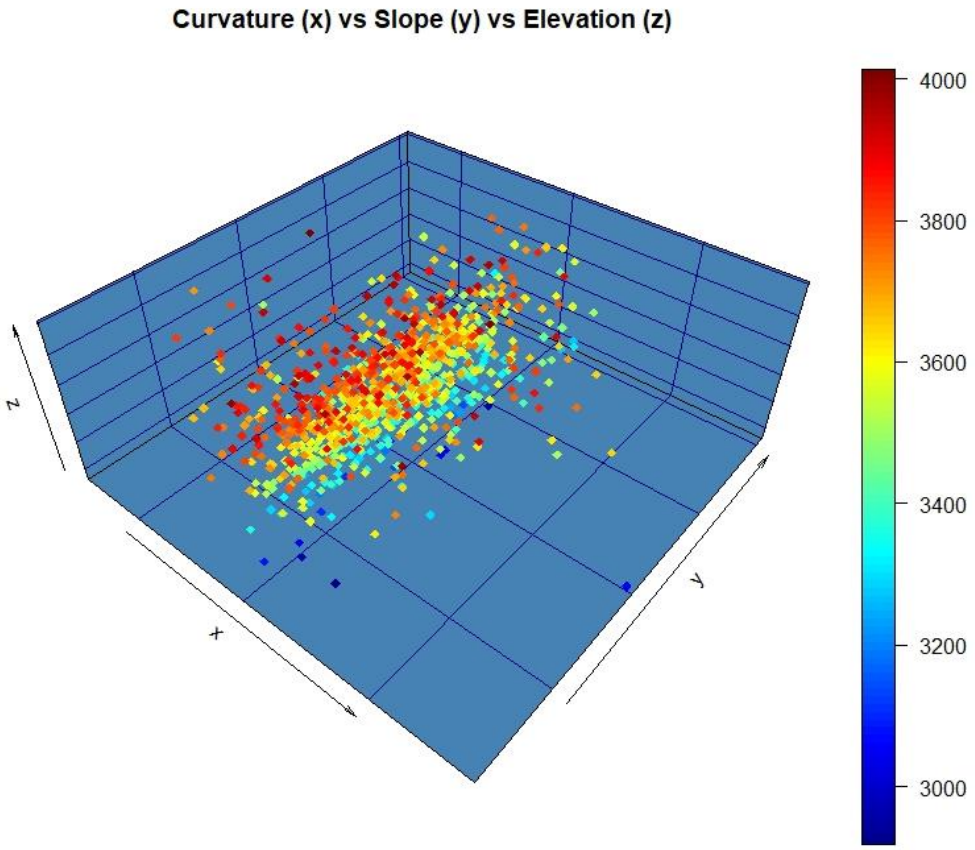

Fig. 35 - Raw data from 1,052 manually mapped rock glacier points. Predictive rock glacier variables of curvature (x-axis), slope (y-axis), and elevation (z-axis) demonstrate significant clustering especially for curvature values.

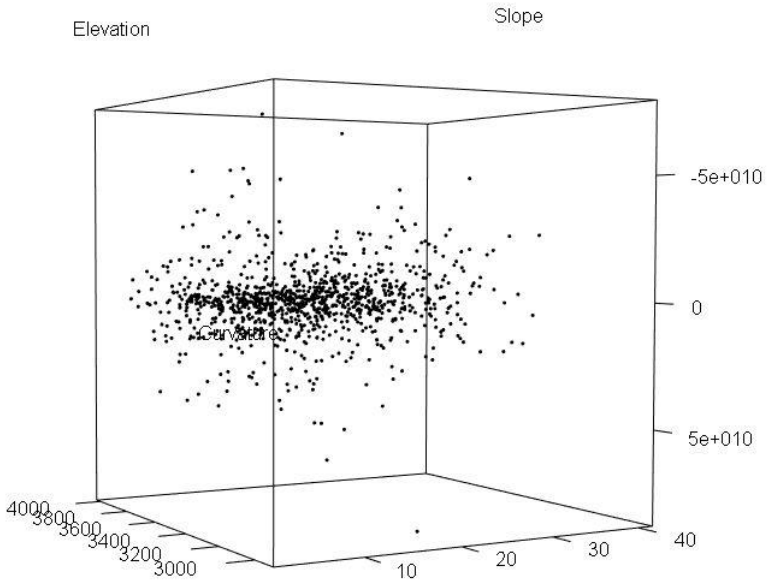

Fig. 36 - Raw data from 1,052 manually mapped rock glacier points. Predictive rock glacier variables of curvature, slope, and elevation showing clustered relationship. Orientation-1.

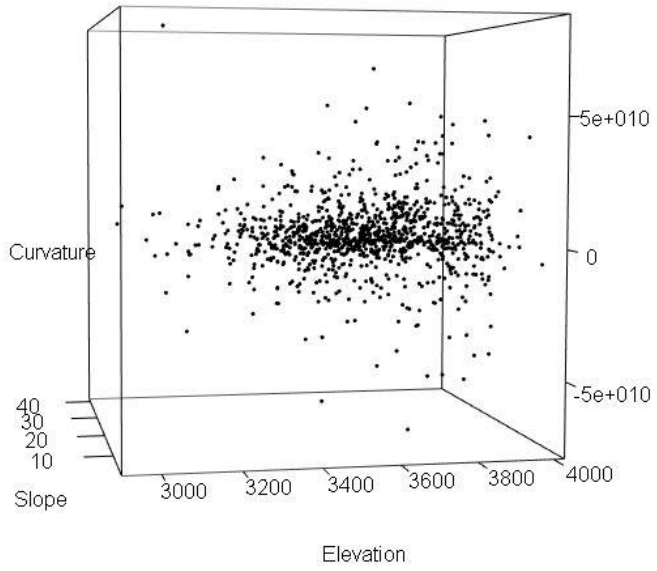

Fig. 37 - Raw data from 1,052 manually mapped rock glacier points. Predictive rock glacier variables of curvature, slope, and elevation showing clustered relationship. Orientation-2.

Furthermore, to fully express the statistical distribution of raw elevation, slope, and curvature data, and to represent the outlier data present between all datasets, box-and-whisker plots were created in Rstudio® (Figures 37 – 39). Mean data values from GEE-1 and GEE-2 for all five predictive rock glacier variables including elevation, slope, curvature, aspect, and hillshade were later graphically compared against mean data values from all 1,052 manually mapped rock glacier point data.

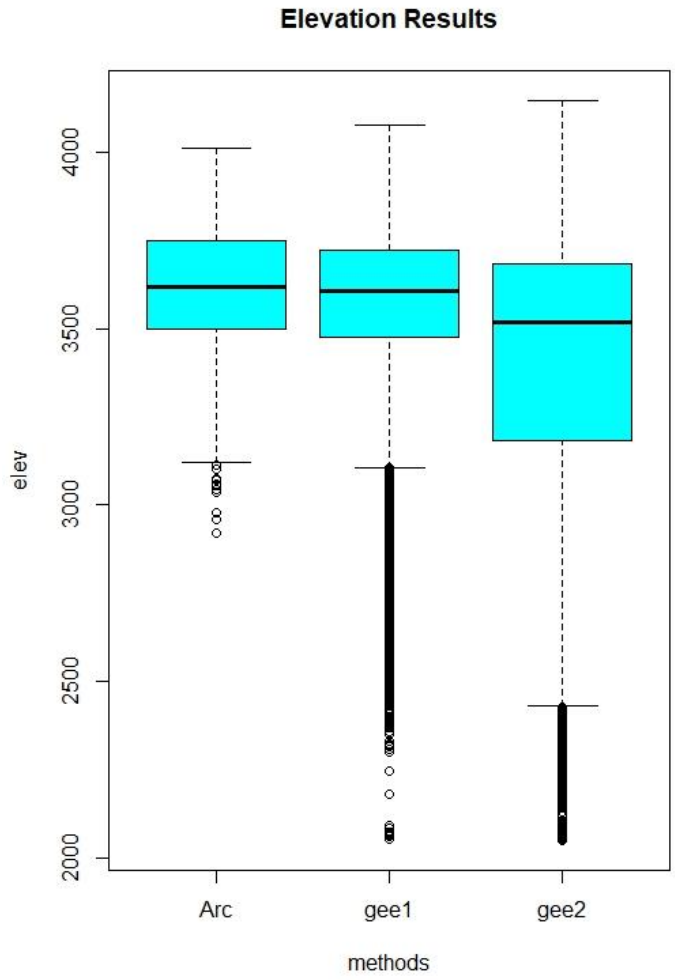

Fig. 38 - Raw elevation data results for GEE-1, GEE-2, and manually mapped rock glacier point data.

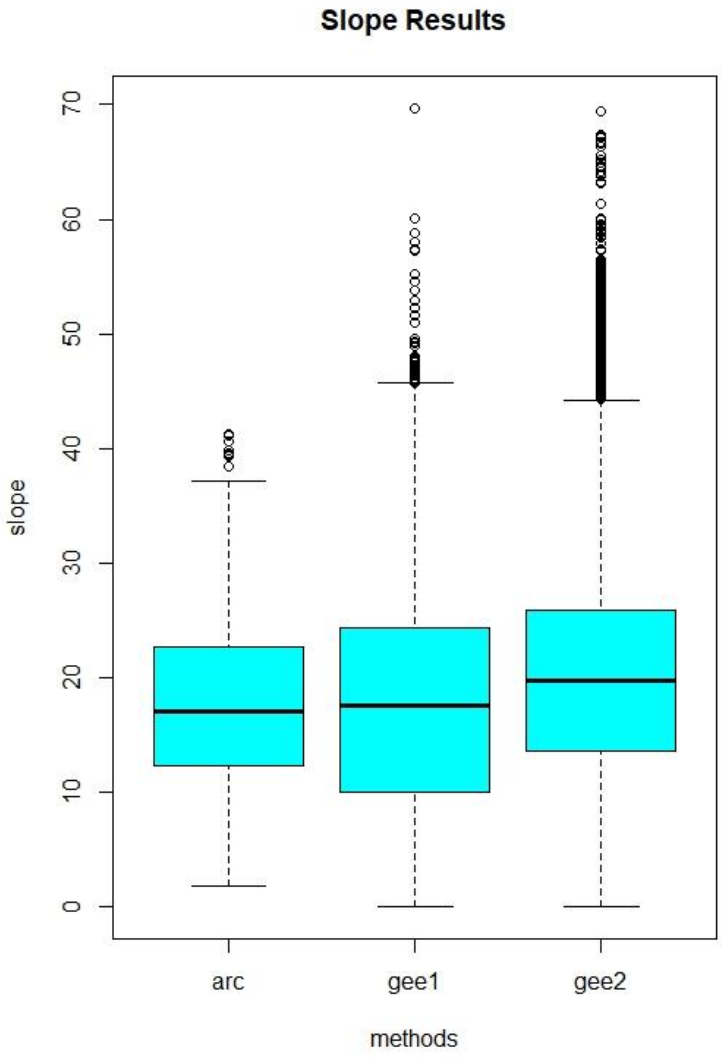

Fig. 39 - Raw slope data results for GEE-1, GEE-2, and manually mapped rock glacier point data.

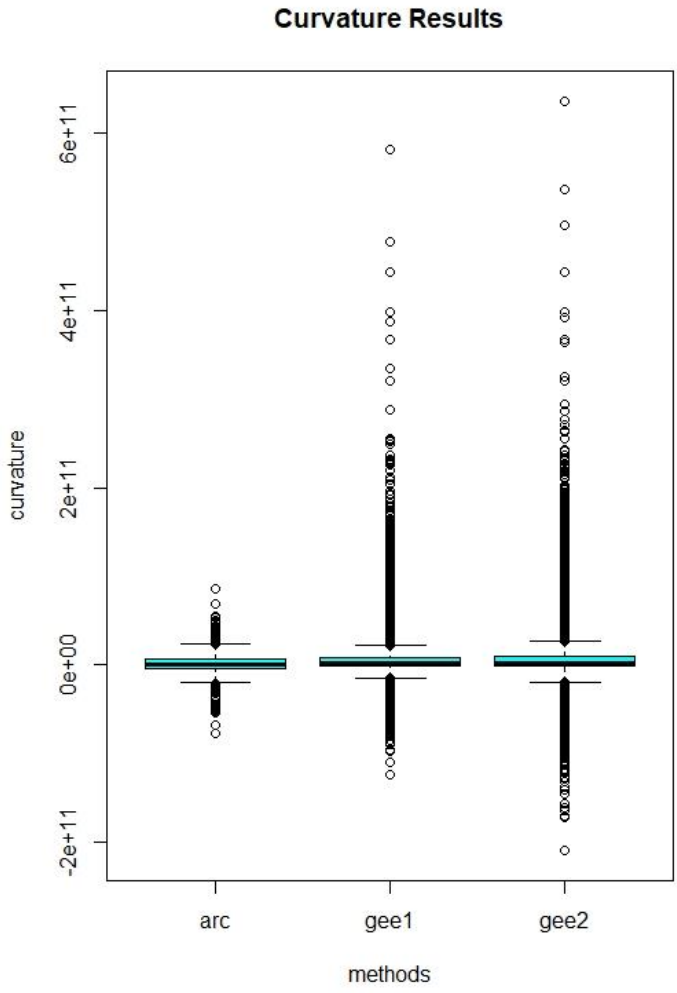

Fig. 40 - Raw curvature data results for GEE-1, GEE-2, and manually mapped rock glacier point data.

The results of the box-and-whisker plots reveal a large amount of outlier data for both GEE-1 and GEE-2 trial runs. It is assumed that the primary reason for the outlier data is a direct result of using a machine-learning image classifier in Google Earth Engine®. In several areas throughout the San Juan Mountains study area, especially during the GEE-1 trial run, the random forest image classifier became confused by the surface terrain, resulting in misclassified rock

glacier landcover. In areas where the image classifier performed poorly, misclassified rock glacier landcover was predicted sporadically at very small, sometimes pixel-sized scales. While a large majority of these misclassified pixel-sized areas were removed during the speckle-filtering step of the volume estimation workflow, many areas retained small clusters of predicted rock glacier pixels, which ultimately yielded small triangular polygons produced after converting the initial GeoTIFF raster image to a series of polygon features (Figure 40).

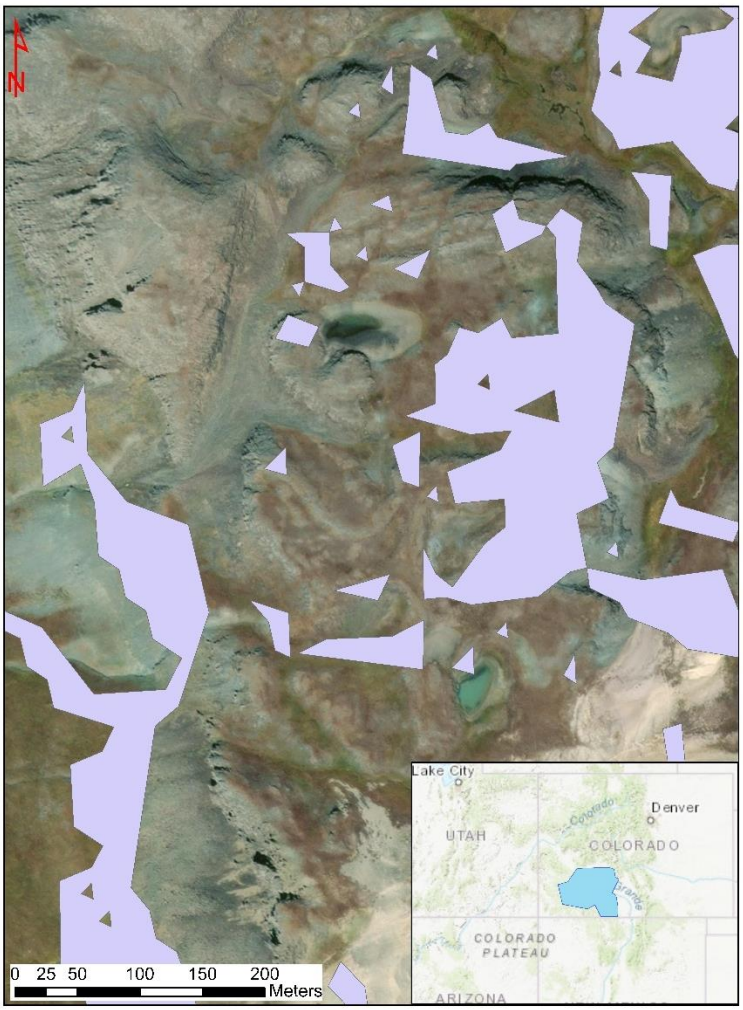

Fig. 41 - Misclassified rock glacier landcover from GEE-1 trial run. Purple polygons represent predicted rock glacier pixel areas.

By iteratively performing the speckle-filter procedure several more times, it is likely that a majority of the misclassified rock glacier polygons constituting the large number of outlier data would be removed. Additionally, by incorporating minimum-contributing rock glacier surface area information into the random forest classifier, it is possible that predicted rock glacier landcover could be contained within a range of predicted surface areas. Regardless, however, mean elevation, curvature, and slope values results for GEE-1, GEE-2, and all 1,052 manually mapped rock glacier points are in rather noteworthy agreement as demonstrated in the box-and-whisker plots in Figures 37-39. As a final step to demonstrate similarities between manual analyst rock glacier mapping procedures, and machine-learning image classification procedures, the mean value results for all five predictive rock glacier variables (i.e., elevation, slope, curvature, aspect, hillshade) generated by GEE-1, GEE-2, and manually mapped rock glacier point data were graphically compared against each other, shown in Appendix A. R-squared values produced from these graphical comparisons range from 0.896 – 0.99, suggesting that the use of machine-learning image classifiers such as decision-trees (i.e. random forest) can provide an effective means of classifying rock glacier landcover using remotely-sensed data.

Overall, the results generated from the random-forest image classifier run in Google Earth Engine® were better than previously expected. As a final measure of validity between predicted rock glacier landcover areas produced in GEE-1 and GEE-2, and manually mapped rock glacier point data, the percentage of overlapping points versus predicted rock glacier area polygons was calculated, with a 90.3% overlap between GEE-1 and manually mapped rock glacier points, and an 85.64% overlap between GEE-2 and manually mapped points. It is assumed that the decrease in overlap percentage for GEE-2 is a direct result of the lower predicted rock glacier surface area of 69.691 km^2 for GEE-2 versus the predicted rock glacier surface area of 76.955 km^2 for GEE-1.

As mentioned before, of the three studies that have examined rock glacier populations in the San Juan Mountains, (Brenning et al., 2007; Johnson, B. 2017; White, P. 1979), only the study by Brenning et al. (2007) attempted to estimate rock glacier water and ice volumes using a predictive statistical generalized additive model. The study by Brenning statistically modeled morphometric parameters, incoming solar radiation, and contributing surface area from a stratified random sample of five landcover classes including 84 rock glacier points, 329 debris points, 1154 grass/shrub points, 663 forest points, and 677 exposed bedrock points. Brenning's study additionally included an accuracy assessment for the predictive power of the generalized additive model (GAM) used. The accuracy assessment was performed via the area under the receiver-operating characteristic curve (ROC or AUROC), which bases accuracy on a 0.5-1 scale, with values closer to 1 demonstrating an "excellent" measure of fit for the GAM model. The results from Brenning's study produced an AUROC value of 0.91, suggesting that the estimated rock glacier population of 900-1300 features, the estimated total rock glacier surface area of 70 km^2, and the estimated rock glacier water volumes of 0.5-0.76 km^3 (40-60% internal content) are reasonable estimates. The results of this thesis confirm the estimated rock glacier population of 900-1300 features via the manually mapped population of 1,052 rock glaciers, and additionally confirm the validity of an estimated 70 km^2 rock glacier surface area by reproducing a similar surface area of 69.691 km^2. The estimated water volumes generated by the volume estimation procedure developed in this thesis are higher than the water volumes estimated in Brenning's study. Major differences in estimated water volumes are almost certainly the direct result of an assumed thickness of 20 m for all rock glaciers in Brenning's study, whereas rock glacier thicknesses used in this thesis are estimated based off differences in rock glacier surface elevations and interpolated rock glacier base elevations produced via the use of a 10 m USGS DEM and the

aforementioned volume estimation procedure. Because estimated rock glacier thicknesses in this study are directly derived from LiDAR elevation data and interpolated rock glacier base elevations, these results asuggest that a significantly larger water inventory of 0.94 – 1.41 km^3 may be more reasonable. By utilizing raw DEM elevation data in lieu of the empirical area-thickness power-law relationship proposed by Brenning (2005) and Azocar & Brenning (2010) for estimating rock glacier ice-debris thicknesses, based off observations of rock glaciers in the Swiss Alps by Barsch (1977b), this thesis proposes an alternate approach towards volumetric water and ice estimation for rock glaciers in the San Juan Mountains.

7. CONCLUSION

This primary motivation for this thesis stems from global concerns of water availability as it relates to climate change and population expansion. The implications of these methods and results pertain to alpine regions, where many communities are almost entirely reliant on seasonal meltwater runoff. It is hoped that by addressing water availability issues at more localized scales, water budgets can be more effectively monitored and protected, ultimately lending towards better management of global water resources.

A variety of estimation approaches for rock glacier water volumes were examined, including the combination of a generalized rock glacier volume model and ICESat-2 data, the in-situ collection of rock glacier morphometric and GPS data and manual creation of digital elevation models, and the ultimate integration of a machine-learning random forest image classifier and volume estimation procedure. The results of integrating the generalized rock glacier volume model with ICESat-2 data were compared against the results of an in-situ derived DEM and subsequent volume estimate for the Camp Bird rock glacier. It was shown that ICESat-2 data, and the use of a generalized rock glacier volume model, greatly overestimate water volumes as compared against estimated water volumes produced via the use of in-situ field data and a manually generated DEM.

Ultimately, the combination of a random forest image classifier, a 10 m USGS DEM, and a volume estimation procedure developed for this thesis, yielded estimated rock glacier surface areas, mean morphometric values, and estimated water volumes of great similarity to those produced by a similar study by Brenning et al. (2007) in the same San Juan Mountain study area. Brenning's study constitutes the only proposed water volume estimation for all rock glaciers in the San Juan Mountains. To further validate predicted rock glacier landcover, classified by the

random forest image developed in Google Earth Engine®, all observable rock glaciers in the near-entire San Juan Mountain extent of 21,656 km^2 were manually mapped in ArcMap 10.7®, with a total of 1052 rock glaciers observed. Validation of predicted rock glacier landcover generated by the random forest image classifier was assessed by comparing mean elevation, slope, curvature, aspect, and hillshade values for GEE-1 and GEE-2 trial runs against raw elevation, slope, curvature, aspect, and hillshade values from the 1,052 manually mapped rock glacier point data. The results of these comparisons are shown via box-and-whisker plots (Figures 37 – 39) with mean values for GEE-1, GEE-2, and manual point data graphically compared (Appendix A).

While all results in this thesis may still be considered first-order approximations, the strong statistical similarities between morphometric values like elevation, slope, curvature, aspect, and hillshade between GEE-1, GEE-2, and all 1,052 manually mapped rock glacier point data, suggest that machine-learning image classification approaches for rock glacier landcover predictions may be effective. Furthermore, the similarities of predicted rock glacier surface area, mean morphometric values, and estimated water and ice volumes between the results presented herein, and the results of Brenning et al. (2007), suggest that the volume estimation methodologies proposed in this thesis may offer a different approach for estimating water and ice volumes contained within rock glaciers, especially those contained within the San Juan Mountains, CO. In light of these findings, the proposed hypothesis of this thesis is considered valid.

Lastly, the results of this thesis highlight many shortcomings of these methods, namely the inaccuracies that arise from inferring rock glacier bases by means of interpolation, the uncertainties that exist from using coarse spatial resolution DEM data such as the 10 m USGS

DEM utilized in this thesis, and the water/ice volume underestimation that results from the rock glacier thickness estimation procedure. It is expected that bolstering the predictive power of the random forest image classifier via the addition of landcover class training polygons, and by incorporating higher spatial resolution DEM data, the estimation of water and ice volumes contained within rock glaciers can be greatly improved. For now, I consider the estimation of rock glacier water and ice volumes an important step towards understanding the water resources available to alpine communities, a step which may further provide means of allocating water resources as climate changes persist. Perhaps, one day similar methodologies may even be employed for the exploration of water resources contained within Martian rock glaciers for future colonies.

REFERENCES

Apaloo, J., 2013. Thermal and Hydrological Response of Rock Glaciers to Climate Change: A Scenario Based Simulation Study. [M.S. thesis]: Ontario, Canada. University of Waterloo. 1–171.

Atwood, W.W., Mather, K.F., 1932. Physiography and Quaternary Geology of the San Juan Mountains, Colorado. U.S. Geological Survey Professional Paper 166, 1–122.

Azócar, G.F., Brenning, A., 2010. Hydrological and geomorphological significance of rock glaciers in the dry Andes, Chile (27°-33°s). Permafr. Periglac. Process. 21, 42–53. https://doi.org/10.1002/ppp.669

Bailey, B.K., 2020. Rock Glacier Development in the San Juan Mountains. [M.S. thesis]: Denver, Colorado. University of Denver. 1–70.

Bajewsky, I., Gardner, J.S., 1989. Discharge & Sediment-Load Characteristics of the Hilda Rock-Glacier Stream, Canadian Rocky Mountains, Alberta. 3646. https://doi.org/10.1080/02723646.1989.10642384

Baltensperger, U., Gaggler, H., Gloor, M., Hoehn, E., Keil, R., 1990. Chemical composition. In: (Eds.), Pilot Analyses of Permfrost Cores from the Active Rock Glacier Murtel, Piz Corvatsch, Eastern Swiss Alps. A Workshop Report. Arbeitsheft VAW/ETHZ, Haeberli W pp. 24–26.

Barcaza, G., Nussbaumer, S.U., Tapia, G., Valdés, J., García, J.L., Videla, Y., Albornoz, A., Arias, V., 2017. Glacier inventory and recent glacier variations in the Andes of Chile, South America. Annals of Glaciology 58, 166–180. https://doi.org/10.1017/aog.2017.28

Barsch, D., 1971a. Rock Glaciers and Ice-Cored Moraines. Geografiska Annaler: Series A, Physical Geography 53, 203–206. https://doi.org/10.1080/04353676.1971.11879846

Barsch D., 1977b. Ein Permafrostprofi1 aus Graubunden, Schweizer Alpen. Z Geo- morpho1 NF 21:79-86.

Barsch, D., 1996a. Rockglaciers: Indicators for the Present and Former Geoecology in High Mountain Environments. Springer-Verlag, Berlin, 331 pp.

Barsch, D., 1996b. Summary and Outstanding Problems 269–271. https://doi.org/10.1007/978-3-642-80093-1_12

Barsch, D., 1996c. Rockglaciers: Description and Morphometry 18–30. https://doi.org/10.1007/978-3-642-80093-1_4

Barsch D, Hell G., 1975. Photogrammetrische Bewegungsmessungen am Blockgletscher Murtel I Oberengadin, Schweizer Alpen. Z Gletscherk Glazialgeol 11: 111-142.

Barsch, D., Updike, R., 1971b. Late Pleistocene Periglacial Geomorphology (Rock Glaciers and Blockfields) at Kendrick Peak, Northern Arizona. Arizona Geological Society Digest IX, 225–243.

Berta, S.M., 1982. The analysis and interpretation of spectral reflectance signatures from rock glaciers. [M.S. thesis]: Flint, Michigan. University of Michigan. 1-88.

Berthling, I., 2011. Beyond confusion: Rock glaciers as cryo-conditioned landforms. Geomorphology, 131, 98–106. https://doi.org/10.1016/j.geomorph.2011.05.002

Bhardwaj, A., Kumar, P., Kumar, M., Sam, L., Gupta, R.D., 2014. Mapping debris-covered glaciers and identifying factors affecting the accuracy. Cold Regions Science and Technology 106–107, 161–174. https://doi.org/10.1016/j.coldregions.2014.07.006

Bishop, M., Bonk, R., Kamp, U., 2001. Terrain Analysis and Data Modeling for Alpine Glacier Mapping. Polar Geography. 25. 182-201. 10.1080/10889370109377712.

Bishop, M.P., Olsenholler, J.A., Shroder, J.F., Barry, R.G., Raup, B.H., Bush, A.B.G., Copland, L., Dwyer, J.L., Fountain, A.G., Haeberli, W., Kääb, A., Paul, F., Hall, D.K., Kargel, J.S., Molnia, B.F., Trabant, D.C., Wessels, R., 2004. Global Land Ice Measurements from Space (GLIMS): Remote sensing and GIS investigations of the Earth's Cryosphere. Geocarto International 19, 57–84. https://doi.org/10.1080/10106040408542307

Bolch, T, Buchroithner, M., Pieczonka, T., Kunert, A., 2008. Planimetric and volumetric glacier changes in the Khumbu Himal, Nepal, since 1962 using Corona, Landsat TM and ASTER data, Journal of Glaciology, 54, 592-600.

Bolch, T., Kamp, U., 2006. Glacier mapping in high mountains using DEMs, Landsat and ASTER data. In Kaufmann V and Sulzer W eds. Proceedings of the 8th International Symposium on High Mountain Remote Sensing Cartography, 21–27 March 2005, La Paz, Bolivia. Karl Franzens University, Graz, 13–24 (Grazer Schriften der Geographie und Raumforschung 41).

Bonk, R., 2002. Scale-dependent geomorphometric analysis for glacier mapping at Nanga Parbat: GRASS GIS approach. Proceedings of the open source GIS-Grass users conference, pp. 1–4.

Breiman, L., Friedman, J.H., Olshen, R.A., Stone, C.J., 1998. Classification and Regression Trees.

Brenning, A., 2009. Benchmarking classifiers to optimally integrate terrain analysis and multispectral remote sensing in automatic rock glacier detection. Remote Sensing of Environment 113, 239–247. https://doi.org/10.1016/j.rse.2008.09.005

Brenning, A., 2005. Climatic and geomorphological controls of rock glaciers in the Andes of Central Chile: Combining statistical modelling and field mapping. Dissertation 153. https://doi.org/10.1002/ppp.528

Brenning, A., Grasser, M., Friend, D.A., 2007. Statistical estimation and generalized additive modeling of rock glacier distribution in the San Juan Mountains, Colorado, United States. Journal of Geophysical Research: Earth Surface 112. https://doi.org/10.1029/2006JF000528

Brenning, A., Long, S., Fieguth, P., 2012. Detecting rock glacier flow structures using Gabor filters and IKONOS imagery. Remote Sens. Environ. 125, 227–237. https://doi.org/10.1016/j.rse.2012.07.005

Brenning, A., Peña, M.A., Long, S., Soliman, A., 2011. Thermal remote sensing of ice-debris landforms using ASTER. The Cryosphere Discussions 5, 2895–2933. https://doi.org/10.5194/tcd-5-2895-2011

Brenning, A., Trombotto, D., 2006. Logistic regression modeling of rock glacier and glacier distribution: Topographic and climatic controls in the semi-arid Andes. Geomorphology 81, 141–54.

Brighenti, S., Tolotti, M., Bruno, M.C., Engel, M., Wharton, G., Cerasino, L., Mair, V., Bertoldi, W., 2019. After the peak water: the increasing influence of rock glaciers on alpine river systems. Hydrological Processes 33, 2804–2823. https://doi.org/10.1002/hyp.13533

Brown, W.H., 1925. A Probable Fossil Glacier 67, 464–466.

Burbank, W.S., Luedke, R.G., 2008. Geology and Ore Deposits of the Uncompahgre (Ouray) Mining District, Southwestern Colorado.

Caine, N., 2010. Recent hydrologic change in a Colorado alpine basin: An indicator of permafrost thaw?, Ann. Glaciol., 51(56), 130–134. https://doi.org/10.3189/172756411795932074

Capps, S.R., 1910. Rock glaciers in Alaska. J. Geol., 18(4), 359–375.

Carrara, P., Andrews, J., 1975. Holocene glacial/periglacial record, Northern San Juan Mountains, Southwestern Colorado. Z Gletscherkd Glazia1geol 11:155-174.

Charbonneau, A.A., Smith, D.J., 2018. An inventory of rock glaciers in the central British Columbia Coast Mountains, Canada, from high resolution Google Earth imagery. Arctic, Antarctic, and Alpine Research 50. https://doi.org/10.1080/15230430.2018.1489026

Corte, A., 1976. The Hydrological Significance of Rock Glaciers. Journal of Glaciology 17, 157-158.

Cross, W., Howe, E., Ransome, L., 1905. Silverton Folio: USGS Atlas. Folio 120: 40.

Cross, W., Larsen, E.S., 1935. A brief review of the geology of the San Juan region of southwestern Colorado. U.S. Geological Survey Bulletin 00, 138.

Degenhardt, J.J., 2002. A MODEL FOR THE DEVELOPMENT OF A LOBATE ALPINE ROCK GLACIER IN SOUTHWEST COLORADO, USA: IMPLICATIONS FOR WATER ON MARS.

Degenhardt, J.J., Giardino, J.R., 2003. Subsurface investigation of a rock glacier using ground-penetrating radar : Implications for locating stored water on Mars 108, 1–17. https://doi.org/10.1029/2002JE001888

Delaloye, R., Lambiel, C., 2005. Evidence of winter ascending air circulation throughout talus slopes and rock glaciers situated in the lower belt of alpine discontinuous permafrost (Swiss Alps). Nor. Geogr. Tidsskr. 59, 194–203. doi: 10.1080/00291950510020673

Derry, J., 2019. Dust-on-Snow: Impacts on Snowmelt & Streamflow. Water Rep. 15–32.

Emmert, A., Kneisel, C., 2017. Internal structure of two alpine rock glaciers investigated by quasi-3-D electrical resistivity imaging 841–855. https://doi.org/10.5194/tc-11-841-2017

Fisch, W. Sen., Fisch, W. Jun., Haeberli, W., 1978. Electrical DC resistivity soundings with long profiles on rock glaciers and moraines in the Alps of Switzerland. Z Glet- scherkd Glazialgeol 13:239-260.

Foster, L.A., 2010. Utilisation of remote sensing for the study of debris-covered glaciers : development and testing of techniques on Miage Glacier , Italian Alps 1–274.

Gamache, K., Giardino, J.R., Zhao, P., Owens, R.H., 2018. Bivouacs of the Anthropocene: Urbanization, Landforms, and Hazards in Mountainous Regions. Urban Geomorphology 205–230. https://doi.org/10.1016/b978-0-12-811951-8.00011-4

Gerhold, N., 1964. Die Blockgletscher - eine besondere Moranenform? [Ph.D Dissertation]: Geogr Inst Univ Innsbruck, 1-200.

Giardino, J.R., 1979. Rock Glacier Mechanics and Chronologies: Mount Mestas, Colorado.

Giardino, J.R., 1983. Movement of ice-cemented rock glaciers by hydrostatic pressure: an example from Mt. Mestas, Colorado. Zeitschrift für Geomorphologie 27, 297-310.

Giardino, J.R., Shroder, J.F., Lawson, M.P., 1978. Movement mechanisms for ice- cemented rock glaciers. American Quaternary Association Abstracts 5:202.

Giardino, J. R., Shroder, J. F., Lawson, M. P., 1984. Tree- ring analysis of movement of a rock glacier complex on Mount Mestas, Colorado, U.S.A. Arctic, Antarctic, and Alpine Research 16, 299–309.

Giardino, J.R., Vick, S.G., 1987. Geologic engineering aspects of rock glaciers. In: Giardino, J.R., Shroder, J.F., Vitek, J.D. (Eds.), Rock Glaciers. Allen and Unwin, Boston, pp. 265–288.

Giardino, J.R., Vitek, J.D., 1985. A Statistical Interpretation of the Fabric of a Rock Glacier. Arctic and Alpine Research 17, 165–177. http://www.jstor.org/stable/1550846

Giardino, J.R., Vitek, J.D., 1988. Interpreting the Internal Fabric of a Rock Glacier. Geogr. Ann. Ser. A Phys. Geogr. 70, 15–25.

Giardino, J.R., Vitek, J.D., Demorett, J.L., 1992. A model of water movement in rock glaciers and associated water characteristics. In: Dixon, J.C., Abrahams, A.D. (Eds.): Periglacial Geomorphology. Wiley, Chichester, pp. 159–184.

Goodrich, L.E., 1982. The influence of snow cover on the ground thermal regime, Can. Geotech. J., 19, 421–432, doi:10.1139/t82-047.

Grasser, M.W., 2006. Statistical estimation and automated mapping of rock glacier occurrence in the San Juan Mountains/Colorado. Diplomarbeit, Institut für Geographie. Erlangen: Friedrich-Alexander-Universität Erlangen–Nürnberg.

Haeberli, W., 1985. Creep of mountain permafrost: internal structure and flow of alpine rock glaciers. Mitt Versuchsanst Wasserbau Hydrol Glaziol ETH Zur 77:142.

Haeberli, W., 1989. Pilot analysis of permafrost cores from the active rockglacier Murtel I, Piz Corvatsch, Eastern Swiss Alps. Versuchsanst Wasserbau Hydrol Glaziol ETH Zur Arbeitsh 9:38.

Haeberli, W., Hallet, B., Arenson, L., Elconin, R., Humlum, O., Ka, A., 2006. Permafrost Creep and Rock Glacier Dynamics 214, 189–214. https://doi.org/10.1002/ppp

Haeberli, W., Hoelzle, M., Kääb, A., Keller, F., Vonder Mühll, D., Wagner, S., 1998. Ten years after drilling through the permafrost of the active rock glacier Murtèl, Eastern Swiss Alps: answered questions and new perspectives. Proc. 5th Int. Conf. on Permafrost, Yellowknife: 403–410.

Hauck, C., Vonder Muhll, D., 2003. Inversion and interpretation of two-dimensional geoelectrical measurements for detecting permafrost in mountainous regions. Permafrost and Periglacial Processes 14, 305–318.

Hauck, C., Vonder Muhll, D., Maurer, H., 2003. Using DC resistivity tomography to detect and characterize mountain permafrost. Geophysical Prospecting 51, 273–284.

Hendrickx, H., Vivero, S., de Cock, L., de Wit, B., de Maeyer, P., Lambiel, C., Delaloye, R., Nyssen, J., Frankl, A., 2019. The reproducibility of SfM algorithms to produce detailed

Digital Surface Models: the example of PhotoScan applied to a high-alpine rock glacier. Remote Sensing Letters 10, 11–20. https://doi.org/10.1080/2150704X.2018.1519641

Hoelzle M, Wegmann M, Krummenacher B. 1999. Min- iature temperature dataloggers for mapping and monitoring of permafrost in high mountain areas: first experiences from the Swiss Alps. Permafrost and Periglacial Processes 10(2): 113–124.

Holt, JW., Safaeinili, A., Plaut, JJ., Head, JW., Phillips, RJ., Seu, R., Kempf, SD., Choudhary, P., Young, DA., Putzig, NE., Biccari, D., Gim, Y., 2008. Radar sounding evidence for buried glaciers in the southern mid- latitudes of Mars. Science, 322(5905), 1235–1238. doi: 10.1126/science. 1164246.

Howe, E., 1909. Landslides in the San Juan Mountains, Colorado: including a con- sideration of their causes and their classification. US Geol Surv Prof Pap 67:58.

Humlum, O., 1982. Rock glacier types on Disko , Central West Greenland. Danish Journal of Geography 82, 59–66. https://doi.org/10.1080/00167223.1982.10649152

Ishikawa, M., 2003. Thermal regimes at the snow–ground interface and their implications for permafrost investigations. Geomor- phology 52 (1–2), 105–120.

Janke, J.R., 2001. Rock Glacier Mapping: A Method Utilizing Enhanced TM Data and GIS Modeling Techniques Rock Glacier Mapping: A Method Utilizing Enhanced TM Data and GIS Modeling Techniques 6049. https://doi.org/10.1080/10106040108542199

Janke, J.R., 2005. The occurrence of alpine permafrost in the Front Range of Colorado 67, 375–389. https://doi.org/10.1016/j.geomorph.2004.11.005

Janke, J.R., 2013. Using airborne LiDAR and USGS DEM data for assessing rock glaciers and glaciers. Geomorphology 195, 118–130. https://doi.org/10.1016/j.geomorph.2013.04.036

Janke, J.R., Bellisario, A.C., Ferrando, F.A., 2015. Classification of debris-covered glaciers and rock glaciers in the Andes of central Chile. Geomorphology 241, 98–121. https://doi.org/10.1016/j.geomorph.2015.03.034

Janke, J.R., Regmi, N.R., Giardino, J.R., Vitek, J.D., 2013. Rock Glaciers, Treatise on Geomorphology. Elsevier Ltd. https://doi.org/10.1016/B978-0-12-374739-6.00211-6

Johnson, B., 2017. Rock Glaciers in the San Juan Mountains, Colorado. New Mex. Geol. Soc. 68th F. Conf. 205–208.

Johnson, G., Chang, H., Fountain, A., 2020. Rock glaciers of the contiguous United States: GIS inventory and spatial distribution patterns 1–26.

Johnson, P.G., 1978. Rock glacier types and their drainage systems, Grizzly Creek, Yukon Territory 1496–1507.

Johnson, P.G., 1981. The structure of a talus-derived rock glacier deduced from its hydrology. Can J Earth Sci 18:1422-1430.

Jones, D.B., Harrison, S., Anderson, K., Betts, R.A., 2018. Mountain rock glaciers contain globally significant water stores. Scientific Reports 8, 1–10. https://doi.org/10.1038/s41598-018-21244-w

Jones, D.B., Harrison, S., Anderson, K., Whalley, W.B., 2019. Rock glaciers and mountain hydrology: A review. Earth-Science Reviews 193, 66–90. https://doi.org/10.1016/j.earscirev.2019.04.001

Jorgensen, W.R., 2007. A Validation of Ground Penetrating Radar for Reconstructing the Internal Structure of a Rock Glacier: Mount Mestas, Colorado, USA. [M.S. thesis]: College Station, Texas. Texas A&M University. 1-81.

Juliussen, H., Humlum, O., 2008. Thermal regime of openwork block fields on the mountains Elgahogna and Solen, central-eastern Norway. Permafrost and Periglacial Processes 19, 1-18.

Keller, F., Gubler, HU., 1993. Interaction between snow cover and high mountain permafrost at Murte`l/ Corvatsch, Swiss Alps. Proceedings of the Sixth International Conference on Permafrost, Beijing, China, 5–9 July 1993. South China University of Technology Press: Wushan, Guangzhou, China; 1, 332–337.

Khan, A.A., Jamil, A., Hussain, D., Jabeen, G.U.L., Malik, M.K., 2020. Machine-Learning Algorithms for Mapping Debris-Covered Glaciers : The Hunza Basin Case Study 8, 12725–12734.

King, L., Fisch, W., Haeberli, W., Waechter, H.P., 1987. Comparison of resistivity and radio-echo soundings on rock-glacier permafrost. Zeitschrift fu¨r Gletscherkunde und Glazialgeologie 23, 77–97.

Kneisel, C., Hauck, C., Fortier, R., Moorman, B., 2008. Advances in geophysical methods for permafrost investigations. Permafr. Periglac. Process. 19 (2), 157–178.

Kofler, C., Steger, S., Mair, V., Zebisch, M., Comiti, F., Schneiderbauer, S., 2020. An inventory-driven rock glacier status model (intact vs. relict) for South Tyrol, Eastern Italian Alps. Geomorphology 350, 106887. https://doi.org/10.1016/j.geomorph.2019.106887

Landry, C.C., Buck, K.A., Raleigh, M.S., Clark, M.P., 2014. Mountain system monitoring at Senator Beck Basin, San Juan Mountains, Colorado: A new integrative data source to develop and evaluate models of snow and hydrologic processes. Water Resources Research 1773–1788. https://doi.org/10.1002/2013WR013711.Received

Leopold, L.B., Wolman, M.G., Miller, J.R., 1964. Fluvial Processes in Geomorphology. W.H. Freeman.

Lillesand, T. M., Kiefer, R. W., and Chipman, J. W., 2004. Remote Sensing and Image Interpretation, John Wiley & Sons, New York.

Lu, D., Weng, Q., 2007. A survey of image classification methods and techniques for improving classification performance. International Journal of Remote Sensing 28, 823–870. https://doi.org/10.1080/01431160600746456

Luetschg, M., Lehning, M., Haeberli, W., 2008. A sensitivity study of factors influencing warm/thin permafrost in the swiss alps. Journal of Glaciology, 54, 696–704. doi:10. 3189/002214308786570881.

Mateo, E.I., 2017. Rock Glacier Hydrology in the San Juan Mountains, Colorado 199.

Mateo, E.I., Daniels, J.M., 2019. Surface hydrological processes of rock glaciated basins in the San Juan Mountains, Colorado. Physical Geography 40, 275–293. https://doi.org/10.1080/02723646.2018.1541707

Maurer, H., Hauck, C., 2007. Geophysical imaging of alpine rock glaciers. J. Glaciol. 53, 110–120. doi: 10.3189/172756507781833893

Mihalcea, C., Mayer, C., Diolaiuti, G., D'Agata, C., Smiraglia, C., Lambrecht, A., Vuillermoz, E., Tartari, G., 2008. Spatial distribution of debris thickness and melting from remote-sensing and meteorological data, at debris-covered Baltoro glacier, Karakoram, Pakistan. Annals of Glaciology 48, 49–57. https://doi.org/10.3189/172756408784700680

Millar, C.I., Westfall, R.D., Delany, D.L., 2013. Thermal and hydrologic attributes of rock glaciers and periglacial talus landforms: Sierra Nevada, California, USA 310. https://doi.org/10.1016/j.quaint.2012.07.019

Millar, C.I., Westfall, R.D., 2019. Geographic, hydrological, and climatic significance of rock glaciers in the Great Basin, USA. Arctic, Antarct. Alp. Res. 51, 232–249. https://doi.org/10.1080/15230430.2019.1618666

Monnier, S., Kinnard, C., 2015. Internal Structure and Composition of a Rock Glacier in the Dry Andes, Inferred from Ground-penetrating Radar Data and its Artefacts 346, 335–346. https://doi.org/10.1002/ppp.1846

Muhammad, S., Thapa, A., 2020. An improved Terra – Aqua MODIS snow cover and Randolph Glacier Inventory 6 . 0 combined product (MOYDGL06 *) for high-mountain Asia between 2002 and 2018 0, 345–356.

Munroe, J.S., 2018. Distribution, evidence for internal ice, and possible hydrologic significance of rock glaciers in the Uinta Mountains, Utah, USA. Quaternary Research 50–65. https://doi.org/10.1017/qua.2018.24

Nydick, K., Crawford, J., Bidwell, M., Livensperger, C., Cozzetto, K., 2012. Climate Change Assessment for the San Juan Mountain Regions , Southwestern Colorado , USA: A Review of Scientific Research. Mt. Stud. Inst. www.mountainstudies.org

Outcalt, S.E., Benedict, J.B., 1965. Photo-interpretation of two types of rock glaciers in the Colorado Front Range, USA. J Glaciol 5:849-856

Paul, F., Barrand, N.E., Baumann, S., Berthier, E., Bolch, T., Casey, K., Nosenko, G., Frey, H., Joshi, S.P., Konovalov, V., Bris, R.L.E., Mo, N., Steffen, S., Winsvold, S., 2013. On the accuracy of glacier outlines derived from remote-sensing data. Annals of Glaciology 54, 171–182. https://doi.org/10.3189/2013AoG63A296

Paul, F., Huggel, C., Kääb, A., 2004. Combining Satellite Multispectral image data and a digital elevation model for mapping of debris-covered glaciers, Remote Sensing of Environment, 89 (4): 510-518.

Petersen, E.I., Levy, J.S., Holt, J.W., Stuurman, C.M., 2020. New insights into ice accumulation at Galena Creek Rock Glacier from radar imaging of its internal structure. Journal of Glaciology 2–11.

Pfeffer, W.T., Arendt, A.A., Bliss, A., Bolch, T., Cogley, J.G., Gardner, A.S., Hagen, J., Hock, R., Kaser, G., Kienholz, C., Miles, E.S., Moholdt, G., Rastner, P., Raup, B.H., Paul, F., Radic, V., Mo, N., Rich, J., Sharp, M.J., Consortium, T.H.E.R., 2014. The Randolph Glacier Inventory : a globally complete inventory of glaciers 60, 537–552. https://doi.org/10.3189/2014JoG13J176

Plaut, J.J., Safaeinili, A., Holt, J.W., et al., 2009. Radar evidence for ice in lobate debris aprons in the mid-northern latitudes of Mars. Geophysical Research Letters 36, L02203.

Potter, N., 1972. Ice-cored rock glacier, Galena Creek, northern Absaroka Mountains, Wyoming. Bull Geol Soc Am 83:3025-3058

Rau, F., Mauz, F., Vogt, S., Jodha, S., Kalsa, S., Raup, B., 2005. Illustrated GLIMS Glacier Classification Manual Glacier, Classification Guidance for the GLIMS Glacier Inventory 36.

Robson, B.A., Bolch, T., MacDonell, S., Hölbling, D., Rastner, P., Schaffer, N., 2020. Automated detection of rock glaciers using deep learning and object-based image analysis. Remote Sensing of Environment 250. https://doi.org/10.1016/j.rse.2020.112033

Rothlisberger, H., 1972. Seismic exploration in cold regions. Cold Regions Sci Engin Monogr II-A2a:I-139

Rowley, T., Giardino, J.R., Granados-Aguilar, R., Vitek, J.D., 2015. Periglacial Processes and Landforms in the Critical Zone, Developments in Earth Surface Processes. Elsevier B.V. https://doi.org/10.1016/B978-0-444-63369-9.00013-6

Schaffer, N., MacDonell, S., Réveillet, M., Yáñez, E., Valois, R., 2019. Rock glaciers as a water resource in a changing climate in the semiarid Chilean Andes. Regional Environmental Change 19, 1263–1279. https://doi.org/10.1007/s10113-018-01459-3

Schmid, M.O., Baral, P., Gruber, S., Shahi, S., Shrestha, T., Stumm, D., Wester, P., 2015. Assessment of permafrost distribution maps in the Hindu Kush Himalayan region using rock glaciers mapped in Google Earth. Cryosphere 9, 2089–2099. https://doi.org/10.5194/tc-9-2089-2015

Schrott, L., Sass, O., 2008. Application of field geophysics in geomorphology: advances and limitations exemplified by case studies. Geomorphology 93, 55–73.

Shao, Y., Lunetta, R.S., 2012. Comparison of support vector machine, neural network, and CART algorithms for the land-cover classification using limited training data points. ISPRS Journal of Photogrammetry and Remote Sensing 70, 78–87. https://doi.org/10.1016/j.isprsjprs.2012.04.001

Sheppard, P.R.., Comrie, A.C., Packin, G.D., Angersbach, K., Hughes, M.K., 2002. The climate of the US Southwest. Climate Research 21 (3): 219-238.

Spencer, A.C., 1900. A peculiar form of talus. Science (NS) 11:188

Staub, B., Marmy, A., Hauck, C., Hilbich, C., Delaloye, R., 2015. Ground temperature variations in a talus slope influenced by permafrost: A comparison of field observations and model simulations. Geogr. Helv. 70, 45–62. https://doi.org/10.5194/gh-70-45-2015

Steenstrup, KJV., 1883. Bidrag til Kjendskab til Braeerne og Brae-Isen i Nord-Gronland. Medd Gronl 4:69-112

Stine, M., 2013. Clyde Wahrhaftig and Allan Cox (1959) Rock glaciers in the Alaska Range. Bulletin of the Geological Society of America 70(4): 383-436. Progress in Physical Geography 37, 130–139. https://doi.org/10.1177/0309133313475693

Vonder Mühll, D., Arenson, L.U., Springman, S.M., 2003. Temperature conditions in two Alpine rock glaciers. Proceedings of the Eighth International Conference on Permafrost, Zurich, Switzerland, 21–25 July 2003, PhillipsM, Springman SM,Arenson LU(eds). Balkema Publishers: Lisse, The Netherlands. 1195–1200.

Vonder Muhll, D.S., Klingele, E.E., 1994. Gravimetrical investigation of ice-rich permafrost within the Rock Glacier Murtel-Corvatsch (Upper Engadin, Swiss Alps). Permafrost and Periglacial Processes 5, 13–24.

Wagner, S., 1996. DC resistivity and seismic refraction soundings on rock glacier permafrost in northwestern Svalbard. Norsk geografisk Tidsskrift 50: 25–36.

Wagner, T., Kainz, S., Krainer, K., Winkler, G., 2020. Storage-discharge characteristics of an alpine active rock glacier catchment – a multidisciplinary approach applied to the Innere Austrian Alps 1–22.

Wahrhaftig, C., 1987. Foreword. In: Giardino JR, Shroder JF, Vitek JD (ed) Rock glaciers. Allen & Unwin, London, pp 7-42

Wahrhaftig, C. and Cox, A., 1959. Rock Glaciers in the Alaska Range. Geological Society of America Bulletin. 70, 383-436.

Wakonigg, H., 1996. Unterkühlte Schutthalden. Arb. aus dem Inst. für Geogr. der Karl Franzens Universität Graz 33, 209–223.

Whalley, W.B., Martin, E., Gellatly, A.F., 1986. THE PROBLEM OF " HIDDEN " ICE IN GLACIER MAPPING 181–183.

White, P.G., 1973. Rock glaciers in the San Juan Mountains, Colorado. [Ph.D. thesis]: Denver, Colorado. University of Denver.

White, P.G., 1979. Rock glacier morphometry, San Juan Mountains, Colorado. Bull. Geol. Soc. Am. 90, 924–952. https://doi.org/10.1130/GSAB-P2-90-924

White, S.E., 1971. Rock glacier studies in the Colorado Front Range, 1961 to 1968. Arct Alpine Res 3:43-64

Wicky, J., Hauck, C., 2017. Numerical modelling of convective heat transport by air flow in permafrost talus slopes. Cryosph 11, 1311–1325. doi: 10.5194/tc- 11-1311-2017

Wicky, J., Hauck, C., 2020. Air Convection in the Active Layer of Rock Glaciers. Front. Earth Sci. 8, 1–17. https://doi.org/10.3389/feart.2020.00335

Winsor, K., Swanger, K.M., Babcock, E.L., Dickson, J.L., Valletta, R.D., Schmidt, D.F., 2020. Origin, structure and geochemistry of a rock glacier near Don Juan Pond, Wright Valley , Antarctica 32, 273–287. https://doi.org/10.1017/S0954102020000139

Xie, Z., Haritashya, U.K., Asari, V.K., Member, S., Young, B.W., Bishop, M.P., Kargel, J.S., 2020. GlacierNet : A Deep-Learning Approach for Debris-Covered Glacier Mapping XX, 1–15. https://doi.org/10.1109/ACCESS.2020.2991187

Zahs, V., Sailer, R., Hämmerle, M., Rutzinger, M., Anders, K., Hecht, S., Williams, J.G., Höfle, B., 2019. Multi - temporal 3D point cloud - based quantification and analysis of

geomorphological activity at an alpine rock glacier using airborne and terrestrial LiDAR 222–238. https://doi.org/10.1002/ppp.2004

Zhang, J., Jia, L., Menenti, M., Hu, G., 2019. Glacier Facies Mapping Using a Machine-Learning Algorithm: The Parlung Zangbo Basin Case Study. https://doi.org/10.3390/rs11040452

APPENDIX A

GRAPHICAL RESULTS

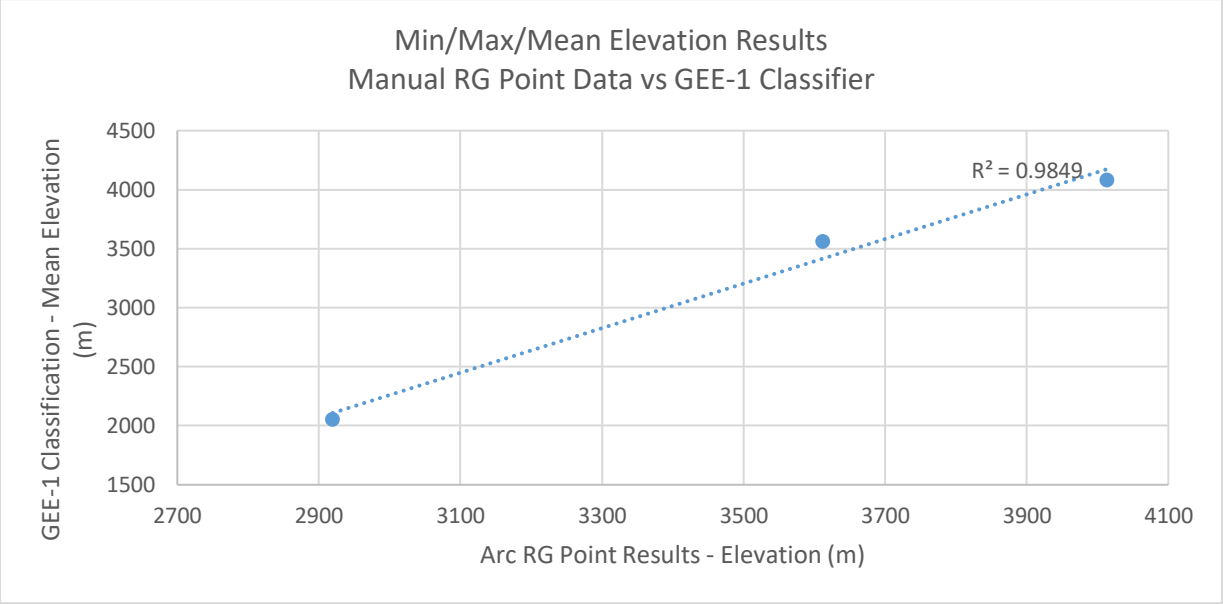

Fig. A.1 - Validation results showing min, max, and mean elevation results from GEE-1 predicted rock glacier landcover versus manually mapped rock glacier points.

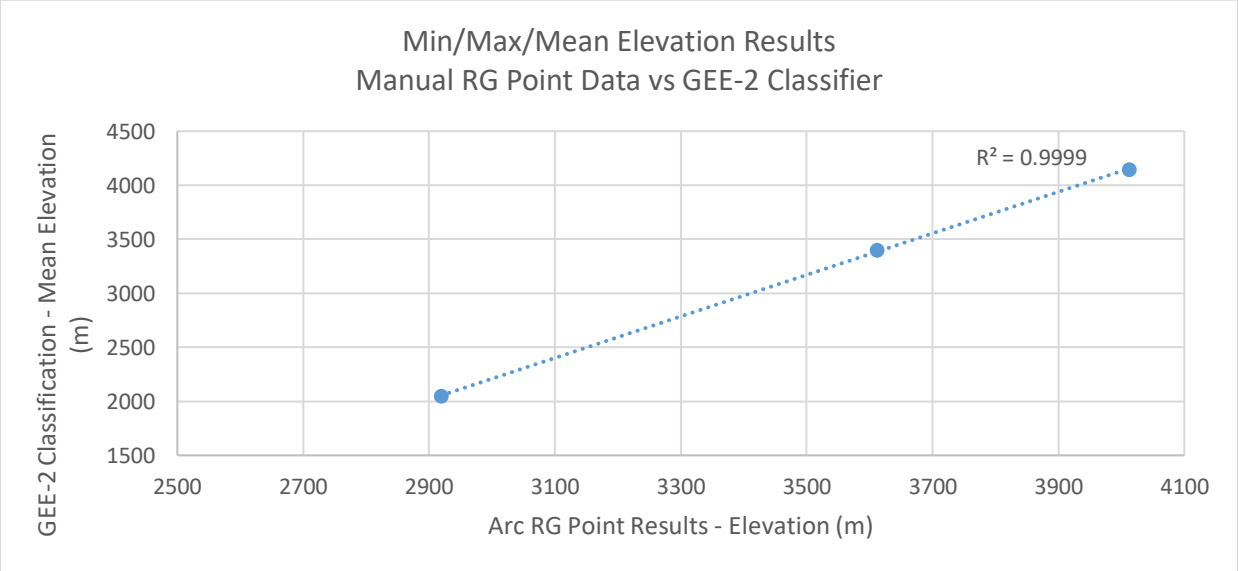

Fig. A.2 - Validation results showing min, max, and mean elevation results from GEE-2 predicted rock glacier landcover versus manually mapped rock glacier points.

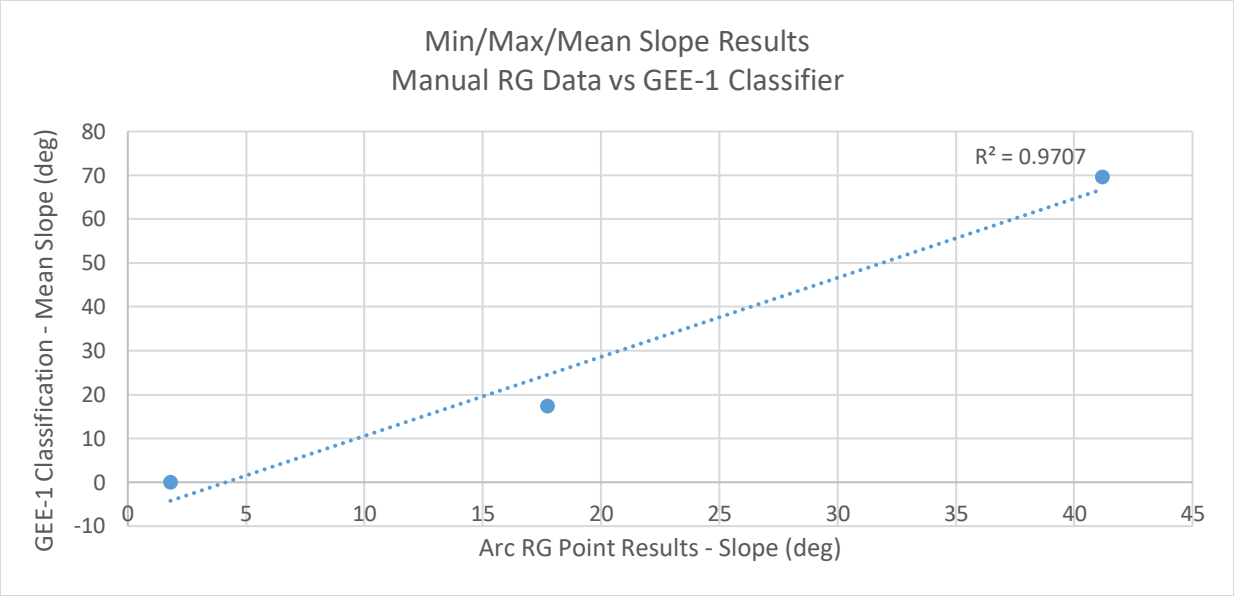

Fig. A.3 - Validation results showing min, max, and mean slope results from GEE-1 predicted rock glacier landcover versus manually mapped rock glacier points.

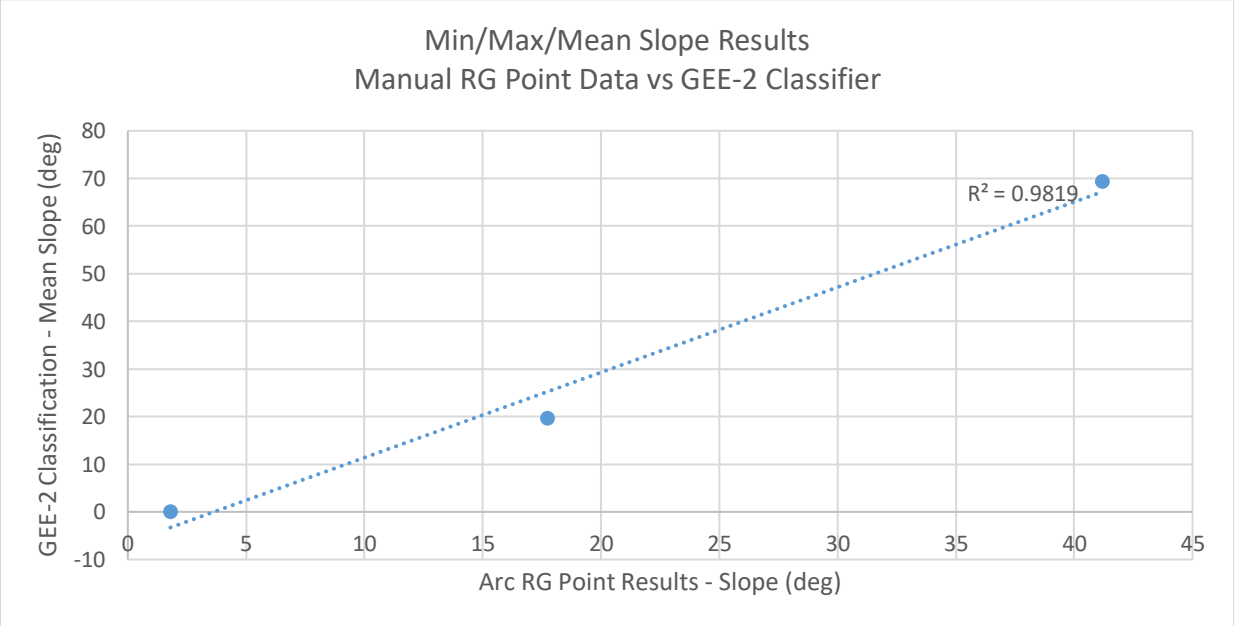

Fig. A.4 - Validation results showing min, max, and mean slope results from GEE-2 predicted rock glacier landcover versus manually mapped rock glacier points.

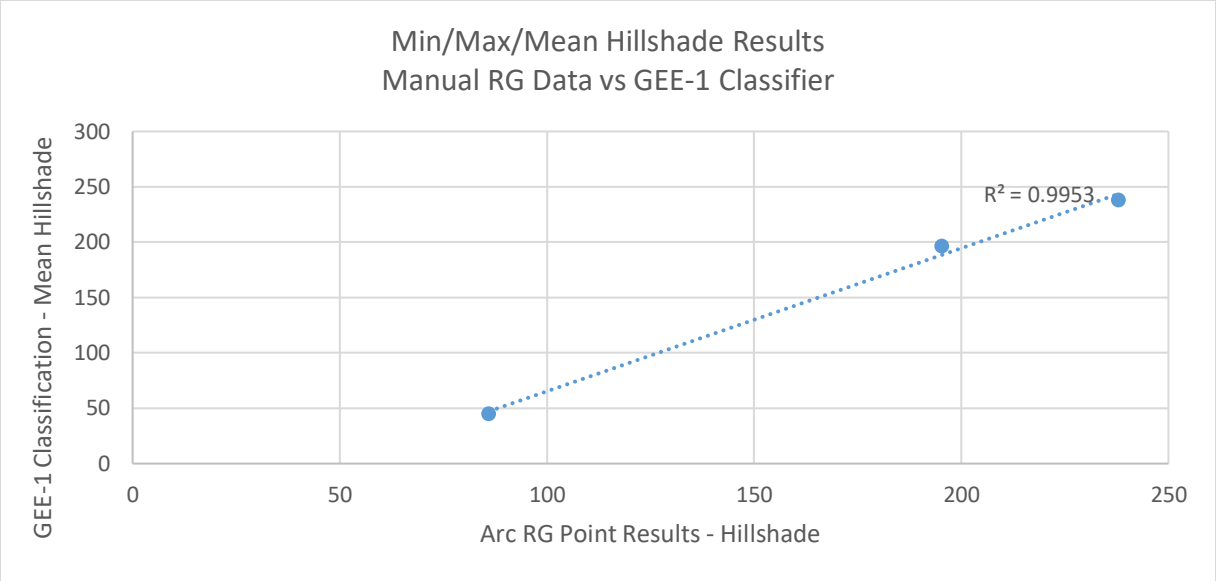

Fig. A.5 - Validation results showing min, max, and mean hillshade results from GEE-1 predicted rock glacier landcover versus manually mapped rock glacier points.

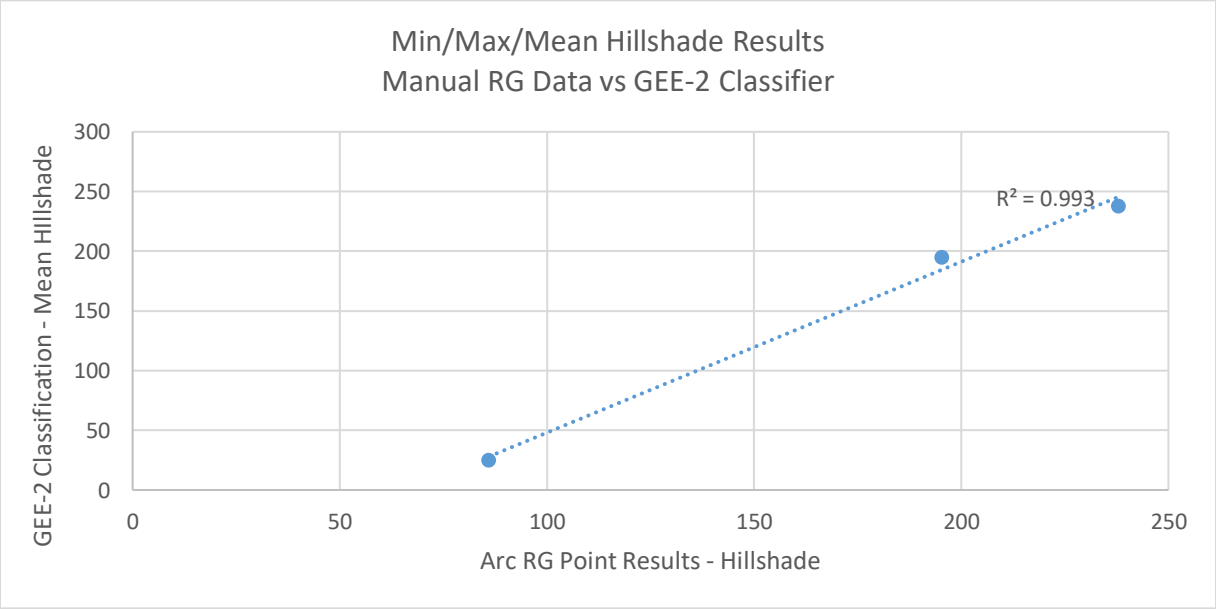

Fig. A.6 - Validation results showing min, max, and mean hillshade results from GEE-2 predicted rock glacier landcover versus manually mapped rock glacier points.

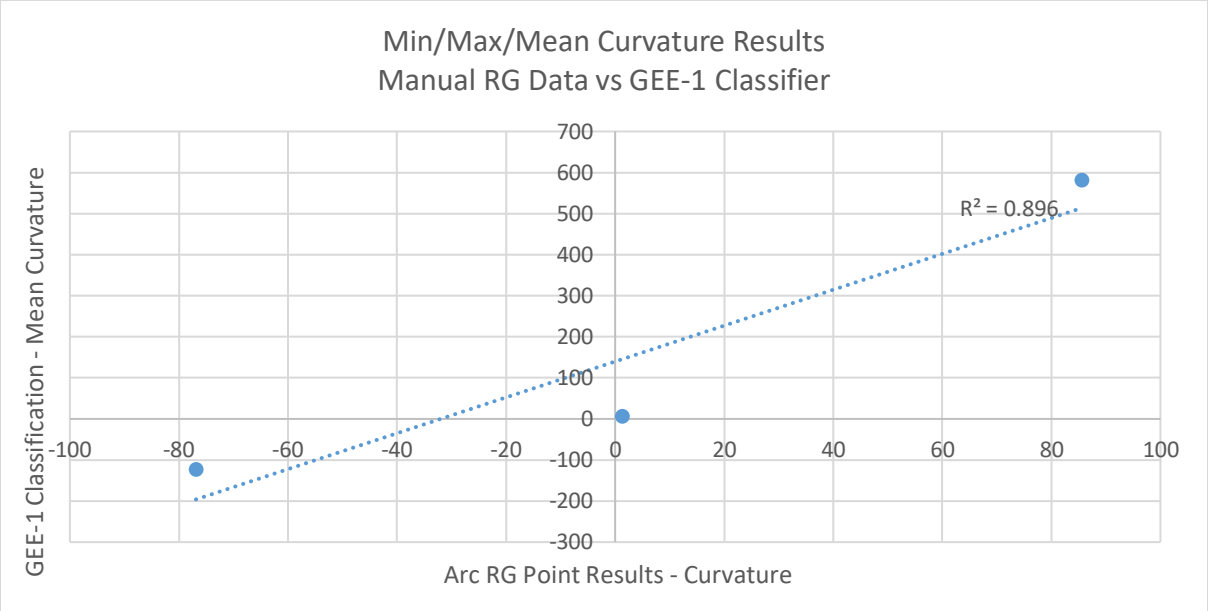

Fig. A.7 - Validation results showing min, max, and mean curvature results from GEE-1 predicted rock glacier landcover versus manually mapped rock glacier points.

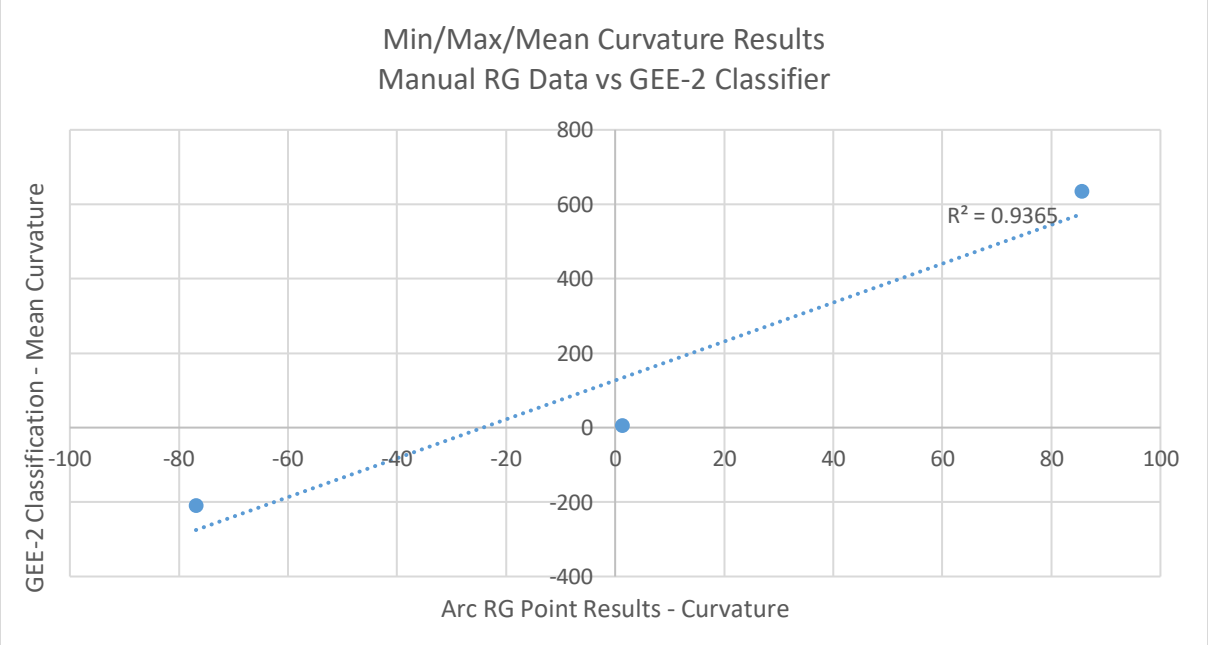

Fig. A.8 - Validation results showing min, max, and mean curvature results from GEE-2 predicted rock glacier landcover versus manually mapped rock glacier points.

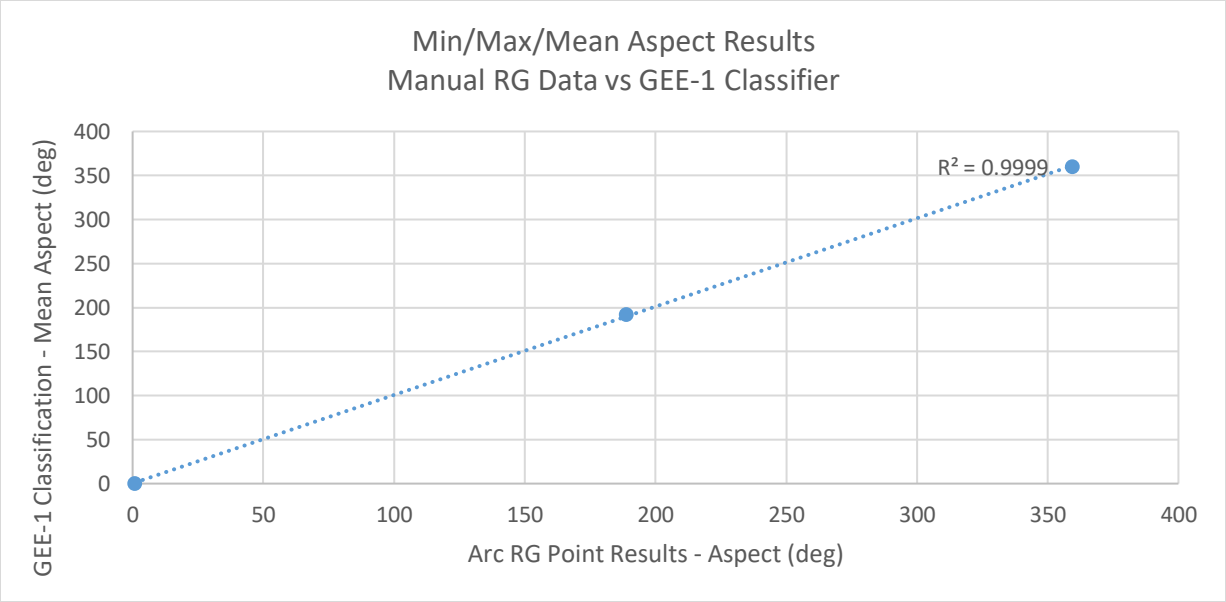

Fig. A.9 – Validation results showing min, max, and mean aspect results from GEE-1 predicted rock glacier landcover versus manually mapped rock glacier points.

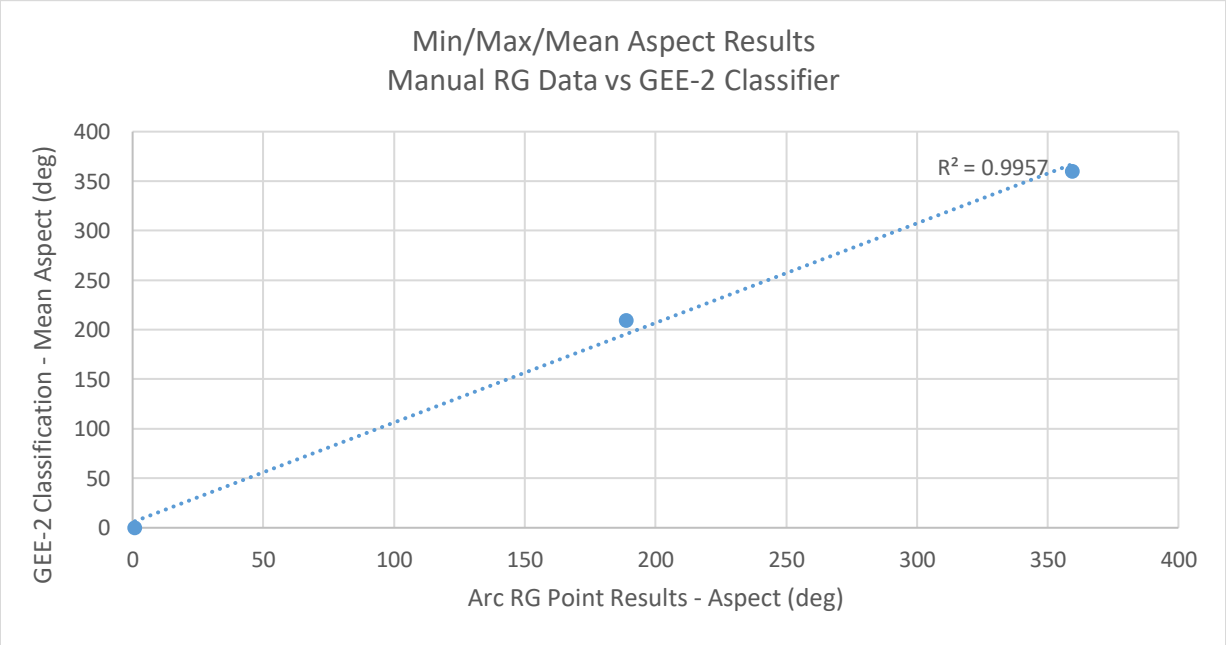

Fig. A.10 – Validation results showing min, max, and mean aspect results from GEE-2 predicted rock glacier landcover versus manually mapped rock glacier points.

APPENDIX B

ROCK GLACIER DISTRIBUTION MAPS

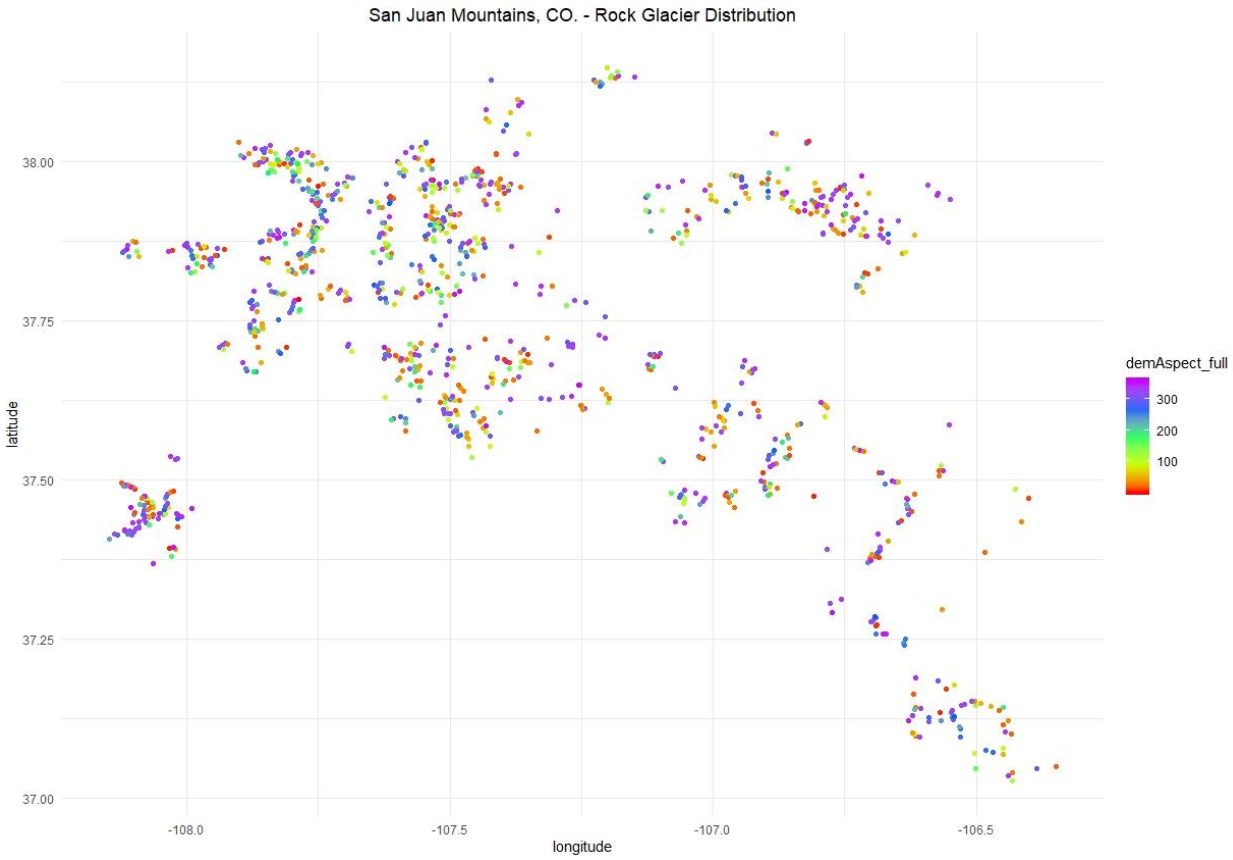

Fig. B.1 - Rock glacier distribution map displaying all 1052 manually mapped rock glaciers in the San Juan Mountains, CO. Points colored by respective aspect values.

Fig. B.2 - Rock glacier distribution map displaying all 1052 manually mapped rock glaciers in the San Juan Mountains, CO. Points colored by respective curvature values.

Fig. B.3 - Rock glacier distribution map displaying all 1052 manually mapped rock glaciers in the San Juan Mountains, CO. Points colored by respective elevation values.

Fig. B.4 - Rock glacier distribution map displaying all 1052 manually mapped rock glaciers in the San Juan Mountains, CO. Points colored by respective hillshade values.

Fig. B.5 – Rock glacier distribution map displaying all 1052 manually mapped rock glaciers in the San Juan Mountains, CO. Points colored by respective slope values.